Design, Simulation and Characterization of Compliant Microfluidic Devices

BY

TATJANA DANKOVIC
B.S., University of Belgrade, 1995
M.S., University of Illinois at Chicago, Chicago, 2006

THESIS
Submitted as partial fulfillment of the requirements
for the degree of Doctor of Philosophy in Electrical and Computer Engineering
in the Graduate College of the
University of Illinois at Chicago, 2013

Chicago, Illinois

Defense Committee:
Alan Feinerman, Chair and Advisor
Mitra Dutta
Siddhartha Ghosh
Constantine Megaridis, Mechanical & Industrial Engineering
Heinz Busta, Prairie Prototypes, LLC

ACKNOWLEDGMENTS

First and foremost I would like to express my gratitude to my supervisor, Professor Alan Feinerman, for his invaluable assistance, guidance, and encouragement throughout my work on the thesis. It gives me great pleasure in acknowledging the support and help of the members of the supervisory committee, Professor Mitra Dutta, Professor Heinz Busta, Professor Constantine Megaridis, and Professor Siddhartha Ghosh. I wish to thank Professor Vitali Metlushko, who was member of the preliminary examination committee. I would also like to acknowledge Robert Lajos and Hongjun Zeng for their helpful discussions during my experimental work in NCF. Special thanks to all my friends both in Belgrade and Chicago for their friendship and support during the last few years. Finally, I would like to express my love and gratitude to my family and Ken Takata for their continued support and encouragement to apply to the graduate program.

TD

TABLE OF CONTENTS

CHAPTER			PAGE
I.	INTRODUCTION		1
	A.	Motivation	1
	B.	Materials used in microfluidics	2
	C.	Fabrication of microfluidic devices	6
	D.	The laser welding	10
	E.	The proposed fabrication method	12
II.	MICROVALVES		18
	A.	Introduction	18
	B.	Previous work	21
	C.	Materials	40
	D.	Fabrication	42
	E.	Theory	47
	F.	Simulation results	49
	G.	Experimental results	52
	H.	Conclusion	58
III.	MICROMIXERS		60
	A.	Introduction and motivation	60
	B.	Previous work	65
	C.	Fabrication	84
	D.	Proposed mixer structures	86
		1. Serpentine micromixer	87
		2. Micromixer with obstacles	88
		3. Split and recombine micromixer	89
		4. Y-mixer	90
	E.	Experimental results	91
		1. Serpentine micromixer	95
		2. Micromixer with obstacles	102
		3. Split and recombine micromixer	109
		4. Y-mixer	115
	F.	Conclusions and future work	118
IV	CONCLUSIONS		121
	CITED LITERATURE		125
	VITA		140

LIST OF TABLES

TABLE		PAGE
I.	COMPARING MIXING RESULTS OF FABRICATED MICROMIXERS ...	119

LIST OF FIGURES

FIGURE		PAGE
1.	The weld apparatus.....	13
2.	SEM image of the weld line	16
3.	Electrostatically actuated microvalve	20
4.	Laser welding of thermoplastic films	43
5.	A typical path for a microvalve	44
6.	SEM image of the weld line	44
7.	Multiple microvalves can be made in same laser welding step	45
8.	Electrostatically actuated microvalve	46
9.	A packaged microvalve after assembly. The LDPE donut provides structural support	46
10.	Schematic cross-sectional view of microvalve	48
11.	Coventor™ predicted values of closing voltages for different valve widths (0.1 mm – blue rhomboids, 0.5 mm-green squares, and 1mm-red triangles) and applied pressures from 100 Pa to 2000 Pa.	50
12.	Coventor™ predicted values of maximum opening of the microvalve channels for applied pressures of 100 Pa, 1 kPa and 10 kPa	51
13.	Coventor™ predicts 544 μm total opening for 1 mm valve at gauge pressure of 1kPa	51
14.	Experimental set up for testing the closing voltages for microvavles	53
15.	Experimental values of closing voltages for 0.9 mm wide valve	54

LIST OF FIGURES (continued)

FIGURE		PAGE
16.	Measured outlet flow rate as a function of applied voltage ……	54
17.	Measured flow rate (normalized to 10 sccm) versus applied closing voltage for a 1 mm wide microvalve and 450 Pa air pressure …….	56
18.	Measured leak as a function of inlet flow rate (range 10-150 sccm) for 1mm wide microvalve …….	56
19.	Measured leak as a function of inlet flow rate (range 1-15 sccm) for 1mm wide microvalves ……	57
20.	Laser welding of thermoplastic films ……..	85
21.	Assembling the device ……	86
22.	Serpentine mixer …….	87
23.	The welded mixer channel with 6 obstacles ……	88
24.	Mixer with obstacles ……..……	89
25.	Split and recombine mixer …..……...	90
26.	Y-mixer ……..	91
27.	Illustration of Mylar reflection (bright spots) and Mylar folding (dark lines) ……..	93
28.	Images showing the mixing results for wider serpentine channel and Reynolds numbers from 0.01 to 10 ……	95
29.	Standard deviation of pixel intensity (a) along the main channel direction of the wide serpentine micromixer; (b) as a function of Reynolds number.	96
30.	Standard deviation of pixel intensity at the cross section of the mixer channel …….	98

LIST OF FIGURES (continued)

FIGURE		PAGE
31.	Images showing the mixing results for narrower serpentine channel and Reynolds numbers from 0.01 to 10 ……..	99
32.	Standard deviation of pixel intensity (a) along the main channel direction of the narrower serpentine micromixer. (b) as a function of Reynolds number …….	100
33.	Standard deviation of pixel intensity at the cross section of the mixer channel …….	101
34.	Images showing the mixing results for mixer with obstacles with wider channel and Reynolds numbers from 0.01 to 10 ……	103
35.	Standard deviation of pixel intensity (a) along the main channel direction of mixer with obstacles and wide channel; (b) as a function of Reynolds number …….	103
36.	Standard deviation of pixel intensity at the cross section of the mixer channel …….	104
37.	Images showing the mixing results for mixer with obstacles with narrower channel and Reynolds numbers from 0.01 to 10 ……	105
38.	Standard deviation of pixel intensity (a) along the main channel direction of the mixer with obstacles and narrow channel; (b) Standard deviation as a function of Reynolds number ……...	106
39.	Standard deviation of pixel intensity at the cross section of the mixer channel …….	107
40.	Images showing the mixing results for mixer with obstacles with short channel and Reynolds numbers range from 0.008 to 8.4 ……	108
41.	Images showing the mixing results for split and recombine mixer and Reynolds numbers from 0.01 to 10 …….	109
42.	Standard deviation of pixel intensity (a) along the main channel direction of the split and recombine mixer with 4 mm segment length; (b) as a function of Reynolds number …….....	110

LIST OF FIGURES (continued)

FIGURE		PAGE
43.	Standard deviation of pixel intensity at the cross section of the mixer channel ……...……...	111
44.	Images showing the mixing results for split and recombine mixer with 5 mm segment length and Reynolds numbers from 0.01 to 10 …….	112
45.	Standard deviation of pixel intensity (a) along the main channel direction of the split and recombine mixer with 5 mm segment length; (b) as a function of Reynolds number …….....	113
46.	Standard deviation of pixel intensity at the cross section of the mixer channel ……...……..	114
47.	Images showing the mixing results for Y-mixer and Reynolds numbers from 0.01 to 10 ……...…….	115
48.	Standard deviation of pixel intensity for the Y-mixer channel as a function of Reynolds number ……...…….	116
49.	Standard deviation of pixel intensity at the cross section of the mixer channel ……...……..	117
50.	Patterned gold structure on Mylar film after etching the 10 nm gold layer, using standard photolithography process …….	122
51.	Schematic representation of the micropump …….	123
52.	Voltages applied to micropump ……...	124

LIST OF ABBREVIATIONS

AC	alternating current
AMANDA	Abforming, Oberflachenmikromechanik und Membranubertragung (surface micromachining, molding, and diaphragm transfer)
ASM	asymmetric serpentine micromixer
AW	alternating whirl
AWL	with alternating whirl and lamination
BEM	barrier embedded mixer
CCD	Charge-coupled device
CE	Capillary electrophoresis
CNC	computer numerical control
COC	cyclic olefin copolymer
CVD	Chemical vapor deposition
D	Diffusion coefficient
DC	direct current
DI	Deionized Water
DNA	Deoxyribonucleic acid
FD&C	Federal Food, Drug, and Cosmetic Act
FTIR	Fourier transform infrared spectroscopy
GC	Gas chromatography
HEMA	hydroxyl ethyl methacrylate
HF	hydrofluoric acid
HPDFO	High Power Density Focusing Optics

LIST OF ABBREVIATIONS (continued)

IC	Integrated circuit
ID	Inner diameter
IgG	Immunoglobulin G
IR	Infrared
LDPE	Low density polyethylene
LLDPE	linear low density polyethylene
LIGA	Lithographie, Galvanoformung, Abformung (Lithography, Electroplating, and Molding
MBA	Molecular Beam Epitaxy
MEMS	micro electro mechanical systems
µEDM	micro electro discharge machining
µTAS	Micro total analysis system
OD	Outer diameter
PCB	Printed Circuit Board
PCR	polymerase chain reaction
Pe	Pecklet number
PDMS	Polydimethylsiloxane
PET	Polyethylene Terephthalate
PFTE	Polytetrafluoroethylene
PIBA	poly isobornyl acrylate
PMMA	Poly methyl methacrylate
PPI	Pulses per inches

LIST OF ABBREVIATIONS (continued)

P-SAR	planar split and recombine
Re	Reynolds number
RIE	Reactive ion etching
SEM	scanning electron microscope
SGM	slanted groove mixer
SHM	staggered herringbone mixer
SOI	Silicon on insulator
TMEA	touch mode electrostatic actuator
TPE	Thermoset polyester
UV	Ultraviolet

SUMMARY

A new technique has been developed to make valves and other microfluidic structures by patterned welding of compliant thermoplastic films. Electrical contacts, packaging, and low leakage connections with external tubing to these structures have also been demonstrated.

An electrostatically driven normally open microvalve made of thermoplastic materials is presented. The microvalves are compatible with a wide range of fluids. The microvalve is limited to actuation voltages less than 600 V because of the breakdown voltage limitation of 1.4 μm thick Mylar film. The pressure range is limited by the value of the closing voltages to few kPa, although the valve can withstand much higher applied pressures (~20 kPa). The operating temperature should be limited to 100 ºC because of the low melting point of the LLDPE tubing and support rings. The measured leak rate for well manufactured microvalves was less than 10% of the flow rate.

The proposed fabrication method for welding very thin polyester sheets is used to produce several types of micromixers and demonstrate its potential use for producing different designs of mixer structures that can be modified as needed without the need for a photolithography or microfabrication facilities.
The proposed fabrication technique is applicable for the design of the planar microfluidic devices.

I. INTRODUCTION

A. Motivation

Microfluidics is the technology that is expected to have significant applications in biomedical and molecular analysis, chemical analysis and molecular biology. The early research started in seventies when Terry et al. published a paper on gas chromatography system made on silicon wafer and consisting of injection valve, capillary column and thermal conductivity detector (Terry et al., 1979).

Research was continued to design and fabricate different microfluidic devices (valves, pumps, chemical sensors, electrophoresis channels) intended for use in automotive and aviation industries, and other manufacturing industrial or household applications (Shoji and Esashi, 1994; Henning, 1998). In 1990 the term 'micro total analysis' or μTAS was proposed by Manz (Manz et al., 1990), and research was directed toward use of microfluidic systems in the analytical chemistry (Reyes et al., 2002; Auroux et al., 2002; West et al., 2008; Arora et al., 2010; Gorkin et al., 2010). Microfluidic devices are also important in the detection of material substances such as biomedical hazards or explosive or flammable materials (Whitesides, 2006). In microelectronics, microfluidic channels and devices are investigated for better cooling of microprocessors (Koo et al., 2005). In macromolecular analysis microfluidic devices are used for Deoxyribonucleic acid (DNA) analysis, especially polymerase chain reaction (PCR), enzyme assays, or immunoassays (Beebe et al., 2002). Complex devices (consisting of array of channels, valves, mixers, reservoirs etc.) that can perform multiple operations at the same time are often described as lab on a chip (Stone et al., 2004).

Often mentioned application of the microfluidic devices and systems is for the use in the diagnostics especially in the remote areas of developing countries as well as in military operations (Yager et al., 2006). For those purposes, the devices would have to be portable, low energy consuming, low-cost, disposable (Fiorini and Chiu, 2005) and easy to use by medical personnel. Those requirements are investigated by many researchers and may be one of the reason that microfluidics is still not used at such degrees as expected (Whitesides, 2006). Low cost disposable devices require low cost manufacturing process and low cost materials. The motivation for this work was to develop a new low cost fabrication technique that may be used in microfluidic applications.

The first two sections in Chapter 1 discuss the choice of materials and technology used for fabrication microfluidic devices. In the following two sections, laser welding and details on proposed fabrication methods are described.

B. Materials Used in Microfluidics

Microfluidic devices were developed using same techniques as for micro electro mechanical systems (MEMS) devices and was considered as type of the MEMS devices. Techniques such as etching (wet, dry), photolithography, layer deposition, etc. were well known as well as materials already used (mostly silicon, glass, metals, photoresist).

However, this specific area has developed independently, and has outgrown the boundaries set by MEMS technology. New techniques that do not require use of the clean room were developed, as well as new materials introduced. There were few requirements to satisfy: the technology should not be expensive if devices are to be produced for one-time consumption (disposable), and the materials for specific use had to be properly chosen. The choice of

materials depends on the intended use of the device, but mostly the material should be transparent, chemically inert, and inexpensive.

Materials used for the earliest microfluidic devices were silicon, metals or glass. Silicon, as a very well-known material used in integrated circuits (IC) industry with highly developed technologies was an obvious choice. A number of microfluidic devices were initially made of silicon (Shoji and Esashi, 1994), however a few problems were noticed. First, the cost of material used per device becomes much larger since microfluidic devices in general use larger areas then IC chips, and for the mass production this was not acceptable. The other problem was that silicon is not optically transparent material and for many microfluidic devices transparency is required for optical detection of processes within the device.

Metal devices can also be used for applications where the observation is not needed. Parts can be manufactured using advanced tools in mechanical machining where features size of 5 to 10 microns can be obtained. The disadvantage is electrical conductivity of material which is not suitable for some microfluidic applications such as capillary electrophoresis (CE), where large voltage difference is applied along the channel. Similar problem exists for silicon devices, so for CE applications glass is the main material of choice.

Glass has a very important advantage of being transparent in the visible wavelength region, so the easy observation of the processes in the device is possible. It also shows less chemical bonding to working fluids then silicon. The manufacturing of devices is still expensive, and devices are less sturdy.

As the applications for the microfluidic devices expand from laboratory experimental usage to mass production, the search for better suited materials becomes more important. The ideal

material should be inexpensive, transparent, not conductive (in some cases), easy to manufacture, biocompatible (depending on applications) etc.

Many of those requirements are fulfilled by plastic (polymer) materials (Boone et al., 2002). Plastics are becoming the material of choice for many devices in last decade. Plastics are convenient for the following reasons: well-known technology, not expensive, variety of material properties available (can be designed), some plastics are biocompatible, proper (desired) chemical properties, etc. (Fiorini and Chiu, 2005; Becker and Gartner, 2000; Becker and Locascio, 2002; Becker and Gartner, 2008). Fabrication methods used for plastic devices include replication techniques (such as injection and compression molding, embossing, extrusion, or casting) or direct methods (laser ablation, cutting and welding, or mechanical machining). By adding additives (plasticizers) to plastic material its properties (thermal stability, ultraviolet (UV) stability, strength, softness, flexibility etc.) can be changed. In such manner desired properties can be tailored for specific intended use of plastic material. Polymers such as Polydimethylsiloxane (PDMS), SU-8, polyimide, acrylic, Teflon, Poly methyl methacrylate (PMMA) and others are used (Sollier et al., 2011).

SU-8 is well known negative photoresist used in photolithography and in soft lithography. It is biocompatible which enables its use for biological applications. It can be used for defining the channel walls, or the entire device can be made of SU-8. It can be applied in one or more layers of different thicknesses. It is easily etched with high aspect ratios up to 1:50 and smooth vertical walls. It can be exposed using standard UV photolithohraphy systems after which the unexposed photoresist is removed. The work area does not need to be specially designated as in case when working with hydrofluoric acid (HF) to etch glass channels (Ribeiro et al., 2005).

PDMS is the most used polymeric material in microfluidics. It is optically transparent, biocompatible, oxygen permeable, relatively chemically inert, and easy for manufacturing. It can be bonded in oxygen plasma to another PDMS layer or glass which allows fabrication of multilevel structures. It is used in soft lithography technique where first the master is made usually of SU-8 negative photoresist, and then two-component PDMS is applied and cured at elevated temperature. It is often used in devices for separation of biomolecules. The surface of PDMS layer is hydrophobic and presents difficulty when using aqueous solutions. Different methods are used to modify the PDMS surface into hydrophilic, including plasma treatment, UV treatment, wet chemical methods or coating with metals or chemical vapor deposition (CVD) of poly(p-xylylene) film on PDMS (Zhou et al., 2009). The other noticed issue is swelling of PDMS in organic solvents such as benzene, toluene, chloroform, and trichloroethylene (Lee et al., 2003).

Fiorini et al. proposed a novel material to replace PDMS in applications where PDMS is not the best choice of material because of its permeability, swelling and hydrophobic nature, while keeping the fabrication process very similar (Fiorini et al., 2004). The new material to be used is thermoset polyester (TPE) (unsaturated polyester), and the process for device fabrication is about 3 hours. It is less hydrophobic than PDMS and oxygen plasma can help to reduce this hydrophobicity further. The swelling ratio shows good compatibility to water, ethanol, 2-propano, some acids and basis, and as a difference to PDMS, it has swelling ratio 1 for toluene, cyclohexane and n-heptane. By comparing the properties of TPE, PDMS and glass it was concluded that TPE devices can be used for situations when rapid fabrication is needed but device should be rigid, or able to withstand certain solvents.

Kim et al. used thermoset polyester to fabricate the droplet based microfluidic device (Kim et al., 2011). The fabrication procedure involves fabrication of the PDMS mold made on top of the SU-8 patterned structure, then peeled and used as a master for TPE. This is done to avoid damaging of the SU-8 while dissociating it from TPE. The TPE material is convenient because it is transparent in the optical region for wavelengths larger than 400 nm, and the used bonding conditions enables much higher burst pressures (>17 MPa) then for PDMS based devices (0.5-1.2 MPa).

C. Fabrication of Microfluidic Devices

Techniques used for manufacturing the microfluidic devices can be either direct or replication. Direct methods include MEMS technologies, mechanical machining, laser welding, and laser ablation. Replication methods used are hot embossing, replica molding, or injection molding. Both types have some advantages or disadvantages. When the devices are needed in larger quantities for mass production, two important requirements are that the fabrication is not expensive, and that it does not require much time. Therefore the replication methods are desirable. However for the in-house use in laboratories, where comparatively only a small number of devices are needed but the design is changed more frequently, direct methods are preferred.

Replication methods used includes hot embossing, injection molding, replica molding, and casting (Rowland and King, 2008). For most of them, the first step is fabrication of the master. This is also the most expensive and most time consuming step, but since it is done one or few times, it does not increase the total cost significantly. Master can be made using various technologies.

Silicon micromachining methods such as photolithography and wet or dry etching are often used (Kovacs, 1998; Madou, 2002; Nguyen and Wereley, 2002). Wet isotropic etching can produce well defined channels. The shape of the channels depends on the crystal orientation. For the 110 silicon wafers the channel can be almost vertical, while for the (100) silicon the cross section is trapezoidal or triangular. If wet etching is used, deep narrow trenches cannot be made. Dry etching (such as reactive ion etching (RIE) or Bosch) can be useful for such purpose, but is a more expensive method. Etching rate in both dry and wet etching is important since it influences the roughness of the etched surface (roughness is smaller with lower etch rates). This is important for enabling easy removal of plastic material after the molding process. Still many polymers are not suitable for use with silicon masters because surface chemical bonds can be easily established between silicon and those polymers.

MEMS techniques such as LIGA, German acronym for Lithographie, Galvanoformung, Abformung - Lithography, Electroplating, and Molding (Ehrfeld et al., 1999b; Malek and Saile, 2004), and electroplating are also useful since they can produce high aspect ratio devices with very small roughness of the walls. For electroplating a photoresist is spun on top of the conductive electroplating layer. If larger aspect rates are needed, a negative photoresist SU-8 can be used. The photolithography step will define the features by removing the SU-8 from unexposed regions and electroplating of metal such as Ni or its alloys can be done on those regions. At the end the SU-8 and starting electroplating layers are removed and master is ready for use. For achieving very high aspect ratios the LIGA process can be used. Here the starting photoresist (such as PMMA) is exposed by X-rays radiation through a metal mask. The development process removes the unexposed PMMA, which is followed by electroplating of Au,

Co or Ni, to form a metal mold. Less expensive version of LIGA is UV-LIGA where UV light is used for exposure instead of X-ray radiation.

For producing the master, an improved conventional micromachining can also be used, since the tools developed can produce features as small as 10 microns. The advantages of this technique is that is does not require masks, it is often much faster than other described methods, and materials such as stainless steel can be machined for the master.

Hot embossing is a process usually performed by pressing the master on top of the polymer at the temperatures above the glass temperature of the polymer by hydraulic press and preferably in vacuum environment to avoid trapping the air between master and polymer. After the embossing both master and embossed polymer are cooled below the glass temperature, and then separated. Master can be made of metal, for example electroplated nickel on silicon microfabricated features. Master preparation is expensive and can take few days to complete (Kricka et al., 2002; Heckele and Schomburg, 2004).The process has a long thermal cycle and alternative methods have been proposed, such as hot roller embossing where polymer material and master foil (mounted on one of two rolls) are in contact for a short time thus reducing the cooling time (Yeo et al., 2010).

Injection molding is a standard process in the industry for making many plastic products. The polymer material is injected under high pressure and at high temperatures into the molded cavity. After the cooling process the mold master can be opened and the polymer part removed.

Both hot embossing and injection molding require high force and temperature but can provide large throughput with a cycle time less than a few minutes. The cost of making the mold can be high, although the advantage is the possibility of creating various shapes that are not possible to achieve with planar techniques such as hot embossing, replica molding, or casting.

Replica molding of microfluidic devices is usually done using soft lithography process, where master is a silicon wafer with photoresist shaped in the pattern of the microfluidic features. PDMS is applied on top and cured for few hours at elevated temperature. After the curing the shaped PDMS is easily removed from the master, and device is made by placing the glass plate or other PDMS layer on top.

Casting is suitable for planar layouts and does not require any additional force as for hot embossing or injection molding. The materials such as elastomers or epoxies are poured on top of the already prepared master. Master is usually made of silicon wafer using standard photolithography and treated with parylene or Polytetrafluoroethylene (PFTE) in order to provide easier release of the casted material after it hardens. The time needed can be long (~day) unless it is cured at elevated temperatures (Sethu and Mastrangelo, 2004). Both elastomers (such as PDMS) and epoxies can be optically transparent.

When device is fabricated using one of mentioned techniques, an additional step is required to close the channels with flat transparent cover. Either bonding or lamination can be used. Bonding is preferred for PDMS since this material easily bonds to another PDMS layer or glass. Glass-made devices are bonded to glass plates either at high temperatures or at temperatures below 100 ºC in which case the adhesive material is added. For polymer materials it is desirable that no high temperature is used in order to prevent damaging or deformation of the fabricated structure. Lamination with direct thermal bonding is done at temperatures near glass temperature and applied pressure in hot press or using roller laminator (Tsao and DeVoe, 2009; Paul et al., 2007). Inter-diffusion of polymer material leads to strong bonds in short time. This is a simple and low cost technique with fair bonding quality. Adhesives may be used to enhance the bonding but can contribute to channel clogging and non-uniform wall chemistry.

Direct methods include such as mechanical machining, laser welding, laser cutting and laser ablation (Snakenborg et al., 2004; Meijer, 2002; Khan Malek, 2006a; Khan Malek, 2006b). The mechanical machining with its improved tools can manufacture features down to 10 microns. For the laser ablation either excimer or CO_2 lasers are used to remove parts of polymer material and form channels or cavities. The ablated polymer sheet is then sandwiched between two glass (or polymer) plates, or laminated in order to close the channels. Similar approach is for laser cutting where the channels are cut for example in Mylar sheet using CO_2 laser and then laminated to form the enclosed microfluidic system (Matthew, 2004; Schilling et al., 2002).

D. The Laser Welding

Most of the previously developed methods for plastic molding used in the industry can also be readily used in microfluidics. Laser welding of plastic and thermoplastic materials has been used in the industry for many years, but recently it also gets a lot of attention in the fabrication of microfluidic devices. There are many advantages in using the laser for welding, such as delivering the needed energy without the contact of machining tools and therefore reducing the mechanical stress in the material, possibility of defining precisely both delivered energy and duration of the interaction. The limiting factors in some cases may be the width of the weld lines which depends on the type of the laser and optics used in the certain application.

When using the laser welding to join two pieces of thermoplastic materials, there are a few considerations to take into account (Russek et al., 2003). We can choose between many laser types (with different wavelength of operation and different power densities) to find the one suitable for our situation (Khan Malek, 2006a; Khan Malek, 2006b). UV excimer lasers are often used for welding or engraving the thermoplastic materials, since these materials have higher

absorption in the UV optical region and the laser beam energy can easily been transformed into the heat energy within the material. CO_2 lasers which operate in the far infrared optical region are often used for engraving or cutting of materials, as well as for welding primarily metals and ceramics (Khan Malek, 2006a). The optical penetration depth of 10.6 μm laser beam is very small in thermoplastic materials, and CO_2 lasers can be used for welding of thin thermoplastic materials.

There is possibility to use direct laser welding (contour), simultaneous (two or more laser heads at a time) or mask welding (using patterned rastering technique, so the laser beam can pass through the mask only at the desired regions. Different approaches should be taken depending on the thickness of the materials to be welded. If two materials are thick (so called form stable), it is not difficult to clamp them together so the parts do not move during the weld process. If material is thin or flexible, other methods could be used to bring two pieces into the tight contact, for example using the vacuum between the materials, or pressing them and exposing only part needed to be welded.

Russek et al. mention two main joint geometries (Russek et al., 2003). The first one is so called overlap welding where two layers or parts have different optical properties at the laser operation frequency. The top plastic material should be transparent and have higher optical transmission in order to allow the laser beam to reach the second, lower material. The penetration depth of the laser beam should be known and it should be long enough to reach the contact between two materials. The other (lower) material should have high absorption and very small reflection and transmission. The two parts to be welded can be of the same material, however in the lower material often the absorbing particles are induced (sometimes in the form of colors) to enhance its absorption. The absorption of the electromagnetic energy of the laser

beam within the lower welding layer will cause the increase of the temperature in the material and its volume will increase to fill all gaps that were possibly present between the two layers. The top layer would then also get heated and two materials will be joined by forming the plastified regions in both layers. This welded region extends on the contact of two materials, and not though the whole thicknesses of materials. The other joint geometry is so called butt joint. Here both joining parts have thickness that is comparable to the optical penetration depth of the laser beam used for the welding process. The welded region (the plastified volume) is extended through the thicknesses of both joining layers.

E. The Proposed Fabrication Method

When the laser beam of sufficient power and wavelength is applied to two thermoplastic pieces, the laser energy is transformed into the heat energy which will melt and join two pieces. In the proposed devices we used the overlap joint technique of welding two Mylar pieces together. Mylar has a high absorption in the ultraviolet region as most other materials and generally low absorbance in the rest of the spectrum except at some peak wavelengths in the infrared regions as we can see from the reported data by DuPont for the optical material properties of Mylar. For example absorbance is 0.11 at 2.45 μm for 23 μm thick Mylar. DuPont does not give the values for optical absorption of Mylar at wavelengths larger than 2.6 μm on the website: http://usa.dupontteijinfilms.com/informationcenter/downloads/Optical_Properties.pdf, although it is shown that the absorbance is greatly reduced when the layer thickness is very small. Transmission at 10.6 μm is larger than 60% for 23 μm thick Mylar. In a paper published in 1953 by Du Pont researchers (Aiiborski and Flierl, 1953), the value for transmission at 10.6 μm is about 85% for 25 μm thick Mylar sheet.

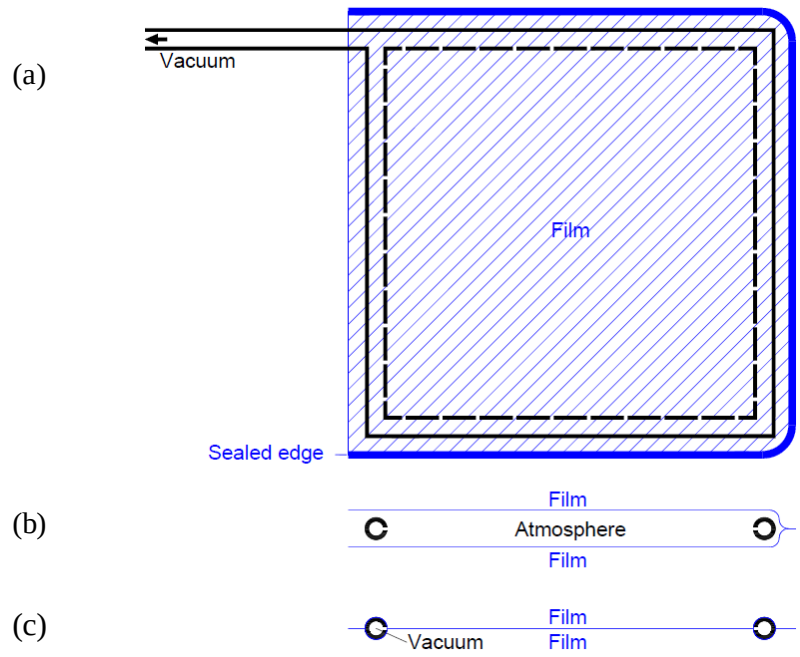

Figure 1. The weld apparatus. (a) Top view of weld apparatus. Vacuum is applied to interior of two sheets of film. Welding, taping, or otherwise clamping three edges of the films improves the vacuum that can be applied to the interior of the films. (b) A cross section view of the weld apparatus before and (c) after vacuum is applied.

The 1.4 μm thin Mylar sheets are coated with thin gold layer (approximately 10 nm). The thermal conductivity of the Mylar is 0.1549 W/m K, and for gold it is 301 W/m K. For gold in the infrared region at 10.6 μm the absorption coefficient is very large and the optical penetration depth is not much larger as the gold layer thickness. Part of the laser energy is absorbed in gold layers (gold layers absorb more laser energy than Mylar layers), and since gold thermal conductivity is high, gold layers have their temperature increased. This also heats Mylar layers and once the melting point of Mylar is reached (254 ºC), Mylar layers in contact are welded together.

The weld apparatus shown in Figure 1 is placed on the platform of the Universal Laser Systems CO_2 laser. The laser beam's path is set with an AutoCAD drawing.

The welding apparatus consists of a closed metal frame constructed from a perforated metal tube. Two pieces of thin thermoplastic material (Mylar sheet) metallized on one side only, are placed below and on top of the metal frame so that the frame is completely surrounded by Mylar sheets as shown in Figure 1. Vacuum is applied between the two Mylar films for a tight and uniform contact with each other so that the welding can be performed. The films are pushed together with a pressure of ~100 kPa (~15 psi) without any solid object contacting the hot plastic during the welding operation. This reduces the amount of heat and time required at the welding temperature.

The laser beam's path is set with an AutoCAD drawing. The order in which welded lines are made can be determined by choosing different layers in AutoCAD drawing, since Universal Laser Systems laser follows the predetermined color-based sequence. Each layer can have different parameter values in situation when different welded line thicknesses are needed. The power used, speed of the laser head and resolution (PPI - number of pulses per unit length) are the parameters that can be changed while using this laser.

The maximum power of the laser is a sum of powers of two laser tubes and nominally it is 100W for this laser. The actual power of tubes is slightly larger than 50W for each tube, and it is not entirely constant during the laser operation, however those small fluctuations did not make any visible influence on the welding, so they were not taken into account.

The PPI is a number which determines how many pulses per inch are made by the laser. Each laser pulse after interaction with the Mylar makes a welded spot, which diameter, shape and weld quality depend on focusing parameters if other parameters are held constant (power,

speed). PPI is set to the highest value (1000) in order to avoid any gaps in welded lines, and to minimize the wave looking edges of the welded lines. Weld lines actually consist of many overlapping welded spots.

Speed of the laser head is also one of the parameters to use. Experimentally it was found that for the used laser system speed changes in percentages is very linear in the range from 1% to 80%. For the experiments on welding the speed used was around 10% which corresponds to ~6.1 cm/s. The optical parts of the laser also have a very important role in determining the best parameters set. The High Power Density Focusing Optics 2" lens (HPDFO) was used to focus the laser beam after it leaves the laser tubes and get deflected by two mirrors in order to direct the laser beam at a right angle toward the working area. Assuming that optical parts (window, mirrors and lenses) are in good condition, the HPDFO lens should focus the laser beam of given power to a minimum spot of 25 μm in diameter. This is theoretically the smallest possible welded line thickness for this lens and laser system. In experiments it was not possible to reach such small weld line widths. When focusing the beam directly to the top Mylar surface, the power density is too high and causes the damage of the polyester material. Reducing the power did not produce a good weld line. Therefore, in order to avoid focusing on a very small area and to obtain reliable weld lines, the focusing was done above the Mylar sheet surface.

A set of experiments were conducted to find the best laser parameters. The power used in most experiments was 3.5 W. This was achieved either as a 3.5% with both laser tubes running on, or as a 7% when only the top laser tube (50W) was connected. The PPI was always set to 1000.

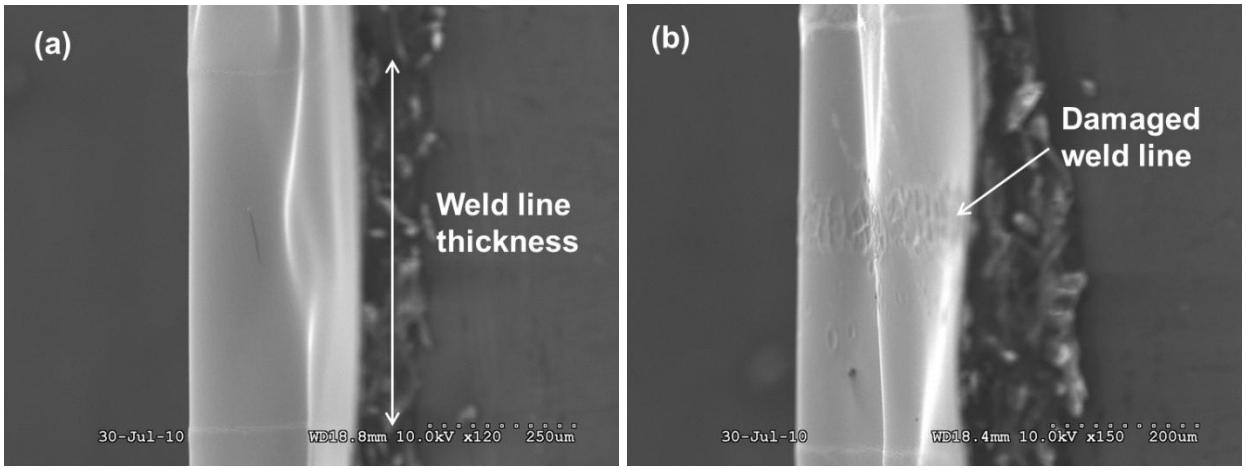

Figure 2. SEM image of the weld line. (a) Weld line is ~0.6 mm wide. (b) Weld line with damage features in its center.

The focusing length determines the welded line thickness. The weld line thickness as thin as 90 μm was obtained, but this result was not repeatable in experiments. The wider weld lines are obtained if Mylar is put further out of focus. Repeatable results with very few damaged devices were obtained when welded line thickness was chosen to 0.5 mm to 1 mm. The weld line thickness was not critical for the microvalve channels since the design did not include any channel bending. However for mixers the wider weld line limits the channel dimensions for proposed micromixers. A scanning electron microscope (SEM) image of a 0.6 mm wide weld line is shown in Figure 2a. Figure 2b shows that in the center of the weld line where the power density was the highest, the surface of the Mylar film was partially damaged.

Welded lines are examined non-destructively by visual test, using the microscope and checking to see if on both sides of the sample the line is well defined and without gaps. It was noticed that when Mylar sheets were not in close contact to each other, the line thickness and quality may differ from the side exposed directly to the laser beam to the other (lower) side. If

the gap was too large, the lower part will not be welded to the top Mylar sheet. Another way of examining the welded line is destructive, by burst pressure test (Russek et al., 2003).

Gaps between the Mylar sheets can cause the voids in the welded lines. In our case gaps are due to bad clamping. This bad clamping occurs when Mylar sheets are not stretched perfectly across the vacuum tool, i.e. Mylar sheets are being pulled more toward one side, and wrinkles appear. If the wrinkles are smaller, it shows that most weld lines are being quite strong and without voids, since smaller gaps are bypassed by melting films together. To make stretching of Mylar sheets better, another vacuum tool was designed. It involves two metal clamps, magnetized sheets that provide paths for air vacuuming from all sides of the stretched Mylar sheet while being in close contact with Mylar, and metal pins that keep the Mylar sheets flat. However this design requires more time to mount and stretch Mylar sheets, and more materials are wasted then in the first design.

The following two chapters describe the microfluidic devices fabricated using the proposed welding technique of thin polyester sheets.

II. MICROVALVE

A. Introduction

The microvalve is an important microfluidic device and a great deal of research is focused on different designs and fabrication techniques. Microvalve is considered to be active if an external force is used for its operation, and passive if that is not the case. There are many active microvalve types where different kinds of externally applied energy are used, such as electromagnetic, magnetic, piezoelectric, electrostatic, thermo-pneumatic, etc. (Kovacs, 1998; Oh and Ahn, 2006). Of those, the electrostatic energy is very attractive because of its quick response time, easy implementation on a chip to connect the device to integrated circuit for operation control or to the controls outside of fluidic chip, and minimal power consumption.

The electrostatic force depends inversely on the distance between the electrodes – when all other parameters are equal, the electrostatic force will be much stronger for smaller distance between the electrodes. The smaller distance between electrodes would require smaller applied voltage which is desirable in many applications, especially for the battery operated devices. Different designs of an electrostatically operated devices where electrodes are separated by only a few microns, thus exploiting the large electrostatic force and relatively small voltage for closing the gap between the parallel electrodes have been reported, for example (Schaible et al., 2001; Xie et al., 2003; Yang et al., 2004b; Yoshida et al., 2010; Messner et al., 2006; Dubois et al., 2001).

In some situations a larger fluid flow is needed or larger stroke of the valve. This can generally be achieved if the electrodes are separated over a larger distance. To avoid very large operating voltages, so-called electrostatic zipping (Legtenberg et al., 1997) can be used, where

the distance between the electrodes is not uniform, but very small at one (or both) sides. At the region where the electrodes are very near each other, the electrostatic force is large, and movable electrode is pulled a little bit toward the other, making the adjacent parts of the electrodes closer to each other. The process continues until the electrodes are fully touching, and the required voltage is smaller than if the electrodes were at larger separation and parallel to each other. For this to be possible, one of the two electrodes (or both) has to be flexible or compliant. The microvalves utilizing this effect are reported by Sato and Shikida (Sato and Shikida, 1994; Shikida et al., 1994), where conductive S-bended elastic film between two parallel electrodes can have 2 mm large stroke. Other microvalves use flexible membranes (Van der Wijngaart et al., 2002; Huff et al., 1990; Yobas et al., 2001; Yobas et al., 2003; Goll et al., 1997; Cabuz et al., 2001; Anjewierden et al., 2012), electrostatically actuated cantilevers to close or open the valve (Ohnstein et al., 1990; Haji-Babaei et al., 1997), T-shaped bridges where the third non-fixed beam is close to the bottom electrode (Dubois et al., 2001), or for example flexible electrode utilized by liquid metal in a closed PDMS channel (Zhang et al, 2009).

The electrostatic microvalve described in this work also uses the electrostatic zipping. The principle of the operation is shown in Figure 3. The top and bottom Au film electrodes are located on the opposite sides of the compliant cylindrical channel. Near the edges electrodes are separated only by the channel material thickness, and electrostatic force is strongest. The zipping effect can be used here without any additional movable parts (membranes, cantilevers or films), since closing the electrodes at the same time closes the channel.

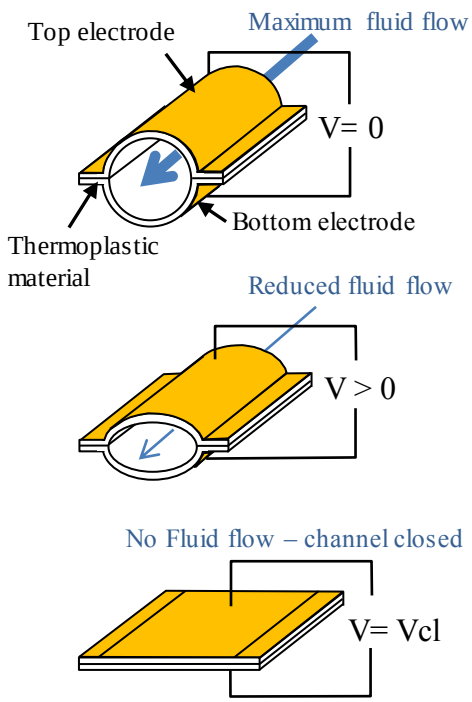

Figure 3. Electrostatically actuated microvalve. (a) When not actuated, channel is open for fluid flow; (b) Applied voltage V > 0 reduces the fluid flow through the valve; (c) Applied voltage V=Vcl closes the channel. (Drawings are not to scale.)

The proposed microvalve is an electrostatically operated normally opened microvalve for gas flow control. The valve is made of thermoplastic materials and uses a new fabrication method. The voltage required to close the 0.9 mm wide microvalve was ~350 V for fluid (air) pressure ~1kPa. A new technique (Feinerman, 2006) has been developed to fabricate valves (Dankovic and Feinerman, 2012), micromixer (Dankovic and Feinerman, 2010; Paya et al., 2008) and other microfluidic structures, by patterned welding of compliant thermoplastic films using Universal Laser System CO_2 laser. The normally opened valve is electrostatically actuated by applying the voltage on its metalized thermoplastic surfaces. There is no movable membrane or cantilever which closes the fluid path as reported in many other electrostatic microvalves. The

walls of the channel collapse toward each other when sufficient voltage is applied, thus effectively closing the fluid path. The material used is 1.4 μm thick Mylar™ sheets (DuPont) coated on one side with ~10 nm of gold.

B. Previous Work

Many researchers mention the valve reported by Terry et al. as one of the first reported microvalves (Terry et al., 1979). They fabricated the microvalve as a part of the gas chromatographic air analyzer (GC). The GC was manufactures on 2" silicon wafer and consisted on a microcvalve, spiral shaped capillary column and thermal conductivity detector. The role of the microvalve was to allow a very small amount (in the order on nanoliters) of the sample gas into the capillary column and at certain time intervals. The inlet and orifice of the microvalve were made by KOH etching through the silicon wafer (the same one that on the other side has manufactured spiral column and detector). The nickel diaphragm and solenoid body and plunger are attached on top and they control the operation of the microvalve and therefore the injection of sample gas into the column. The diameter of proposed valve was 3mm

Sato and Shikida described the electrostatic valve where between two electrodes the flexible movable sheet of metal was placed, which was alternately attracted to each electrode, and in such a way opened or closed the outlet of the valve (Sato and Shikida, 1994; Shikida et al., 1994). The proposed valve was intended for the use in Molecular Beam Epitaxy (MBE) systems where working gases are induced and there is a need for a very responsive valve to enable small amounts of gasses in the chamber for growing thin layers. Small mass of the moving part contributes greatly to the fast response time of the valve.

Goll et al. proposed electrostatic valve made of two molded conductive polymer parts and movable membranes between them (Goll et al., 1997). The membrane had a golden layer sandwiched between polyimide layers. Membrane opens or closes the inlet and outlet, depending on the applied voltage between upper and lower polymer parts (electrodes).

Ohnstein et al. invented a microvalve built on only one silicon wafer (as opposed to many proposed designs where few silicon or Pyrex wafers were bonded together to form the device) (Ohnstein et al., 1990). They used surface micromachining techniques to construct the cantilever which when electrostatically controlled, opened or closed the fluid flow path. As many other silicon made microfluidic devices, there was a need to implement a filter for the gas entering the microvalve so that any particle present in the gas would not affect the performance of the device. The authors also measured the holdback pressure of the valve. When the valve was closed they increased gradually the incoming pressure until the valve was opened again. This type of failure was not catastrophic and the valve would resume its operation when the pressure was reduced. They also observed the hysteresis in flow when applied voltage was increased and decreased, which they speculated as a consequence of the coarse measurements.

Huff et al. fabricated the silicon pressure balanced microvalve by bonding three micromachined silicon wafers to form inlet and outlet, moving part of the valve and a sealed cavity below it (Huff et al., 1990). The valve was electrostatically actuated, and conducting layers were formed by doping n- and p-type silicon wafers during the fabrication, as opposed to other designs where metal sheets or evaporated and patterned metal layers were used. The intention of the authors was to use the shape of the movable part to allow the incoming fluid to make pressure on both base of the moving mass on top of the sealed cavity (and both electrodes) and upper thin layer which closes the outlet. In such a way the applied voltage needed for

electrostatically moving upper electrode (and movable mass) toward the bottom electrode would be reduced. The reported voltage to open the valve was less the 350V which corresponds to the calculated values in the paper (328.4V). However the test results were not available at that time.

Teymoori and Abbaspour-Sani designed a peristaltic micropump which can be suitable for medical applications such as drug delivery because of its small size (7mm x 4mm x 1mm), use of drug compatible materials (silicon, glass, gold, silicon dioxide and Si_3N_4) and the flow rate that is useful for drug delivery systems (Teymoori and Abbaspour-Sani, 2005). The pump consisted of three active electrostatically actuated microvalves. The electrical connections are not in the contact with drug (fluid) and there is no electrolysis of the drug. To operate the micropump using lower voltages, authors propose reducing the spring constant of the membranes, and that was achieved by increasing the membranes degree of freedom – they were fixed on two edges and semi-free on other two edges. Their simulation results showed that threshold voltage was 18.5 V, and the appropriate actuation voltage was suggested to be 23V.

Yobas et al. proposed an electrostatic microvalve with compliant membrane and intended to use such microvalve for pneumatic tactile display (Yobas et al., 2001). The device was fabricated by bonding together two silicon wafers, previously processed separately using bulk micromachining techniques. The advantage of this microvalve the authors contribute to the absence of any initial air gap between the electrodes. Their results with different orifice dimensions show that larger orifice would need smaller applied voltage to close the valve electrostatically (microvalve with 200 μm orifice was closed using 70V with flow rate 80mL/min and differential pressure 18 kPa).

Yobas et al. made a new microvalve for the possible use in pneumatic refreshable Braille display systems (Yobas et al., 2003). This microvalve was fabricated using one silicon wafer and

surface and bulk micromachining techniques to deposit and pattern nitride and polysilicon layers, and to etch the silicon bulk to form an orifice. Nitride layer serves as a dielectric between conducting silicon wafer and polysilicon part. Polysilicon layer is patterned to have a circular rim from which number of beams collects toward the central circular plate. The size of the plate is something larger than the size of the orifice and when the voltage is applied between the electrodes, the plate closes the orifice and stops the flow. They explored the influence of orifice size, number of beams, length of beams and beam profile to the differential pressure, actuation voltage and leakage flow rate. They were able to fabricate a large set of valves, and very good results (68V actuation voltage at 82.7kPa) were obtained for 70 μm x 70 μm orifice, 20 beams and 665 μm beam length. The noticed problems were appearance of the in-use sticking of the polysilicon to nitride layer for valves with longer beams, and fractures of the beams when there was a fast change of the voltage.

Pitchaimani et al. fabricated thermally operated microvalve using plastic materials and operated using Printed Circuit Board (PCB) circuit connected to a battery or a computer (Pitchaimani et al., 2009). Their goal was to reduce the total size of the valve and power accessories to get a portable device, as opposed to few previously mentioned pneumatically operated microvalves. The valve consists of 4 layers (channel layer, membrane, cavity layer and heater layer). The materials used were cyclic olefin copolymer (COC) for all layers except the membrane where polyethylene terephthalate (PET) film was used. The heater was a gold resistor evaporated and then patterned on the heater layer. It does not come into contact with the channel and since there is no problem with clogging the channel solvent was used to bond it to the cavity layer. The cavity volume has to be properly designed to match the volume of the channel segment above. The channel and the cavity are separated by thin PET film which was laminated

to both layers and serves to protect the channel from the cavity fluid, and to expand properly when the cavity fluid is heated and close the valve. The temperature can be precisely controlled by applying a voltage across the resistor and controlling the power of the heater in the heater layer. The valve response time was power dependent, and was somewhat large at powers when the valve was first actuated, but can be reduced if power is enhanced. This however has a limit depending on the properties of the fluid that goes through the channel and thermal properties of the PET film, and it was found that powers larger than 80mW should not be used for this device.

Lee et al. proposed polyimide microvalve made of several layers of polyimide as a cantilever on top of the hole in the silicon wafer (Lee et al., 1996). The valve was electrostatically actuated. Simulations predicted that 50 V applied voltage can sustain the pressure of 130 MPa, however their experiment showed that only 24 kPa was sustained by 55 V. Device used low power (100 mW) and can be used up to 400 C. The problem encountered was the charge build-up in the dielectric (nitride) layer.

Yuen et al. proposed the microvalves made of Plexiglas (Yuen et al., 2000). They used computer numerical control (CNC) machine to drill narrow channels (the minimum channel width depending on CNC tools) of desired depth on one Plexiglas piece. Inlet and outlet channels were brought near each other below the valve closing system constructed in the upper Plexiglas part. The plastic membrane was used to close the channel when valve closing system was pushed toward the channels. The authors investigated different inlet and outlet geometries and membrane materials. For each of the geometries experiments were performed to find the maximum pressure required to open the microvalve. For the incoming flow rate equal 80 μl/min, and given geometries, those pressures were between 60-140 psi (413-965 kPa).

Schomburg et al. describes briefly few microfluidic devices manufactured using the AMANDA (German acronym for Abforming, Oberflachenmikromechanik und Membranubertragung - surface micromachining, molding, and diaphragm transfer) process developed in Karlsruhe Research Center in Germany (Schomburg et al., 1998). The process involves manufacturing of the membrane using standard surface micromachining techniques, and then inserting the membrane between two polymer parts. One such device was the electrostatic valve reported by Goll in 1997. The advantage of this process is the low cost involved, especially because devices can be batch fabricated. For other device fabricated using this process (Goll et al., 1996), the main source of failure was the appearance of the cracks on the membrane surface.

Fahrenberg et al. reported a microvalve made by hot embossing the two microvalve parts: flow element and actuator element (Fahrenberg et al., 1995). The mold inserts were made of brass by micro milling. The membrane element is made of polyimide on which the metal resistive heaters were sputtered and patterned. After the adhesion to the actuator element, the silicon wafer (on which previously the polyimide membrane was made) is separated from the structure. This was enabled by sputtering the thin gold layer on top of the silicon wafer before the fabrication of the polyimide layer. When assembled, the membranes were enclosed on top of the small chambers in the actuator element. To close the microvalve, the resistive heater heats the chamber and thus increases the pressure within the chamber. The membranes were flattened and the outlets were closed.

Shao et al. fabricated polymer piezo microvalve using AMANDA based fabrication process (Shao et al., 2004). Two housing parts are made of PMMA by milling although authors suggest parts can be made either by hot embossing or injection molding. The polyimide membrane was glued by adhesive to the lower housing part except at the region between inlet and outlet. The

piezo actuator is mounted on the upper housing part and space between actuator and membrane filled with silicone. Its nonexpendable property leads to deflecting membrane upwards (valve opened) or downwards (valve closed) depending on piezo actuation. The experiments showed that at pressure difference of 50 kPa over the valve, the valve was closed at 200V and can be opened again when voltage decreases to 100V. The maximum flow rate was ~70 ml/min at ~370V. The response time was measured to be 0.7 ms. The fabricated microvalve had a dead volume of 6nl.

Pattanakul et al. proposed fabrication process for insulator/metal bimorph cantilever structures for electrostatic microvalves, as a low cost alternative to previously reported SiO_2/Cr structures (Pattanakul et al., 2006). Their material of choice was negative photoresist SU-8 covered with thin layers of Cr, Cu and Ni. The structure when released from the substrate (by removing the sacrificial layer) curled away from the substrate as predicted but the radius of curvature was larger than predicted.

Kim et al. reported an electrostatically activated peristaltic micropump consisting of multiple stages where each stage has inlet valve, pump and outlet (exit) valve (Kim et al., 2007). Using bulk micromachining techniques they fabricated chambers for the inlet and exit valves and pumps and released the buckled electrodes. The parylene membrane is sandwiched between two previously made wafers with buckled electrodes and wafers were bonded together. Pumps were fabricated with different number of stages. The achieved pressure difference was 17.5 kPa, air flow rate 4 ml/min and used power only 57 mW. The experiments showed that pump achieved highest flow rates around 15 kHz, as well as the highest pressure difference.

Kim and Najafi fabricated hydraulic microvalve electrostatically operated (Kim and Najafi, 2008). The glass housing has inlet and two outlets, and contains flexible structure made of

parylene and filled with deionized water (DI). Pairs of metal electrodes are on top and bottom surface of the flexible structure. When voltage is applied between one electrode pair, electrode collapse toward each other and the liquid is squeezed out toward the other electrode pair thus enhancing the distance between them and closing the outlet. The valve showed gas conductance of 2.03 ml/min/kPa, and was able to operate against 50kPa backpressure.

Yang et al. proposed and fabricated the electrostatic microvalve able to operate at high temperatures (400 C) and at high pressure of 0.9 MPa (Yang et al., 2004b). The valve was intended to be made of SiC, and be an integrated part of the microengines using gas as a fuel. The desired total flow rate (45 ml/min at 0.9MPa) and power consumption for the microengine valve system were achieved by a set of twenty identical microvalves. The prototype valves were made of silicon on insulator (SOI) wafers, using standard bulk and surface microfabrication techniques. After processing, the set of three wafers (two SOI wafers and one double sided polished) were fusion bonded to form microvalves. Applying the voltage will cause boss part to move toward the top electrode and thus open the valve, for example it was needed to apply 136 V to open the valve when the pressure difference was 0.9 MPa. For the closed valve the leak detected by helium leak detector at 0.17 MPa was 6 μl/min.

Cabuz investigated the failure types that occur in cantilever type micromachined valve, which is electrostatically operated and referred as a touch mode electrostatic actuator (TMEA) (Cabuz, 1999; Cabuz et al., 2000). It was found that device behaves differently depending on the type of driving used, alternating current (AC) or direct current (DC). Humidity has a large effect on the valve operation, for both AC and DC applied voltages, although the dominant failures are different in those two cases. For DC driving, the humidity above 30% contributes to problems in closing the valve at the predicted voltage levels (needed voltages are higher each time the valve

is closed, and larger then theoretically expected), while operation in dry or nitrogen environment contributes to permanent stiction problems. For AC operation when the humidity was above 55% it was noticed that valves were not closing even for very large applied voltage levels. On the other hand, dry air or nitrogen environment helped to reduce stiction problems. since the hydrophilic surfaces are attracting the water and forming the water layer in humid environments, the hydrophobic coatings were applied and devices were tested for both AC and DC driving and at different humidity levels. The experiments showed that achieved electrostatic pressure (measured as a back pressure at which the valve was opened) was not reduced at higher humidity levels when hydrophobic coatings were applied.

Cabuz et al. present a dual diaphragm valve electrostatically operated (Cabuz et al., 2001). The valve body is made of plastic material where specific plastic can be chosen depending on intended application. The electrodes are made by depositing the material on plastic and then depositing the dielectric protection over the metal layers. Two diaphragms are made of Kapton which also has metalized surfaces which are protected by a cast dielectric layer. The valve has three different modes of operation. Moving one, the other or both diaphragms toward the inlet or outlet in such precisely defined steps, the valve performs the pumping of the fluid from inlet to outlet. The voltages used in experiments are up to 200 V, and for 200V the valve can operate at frequencies as high as 95 Hz.

Huff and Schmidt made a microvalve that can be operated both pneumatically and electrostatically (Huff and Schmidt, 1992). The valve is made of three silicon wafers bonded successively and using standard micromachining techniques for shaping the silicon wafers as designed, and one glass wafer with designed metal pattern and holes for inlets and outlets. The valve has a plunger (made of the second and third silicon wafers) that closes or opens the valve

depending on the applied pressure through the actuation port, thus allowing or blocking the fluid flow. The electrostatic actuation is enabled by patterning the metal layers deposited on the bottom silicon wafer and glass wafer. The obtained ration of fluid flow in on and off state was larger than 300 when constant differential pressure of 35 psi was applied between inlet and outlet, and pneumatic pressure was 5 psi.

Messner et al. reported on 3-way silicon microvalve that complies with the industry standards for pneumatic applications (Mesner et al., 2003; Messner et al., 2006). The valve was fabricated by bonding together three silicon wafers (one for outlet and exhaust, one for valve plate and top one for inlet port), and after cutting into separate valves, packaged using ceramic and plastic packaging as well as contact pins and electronic circuit to convert 3V incoming voltage into 200V needed for the valve operation. The valve operates in the normally closed state, and applied voltage will electrostatically open the valve inlet and at the same time close the exhaust outlet. Switching voltage depends on the distance between the electrodes and on the applied pressure – as pressure is increased the switching voltage is lowered. The hysteresis exists between voltage needed to open the valve and the voltage needed to close it back to its normal state. When the valve is opened, the flow rate can be as high as 475 sccm for applied pressure of 6 bar. The leak for the same pressure is below 1sccm, and for the smaller pressures it is somewhat larger since larger pressure helps to press the valve plate tighter to the exhaust outlet. The response time of the valve is ~0.5 ms.

Barth describes four different types of silicon microvalves and compares few of their parameters such as pressure, used power, time response, thermal resistivity and flow rate (Barth, 1995). Valves operate using technologies such as sealed capsule expansion, shape memory

alloys, Ni/Si bimetal and Al/Si bimetal. None of these valves uses electrostatic actuation for its operation.

Haji-Babaei et al. report on the electrostatically operated silicon microvalve (Haji-Babaei et al., 1997). The valve movable part is the silicon oxide cantilever, with Cr strips on top of the cantilever causing the upward curling in the open state. When voltage is applied between top and bottom electrodes, the cantilever deflects and closes the orifice thus stopping the fluid flow. The experiments show linear dependence of fluid flow versus differential pressure across the valve.

Dubois et al. report on a microvalve that can be used for differential pressures of 200 kPa (Dubois et al., 2001). The valve has a Ti-Si-N bridge on top of the very small orifice (10 μm diameter). The bridge is anchored on both sides and the central part is in the shape of the disk that completely covers the orifice. It is electrostatically actuated. Two designs of the bridge are made, one as described, and the other in T-shape, where the third beam is not anchored. When actuated this beam first get in contact with the lower electrode and thus reduces the actuation voltage for the device to 30V, in comparison with the first design which needed 60V. The device can be operated either as a switch to stop or allow the gas flow, or the flow can be controlled using the pulse width modulation.

Bourouina et al. proposed an electrostatically operated micropump made of three parts using standard micromachining techniques for lithography, etching and bonding silicon and glass parts together (Bourouina et al., 1997). The bottom glass part has one electrode and set of micromachined channels. The silicon part has two membranes – the lower is the upper part of condenser, and the upper membrane serves to open or close the valve. It also contains two holes to allow the fluid flow from inlet to outlet. The top part is made of glass and also has a set of channels and a valve seat. The device simulations show that expected flow rates are very small,

with average fluid velocity in the range of 10-100 nm/min, and device would therefore be suitable for drug delivery applications.

Felton gives an overview of main problems that are preventing microvalves to be easily and widely implemented on a chip (Felton, 2003). Problems listed are material choice of the first microvalve designs (silicon and metals) that proved to be not leak tight; complexity of the design steps if standard micromachining techniques are used; a large pressure that can be present in the device and which may not be possible for some materials to withstand. Few applications are discussed as potentially marketable such as liquid chromatography on a chip (where high pressures can be used especially if device is made of materials such as glass), pressure restrictors (where electroosmotic force is used to transfer liquid from one side of the porous material to the other, while there is no flow in another direction), microball valves (there ball is made inside the UV transparent microchannels by polymerization of the specific regions of the polymer previously brought into the channel), or large scale integration systems (where multiple operations can be performed at the same time and controlled by valve system of control channels above the fluid channels).

Goll et al. report on a bistable microvalve consisting of two chambers (fluid and actuator) separated by a buckled diaphragm, and actuated by a heater in an actuator chamber (Goll et al., 1996). Upper, fluid chamber has inlet and outlet posts. Materials used are PMMA for chambers, and polyimide for a diaphragm. The diaphragm was compressively stressed during the bonding process at higher temperature, and buckles once the temperature is reduced. It has two stable states which can be switched by changing the pressure in the actuator chamber. At the 47 kPa inlet pressure, the flow can be closed by 25 kPa in the actuator chamber. The reported leak of the closed valve is smaller than 1 nl/s.

Li et al. present a fluidic device made of thermoplastic elastomer TPE and using hot embossing technique (Li et al., 2010). Fluidic channels are embossed in Zeonor or TPE (two types of devices), while control channels are embossed in TPE layers in both cases. The peristaltic pump has three valves in parallel controlling the fluid flow below in the fluid channel. The closing and opening of the valves is controlled in order to push the fluid in desired direction. The flow rate depends on applied pressure in control channel, and above certain value (12 psi) does not have any influence, since the maximum deflection of TPE material is reached. The frequency increase leads to higher fluid flow rates, but above 6 Hz no change is noticeable – the material cannot follow the frequency of the valve operations above this value. Maximum flow rate at 5 Hz and 12 psi was ~12 μ l/min.

Feng et al. describe two designs of hydrophobic microvalves (Feng et al., 2003). The first is based on geometrical change, i.e. the width of the hydrophobic channel reduces, and additional pressure would be needed to push the liquid through narrower channel, and it can be used as a stop valve below certain pressure. The other design has hydrophobic section in the otherwise hydrophilic channel, and similarly for liquid to flow across this area additional pressure is needed, as predicted by the given formula.

Yang and Lin present three designs of planar check valves (Yang and Lin, 2007). The movable flap is near or touching the solid flap stopper in all three designs. The valves are made of PDMS using the replica molding technique. Since they have a planar configuration they can be used as a part of the system such as lab on a chip. The experiments showed that flow rate was nonlinear when forward pressure was applied and was up to 4 ml/min for pressures in the range of 25 kPa and more depending on the valve type and geometries. For the valve where the distance between the flap and flap stopper was reduced to zero, the forward flow rate was very

small due to the higher flow resistance. The ratio of forward to reverse flow rate was 10^5 for two of the designs.

Kim and Beebe reported on the normally closed microvalve made of two different polymers (Kim and Beebe, 2007). One (poly isobornyl acrylate, PIBA) is used to fabricate the rigid parts of the valve such as channel walls and valve post, while the other (hydroxyl ethyl methacrylate, HEMA) is used for the compliant pars, i.e. valve head and body. The fabrication process (liquid phase photopolymerization) includes double exposing method for better definition of the channel walls. The compliant part is made in situ by exposing the hydrogel prepolymer mixture. The design of the mask is important since it defines the distance of the valve head to the valve neck. If the distance is too small, the valve body buckles and does not close the valve properly, but if too large it does not reach the valve neck. The valve is intended for relatively small pressures up to 200 kPa. The flow rate measured was in the range of 0.025 ml/s (1.5 ml/min) for the forward flow. For the reverse flow it was observed that in the first use the leak was not measurable, but in the repeated tests the flow rate up up to 0.002 ml/s (0.12 ml/min) was measured. If the device is intended for a disposable use this will not affect the operation. The measured response time was ~0.5 s, and restoration time 0.47 s.

Yildirim and Kulah made an electrostatically actuated microvalve from parylene C on a glass substrate (Yildirim and Kulah, 2011) . Parylene is convenient material to replace PDMS in some applications. It is transparent, biocompatible, and solvent resistant, and has lower permeability than PDMS. The valve is an in-plane valve and therefore applicable for the lab on a chip applications. The valve has a disk shape, where electrodes are metal layers on top and at the bottom of the valve chamber. Only bottom electrode is in contact with the fluid. The top side of the valve chamber is circular diaphragm which deflects toward the bottom when actuation

voltage is applied between two electrodes. Because the parylene is not as compliant as PDMS, it does not collapse in such a way to entirely close the fluid path. The diaphragm blocks the central part of the chamber, but the space near the outer valve radius cannot be blocked completely. Therefore valve is never closed, but the leak flow can be controlled by applying a voltage larger than the pull in voltage. The deflection of the diaphragm depends on the equilibrium between the electrostatic pressure on the diaphragm, fluidic pressure and elastic restoring force. The simulated results for the pull in voltages showed the almost linear dependence on the inlet pressure. Pull in voltage is a linear function of the dielectric constant of the working fluid for values of the dielectric constants larger than ~10, and below 10 there is a nonlinear dependence with minimum pull in for dielectric constant values between 3 and 5. The experiment results show that if DI water was used as a working fluid, the valve diaphragm was not pulled in for voltages up to 100 V, and the bubbling of the water was observed if dc voltage was applied. The valves of larger diameter showed smaller pull in voltage, for example for the valve with 450 microns diaphragm the pull in voltage was 19V for air and 14 V for oil. For the valve with 250 microns diaphragm, the pull in voltage was 65 V for air and 47 V for oil.

Yildirim et al. made a normally closed electrostatically operated microvalve made of parylene on silicon substrate and using standard micromachining techniques (Yildirim et al., 2012). It is intended for low inlet pressures (up to 20 kPa). The valve has two chambers, fluid chamber and actuation chamber. The normally closed operation is enabled by parylene wall which prevents fluid flow from inlet to outlet. Applying the voltage on electrodes will pull the upper electrode down toward the lower one to close the actuation chamber, and at the same time it will open the fluid path. The upper electrode near fluid chamber is coated with parylene and there is no contact of the working fluid and electrodes, and thus the main problem that occurs

with electrostatic devices (electrolysis of the liquid or electrode shielding) is avoided. The dimensions of the diaphragm and position of the parylene circular wall will affect the valve operation. The experiments showed no measurable leakage ratio for pressures less than 20 kPa, and up to 9% leakage ratio for increased pressure of 40 kPa. It was also shown that the leak rate would be smaller if the radius of the parylene semi-circular separation wall was larger. The voltage needed to completely open the valve was 60 V, and pull in voltage at which the actuator chamber starts to close (and fluid flow is enabled) was 47 V.

Xie et al. presented the micro flow controller consisting of microvalve and a flow sensor made of parylene on a silicon substrate in the same fabrication sequence (Xie et al., 2003). The valve is electrostatically actuated, and has a circular parylene membrane which closes the fluid path when voltage is applied. The valve is normally open. The distance between electrodes is ~6 microns (4 microns separation and 1 micron of parylene insulation on each electrode). If DC voltage was applied the pull in voltage was found to be 130V. It was also noticed that required pull in voltage will increase after certain number of actuations to 180V. If AC voltage was used this was not observed and pull in voltage was ± 110V at 10 kHz. The valve could not be used with water as a working fluid because of the electrolysis problem, even with electrically insulated electrodes and with AC voltage. Air and Fluorinert oils could be used. Actuation voltage amplitude was changed from 0 to 220 V (AC at 10 kHz) and the valve was not closed for the increased inlet pressure above 28 kPa. In another test where the modulation width of the signal was changed for the constant voltage amplitude (pulse width modulation, with pulse signal 100 Hz), the valve was closed for pressures up to 21 kPa for all Duty Cycle %. The valve is usable for air flow of few μl/min.

Srikar and Spearing discussed the materials suitable for the electrostatically operated MEMS devices (Srikar and Spearing, 2003). The five material indexes were described and used to plot charts showing different materials commonly used in MEMS. For example the charts show that if we need lower actuation voltage and smaller operation speed polymers can be a good choice. Polymers also can be used for high stroke applications where force of the actuation is small. As for electrical resistivity, doping of polymers enables those materials to cover a broad range of electrical resistivity values for small actuation forces and speed of devices. The work was influenced by Ashby (Ashby, 1999) who made similar charts for different materials used in mechanical designs.

Anjewierden et al. made an electrostatically actuated microvalve made of PMMA (Anjewierden et al., 2012). The CO_2 laser was used for cutting the PMMA for the valve chamber and upper part with inlet and outlet holes, and for engraving the valve chamber. The nonflexible electrode is made of chrome (electron beam physical vapor deposition), and the flexible electrode is a very thin copper foil (10 μm). All parts are connected using the double sided tape. When valve is not actuated, the fluid deflects the copper foil so it touches the bottom of the valve chamber while having the curved shape at the edges. When the voltage is applied on the electrodes, the electrostatic force is the strongest at the edges of the chamber where the distance between two electrodes is the smallest and that part of the foil is the first to be attracted to the other electrode. In such a way even large distance between the valves can be closed with not very high voltages. This situation is convenient when larger fluid flow is needed or larger stroke of the valve. A valve with 58 μm deep cavity and with applied pressure of 40 kPa can be closed when 680 V is applied. The flow rate was ~1 μl/min. The dielectric charging is believed to cause the shift in the closing voltage toward higher values after several valve actuations at different

pressures. This could not be completely avoided when switching the control voltage polarity was used, but is believed that AC voltage can be a better solution (as was shown in other papers).

Gilbert et al. present the three-dimensional model of the coupled electromechanical problem and give results obtained in the CoSolve –EM package developed previously by their group (Gilbert et al., 1996). The results of simulated pull in voltage, release voltage, hysteresis, capacitance or contact force, differ from one-dimensional model and are more accurate since the actual beam deflection is taken into account. They also investigated the effect of beam shape, and found that the beam with the narrow flap (where flap reaches the ground electrode first) has smaller pull in voltage, as well as smaller release voltage than the regular beam.

Rollier et al. studied the parallel plate capacitor and pull in voltage for different fluids between the electrodes (Rollier et al., 2006). They developed the analytical model for actuators, and argued that depending on the material (fluid) used the pull in voltage (that in the air occurs after the movable electrode is attracted by one third of the separation) can be avoided and displacement could be controlled accurately by applied voltage. They investigated the three actuator configurations, with different liquids (DI water, isopropyl alcohol, tap water) and air, and showed that theoretical predictions and experimental results were in good agreement. They also pointed out that to be able to work with DI water or tap water, the frequency of AC voltage has to be larger than 1 MHz to avoid the formation of the double charged layers.

Zhang et al. reported on electrostatically actuated microvalve with compliant membrane (Zhang et al., 2009). The valve was made of three layers. The bottom is glass substrate where channels were etched using standard micromachining techniques of etching glass in buffer oxide etch. The bottom electrode is made of aluminum deposited on the glass channels and is not movable. The top layer is made of PDMS using SU-8 mold as a master. The upper electrode is

flexible since it is a liquid metal encapsulated in the upper layer channel, where electrical contact is provided by platinum wire inserted into the channel. The compliant membrane is 2 μm thick PDMS layer which is bonded to the top PDMS layer and also serves as an electrical insulation between two electrodes. Gas flows through the etched channel in the glass substrate. When 200 V are applied to the electrodes, the flexible electrode is pulled toward the bottom one and the channel is closed. The channel shape (trapezoidal) contributes to the closer position of two electrodes near the edges, which helps in minimizing the voltage required to close the channel. They tested the flow of the gas by connecting the outlet of the gas channel into the water container.

Easley and Landers describe two active microvalves which contributed to the increase of research efforts in this area of microfluidics, namely the normally open Quake's valve, and normally closed Mathies' valve (Easley and Landers, 2008). Both were made using PDMS and glass. The Quake's valve can be made in push down configuration, where the actuation pressure is delivered by the channel above the fluidic path, or in push up configuration where very thin layer separates the upper fluidic channel and lower actuation channel. Mathies' valve use micromachined glass layers separated by flexible PDMS membrane. The valve is actuated by applying the vacuum to the upper control channel, which pulls the membrane upwards to open the previously closed fluid channel. The fabrication methods compatible with fabrication of other fluidic devices and channels are encouraged since that would allow valves to be made on the same chip and same process with other devices. However that may become a problem with large number of active valves in the microfluidic system, especially if actuation requires additional tubes and outside equipment. In such cases the passive valves could be a better solution. The

authors also described few methods used to control passive valves, such as fluidic resistance, capillarity, gravity based flow and rectifying fluidic channels.

C. Materials

The first fabricated microvalves were made of materials such as metal, glass or silicon since the technology was highly developed and well known. Recently there has been a large effort among researchers to develop microfluidic devices made of polymer materials. Manufacturing processes for polymer microfluidic devices are simpler and less expensive than those made of standard materials. Another attractive benefit is that for the specific application we can choose the material with desired material properties among large number of available polymer materials (Becker and Locascio, 2002). As discussed in (Srikar and Spearing, 2003), polymers proved to be very good choice for large stroke actuators and low actuation voltage actuators, due to their lower value of Young modulus compared to other materials used for micro devices (such as Si, metals, SiO_2, Si_3N_4, SiC, etc.). Polymers also have lower ratio of Young modulus and density than mentioned MEMS materials ($\sqrt{E/\rho}$ is proportional to the speed of propagation of longitudinal waves), which limits their use for high speed operations. Polymers can have a very large range of electrical resistivity (from conductors to insulators).

Among polymer materials used for fabricating the microvalves are PDMS, SU-8, thermoplastic elastomers (Li et al., 2010; Fiorini et al., 2004; Fiorini et al., 2007; Kim et al., 2011), poly isobornyl acrylate (PIBA), hydroxyl ethyl methacrylate (HEMA) (Kim and Beebe, 2007), parylene C (Xie et al., 2003; Yildirim and Kulah, 2011; Yildirim et al. 2012), poly methyl methacrylate (PMMA) (Anjewierden et al., 2012; Goll et al., 1996), cyclic olefin copolymer (COC), polyester (Pitchaimani et al., 2009), plexiglass (Yuen et al., 2000) and other materials.

Many of those devices require processing in the clean room which can only be economically used for batch processing. There are also proposed technological methods that do not require processing in the clean room, and it becomes affordable to make smaller number of very specific device's design or to change design often and according to specific needs. This would allow the production of microfluidic disposable devices.

Polyester materials show good chemical resistance to weak acids and bases, as well as to alcohols, oils or esters, while for strong acids or bases its chemical resistance is very poor (Becker and Locascio, 2002; Böhm et al., 1999). Polyester material that we used for our device is Mylar (DuPont). Mylar is used for several microfluidic and biomedical devices due to its properties: it is transparent, autofluorescent, and hydrophobic material.

Mylar is used as a part of the device in many reported devices, for example it can be used as surface for in vitro testing of endothelial cell adhesion (Anamelechi et al., 2005), as a movable membrane for the micro pump (Böhm et al., 1999), as part of the T-sensor for capillary electrophoresis-based immunoassays (Hatch et al., 2001), or material to close the channels made of epoxy (Sethu and Mastrangelo, 2004). A number of reported microfluidic devices use lamination of Mylar sheets as a method of manufacturing the device (Neils, 2004; Hsu et al., 2002; Schilling et al., 2002; Levine, L.M.: Developing diagnostic products using polymer laminate technology. Available: http://www.alineinc.com/technical_articles.html, llevine@alineinc.com).

One disadvantage of lamination technique is a difficulty in aligning layers of thin Mylar sheets. The roughness of the microfluidic channel walls due to laser cutting may become an issue for deeper channels, or because of the presence of adhesives between laminated layers. Our proposed technique does not involve an alignment step in device manufacturing. Also there is no

change in surface roughness within the entire microfluidic channel, and no additional materials are involved such as bonding adhesives.

D. Fabrication

The fabrication of the device consists of the following steps: welding of thermoplastic material (1.4 μm thick Mylar films) using welding apparatus and laser power, assembling the device, and welding the assembly to obtain the leak tight contacts and support for the microvalve (Feinerman, 2006).

Our welding apparatus consists of a closed metal frame constructed from a perforated metal tube, and connected to a vacuum pump. Two pieces of thin thermoplastic material (Figure 4a) metallized on one side only (~10 nm of gold), are placed below and on top of the metal frame so that the frame is completely surrounded by Mylar films. The Mylar film is from Knowles Electronics in Itasca, IL. Knowles deposits a gold coating on film they purchase from Steinerfilm in Williamstown, MA. Vacuum is applied between the two Mylar films for a tight and uniform contact with each other so that the welding can be performed (Figure 4b). The gold coated surfaces are on the outer surfaces of the evacuated structure. The films are pushed together with a pressure of ~100 kPa (~15 psi) without any solid object contacting the hot plastic during the welding operation. This reduces the amount of heat and time required at the welding temperature.

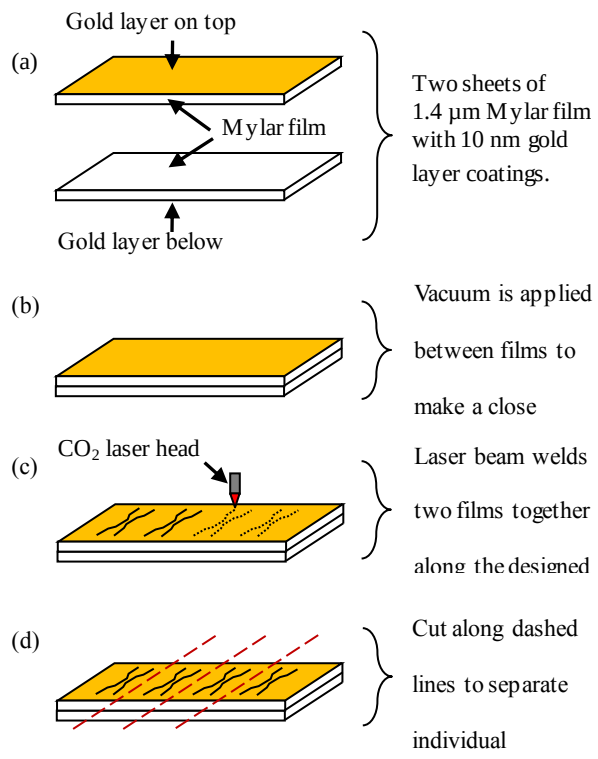

Figure 4. Laser welding of thermoplastic films. (a) Two sheets of Mylar film with metallized layers on opposite sides; (b) vacuum is applied; (c) Laser head follows the computer guided path; (d) individual valves can now be separated. (Drawings are not to scale.)

The whole set-up is placed on the Universal Laser Systems CO_2 laser platform. The laser head follows the path determined by an AutoCAD drawing (Figure 4c). A typical path for a microvalve is in Figure 5. The valve region is the narrow channel between the inlet and outlet regions, and defined by valve width and length, W_{valve} and L_{valve}. Vacuum between the Mylar sheets is maintained throughout the welding process.

The laser power used for welding was 3.5 W (the Universal Laser Systems CO_2 has 100W total power), speed was ~63 - 76 mm/second, and 39 pulses/mm. The focusing was done above the Mylar film surface (approximately 1.5 mm) in order to avoid focusing on a very small area

and burning the polyester material. This produces a maximum spot size of ~0.75mm in diameter. The corresponding welded lines are obtained (Feinerman, 2006). We can choose the width of the weld line by adjusting the focus point further or closer to the film surface. An SEM image of a 0.6 mm wide weld line is shown in Figure 6. In the center of the weld line where the power density was the highest, the surface of the Mylar film was slightly damaged.

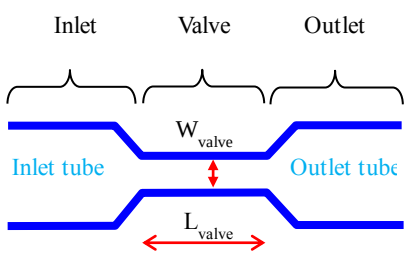

Figure 5. A typical path for a microvalve. The separation in the inlet and outlet regions matches tubing diameter (separation = π*diameter/2).

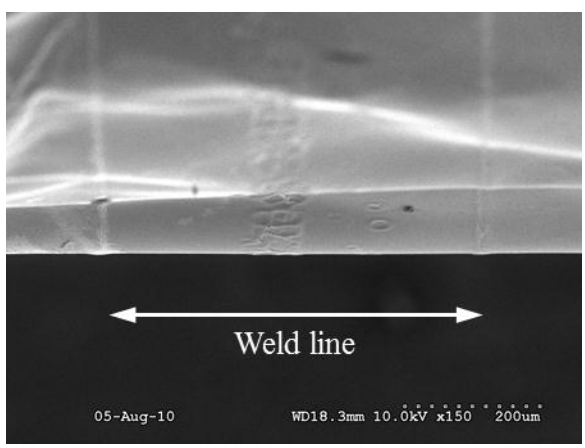

Figure 6. SEM image of the weld line.

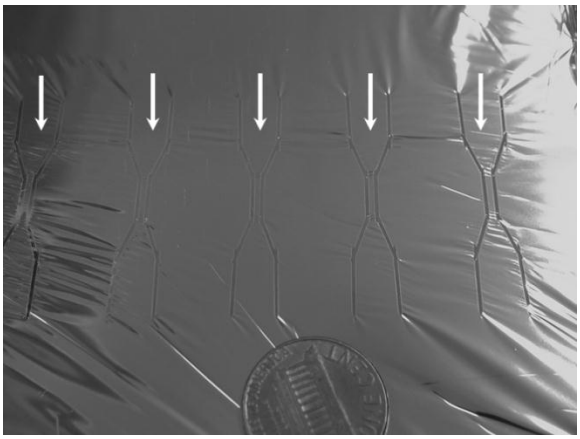

Figure 7. Multiple microvalves can be made in same laser welding step. The weld lines of the five individual channels can be seen on the Mylar surface.

Multiple devices can be welded in the same run, depending on the respective sizes of devices and metal frame for clamping the two Mylar sheets together (Figure 4c and Figure 7). The individual microfluidic devices are separated after the vacuum is released and welded films removed from the weld apparatus (Figure 4d). Linear low-density polyethylene (LLDPE) tubes are inserted into the channel openings with the weld line separation matched to the tube diameter (Figure 8). The Mylar channel and tubes are placed on a thick low-density polyethylene (LDPE) frame to facilitate handling of the microfluidic devices (the frame can be any shape and size). Electrical contacts to each side of the valve are made with conductive thermoplastic material and placed on each metallized Mylar side.

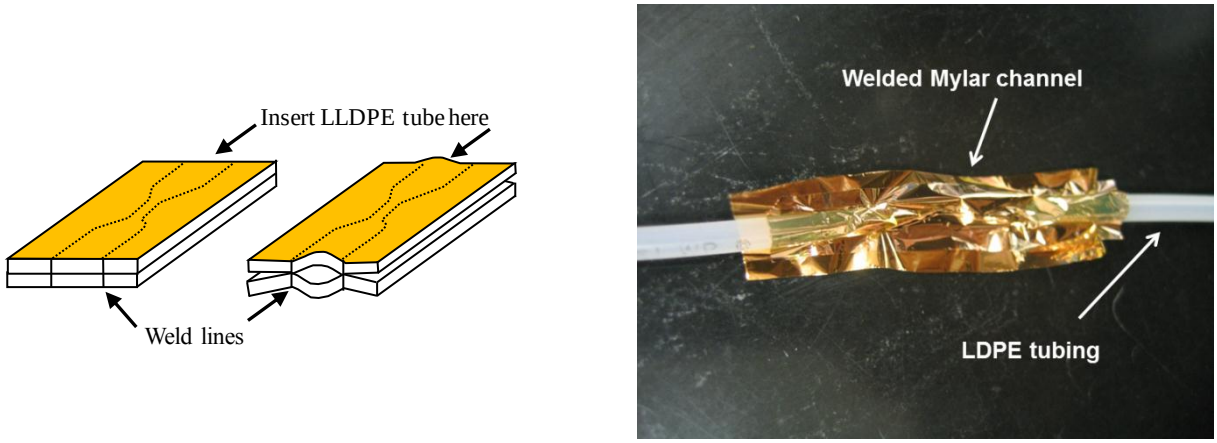

(a) (b)

Figure 8. Electrostatically actuated microvalve. (a) schematic of an individual Mylar valve after welding; (b) LLDPE tubes are inserted in the inlet and outlet regions of individual valves.

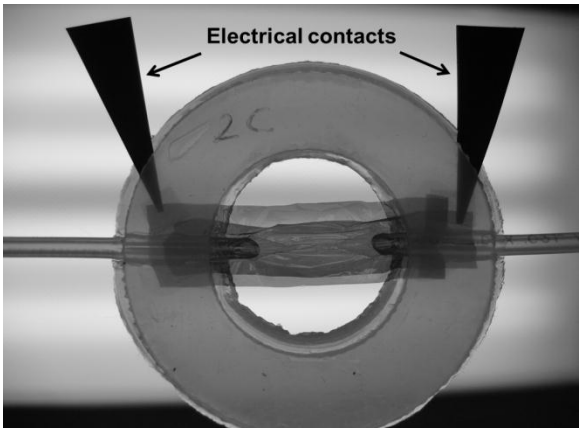

Figure 9. A packaged microvalve after assembly. The LDPE donut provides structural support.

Thin Teflon tubes are inserted into LLDPE tubing to prevent their collapsing while bonding microfluidic devices to the frame. Another piece of thick thermoplastic material of the same shape as the lower one is carefully placed on top and everything is secured between the

aluminum plates to prevent materials shifting while welding. Welding is carried out with sample clamped and at temperature close to melting point of LDPE. The Teflon inserts are removed after the sample cools, and microvalve is ready for testing. A sample microvalve is shown in Figure 9.

E. Theory

As shown in Figure 10, the microvalve width "W_{valve}" is defined by the smallest distance between two welded paths. When the microvalve is filled with a fluid the two sheets of film will separate and the valve will open. The amount the microvalve opens is determined by the pressure difference P_g between the inside (P_c) and the outside (P_o) of the structure and the mechanical characteristics of the thermoplastic film. The capacitance of the closed microvalve is given approximately by the following formula, where W_{valve} is its width, L_{valve} is its length, t_{film} and ε_{film} are the thermoplastic film's thickness and dielectric constant, and ε_o is the permittivity of free space:

$$C_{valve} = \frac{\varepsilon_{film}\, \varepsilon_0\, W_{valve}\, L_{valve}}{2\, t_{film}} \tag{2.1}$$

Assuming that the thermoplastic film doesn't stretch significantly, the maximum opening for the microvalve is if it opens to a circle of diameter:

$$D_{valve} = \frac{2\, W_{valve}}{\pi} \tag{2.2}$$

The cross-sectional area for the microvalve with this diameter is:

$$A_{valve} = \frac{\pi\, D_{valve}^2}{4} = \frac{W_{valve}^2}{\pi} \tag{2.3}$$

The electrostatic energy stored in a closed microvalve is:

$$E_{electrostatic} = \frac{C_{valve}\, \Delta V^2}{2} = \frac{\varepsilon_{film}\, \varepsilon_0\, W_{valve}\, L_{valve}\, \Delta V^2}{4\, t_{film}} \tag{2.4}$$

where ΔV = V1 – V2 is the voltage differential sustained across the closed microvalve. The minimum voltage difference required to close the microvalve can be estimated as follows where z is the direction along the length of the microvalve (L_{valve}).

$$P_g\ A_{valve} = \frac{P_g\ W_{valve}{}^2}{\pi} = -\frac{\partial E_{electrostatic}}{\partial z} = -\frac{\varepsilon_{film}\ \varepsilon_0\ W_{valve}\ \Delta V^2}{4\ t_{film}} \tag{2.5}$$

$$\Delta V = \sqrt{\frac{4\ t_{film}\ W_{valve}\ P_g}{\pi\ \varepsilon_{film}\ \varepsilon_0}} \tag{2.6}$$

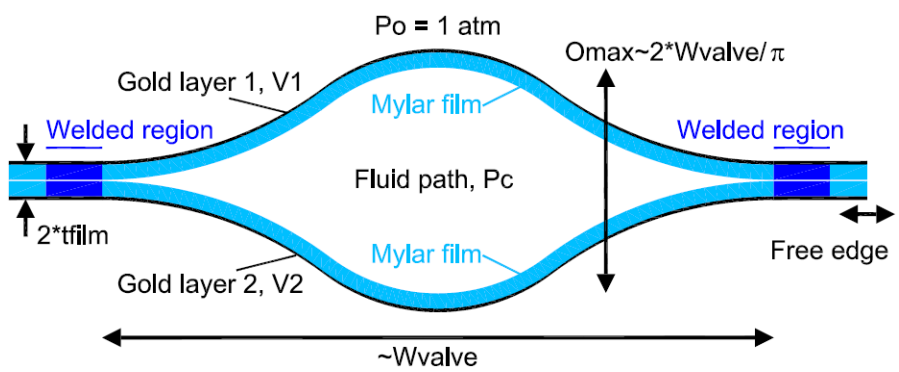

Figure 10. Schematic cross-sectional view of microvalve.

Equation (2.6) is an estimate on the voltage required to close the microvalve, and it doesn't take into account the mechanical forces (deformation and stretching energies of the thermoplastic film) that work to close the structure. These mechanical forces reduce the maximum opening O_{max} of the microvalve to be less than the D_{valve} predicted by equation (2.2). This decreases the

cross-sectional area A_{valve} from the value predicted by equation (2.3) and reduces the voltage required to close the microvalve.

F. Simulation Results

We performed simulations of the structure similar to the valve channel using Coventor™ software for three valve widths (0.1 mm, 0.5 mm, and 1 mm) to investigate the agreement with equation (2.6). The theoretical results according to equation (2.6) are shown in solid lines, and results obtained in Coventor™ simulations in corresponding markers. It is noticeable that there is a large discrepancy between simulated and calculated voltages for 0.1 mm wide valve. The reason for this is that the actual cross sectional area of the small valve channel is much smaller than circular cross section as assumed in equation (2.6) because of the larger stiffness of the small width channels. The elasticity of the valve channel was not taken into account when deriving the equation (2.6). When corresponding adjustments of the valve cross sectional area are taken into account (shown in Figure 11 in dashed black lines) the agreement with Coventor™ results is very good for 0.1 mm valve. For 0.5 mm and 1 mm widths of the valve the mesh used in CoSolve solver was much coarser than for 0.1 mm wide microvalve, which explains the disagreement between Coventor™ and calculated results.

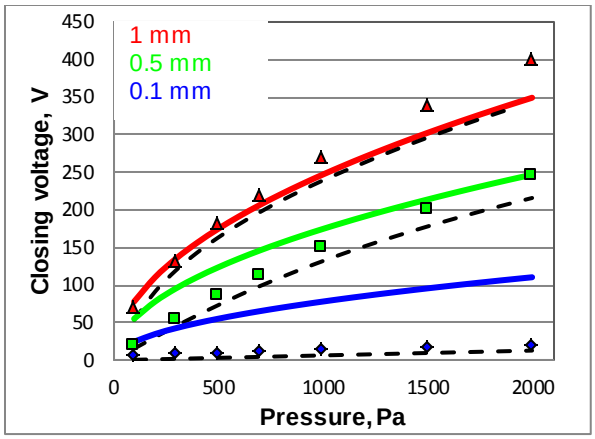

Figure 11. Coventor™ predicted values of closing voltages for different valve widths (0.1 mm – blue rhomboids, 0.5 mm-green squares, and 1mm-red triangles) and applied pressures from 100 Pa to 2000 Pa. Solid lines represent the predicted voltage by equation (2.6), while dashed lines show theoretical prediction when the cross sectional area was adjusted.

To investigate the influence of the valve cross sectional area on closing voltage results, we simulated the maximum opening of valves for a range of applied pressures. The results presented in Figure 12 show that for valves with small widths the maximum opening is much less than predicted by equation (2.2) even when large pressures are applied. As the width approaches the thickness of the valve, the openings becomes practically negligible (on the order of 0.01 μm). The larger width valves open easily and have near maximum cross section of the valve channel. Figure 13 shows the Coventor™ result for 1 mm wide microvalve. Coventor™ software predicts a 272 μm deflection of each surface of a 1 mm wide microvalve that is made from welding two sheets of 1.4 μm thick Mylar film. The total opening would be 544 μm, while equation (2.2) predicts 637 μm. The software assumed a gauge pressure of 1000 Pa.

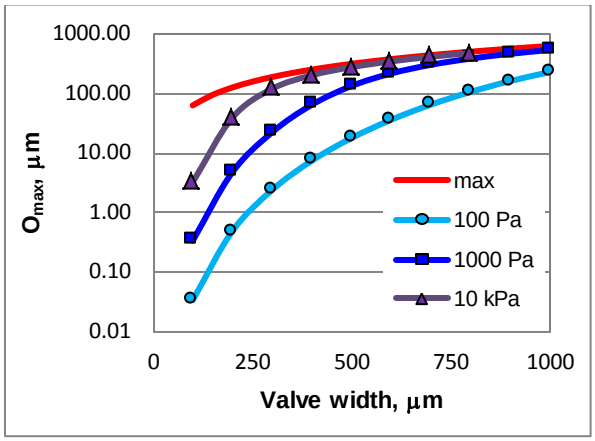

Figure 12. Coventor™ predicted values of maximum opening of the microvalve channels for applied pressures of 100 Pa, 1 kPa and 10 kPa. The red line shows the maximum possible opening (the diameter of the perfect circuit) for each width of the valve.

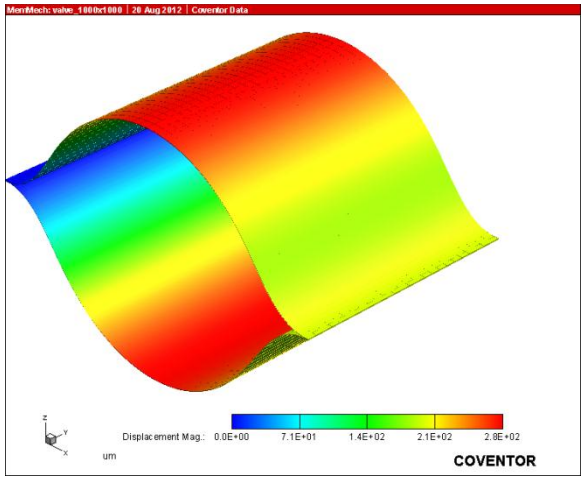

Figure 13. Coventor™ predicts 544 µm total opening for 1 mm valve at gauge pressure of 1kPa.

G. Experimental Results

Experiments were conducted to measure the closing voltage of microvalve and to compare the results with the values predicted by equation (2.6). We tested valves with different widths (0.9 mm, 1 mm) for a range of applied pressure (250 Pa to 2000 Pa). Pressure is applied using Profile Aquarium Air Pump 1000, and measured using the pressure gauge (Ashcroft, Inc., model 1490) at the valve inlet port. The initial air flow rate was controlled by the immersion of the outlet tube below water surface (marked as 'h' in Figure 14a). The air passing through the microvalve exits as air bubbles in a small container filled with water. High DC voltage power supply (Bertan Associates, Inc., model 205B-05R) was used to apply voltage onto electrical contacts on upper and lower metalized surfaces of the microvalve. Closing voltage was recorded as the voltage when no bubbles would appear in the water filled container. Water is saturated with air prior to testing. The experimental set up is shown in Figure 14a.

There is a spread of results obtained for valves of the same size. This is due to non-automated manufacturing process. The actual widths of the valve can vary for each laser run since the films can be at somewhat different distance from the focusing lens. However the main contribution to the variance in results is due to the melting of the LDPE support rings where the melted LDPE material can pull the Mylar film near the LLDPE tubes causing for each valve different stress which will affect the value of the closing voltage.

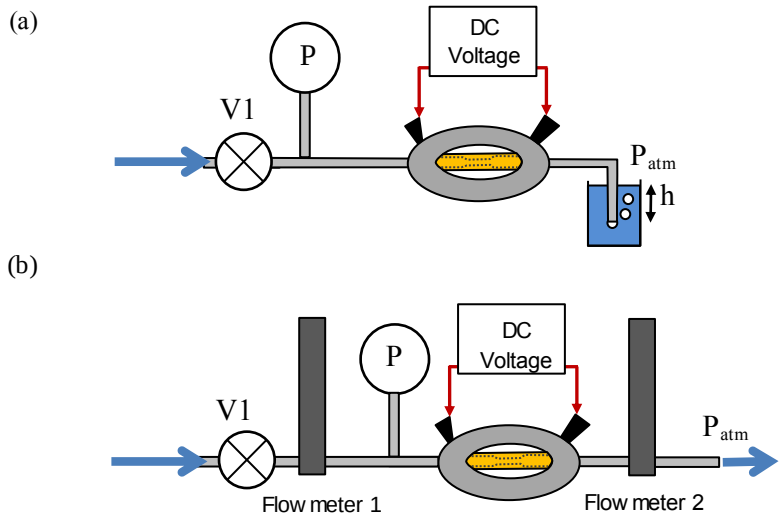

Figure 14. Experimental set up for testing the closing voltages for microvavles. (a) Flow observed as bubbles in a liquid chamber. (b) Flow recorded by two flowmeters.

Multiple experimental data for closing voltage for one 0.9 mm wide microvalve are presented in Figure 15. The solid line on the same figure shows the closing voltages predicted by equation (2.6). Most experimental data for closing voltages fit around the predicted voltage values. We noticed that in repeated experiments with the same valve, different (typically higher) voltage was needed to close the valve. This can be seen in Figure 15. The four consecutive tests of the same 0.9 mm wide valve are performed showing an increase in measured closing voltage. Similar changes in closing voltages were reported for DC voltage actuated electrostatic microvalves made of Parylene C (Xie et al., 2003; Anjewierden et al., 2012; Yildirim et al., 2012) and it is believed that the shift in voltage is due to the dielectric charging of the material. The errors in pressure and voltage measurements also contribute to different response results.

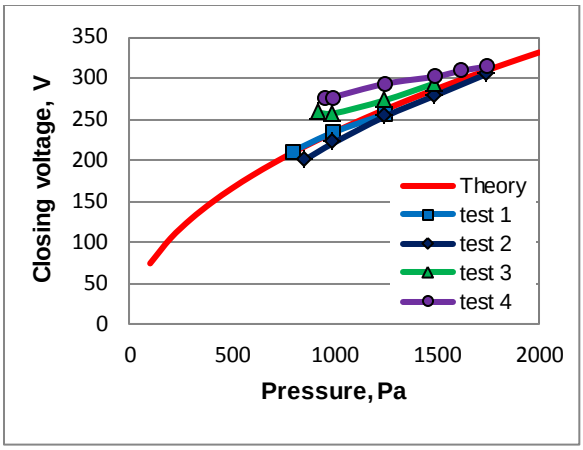

Figure 15. Experimental values of closing voltages for 0.9 mm wide valve.

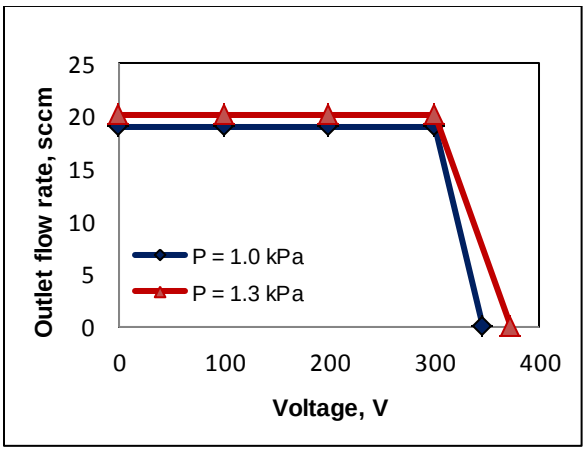

Figure 16. Measured outlet flow rate as a function of applied voltage. The 0.9 mm microvalve is completely closed for applied voltage over 300V and the fluid (air) pressure of 1 kPa.

The similar test is done using the experimental set up as shown in Figure 14b. The air is delivered from the air supply system and the pressure is regulated by valve V1 and measured using the pressure gauge. The air flow rate is measured at the microvalve inlet and outlet ports to investigate leakage. High flow rates were recorded by Gilmont/Cole Parmer GF-5522-2217 rotameters 10-250 sscm ±~5% accuracy. Small range flow rates 1-10 sccm were measured using Omega FMA2701 flowmeters with ±0.1sccm accuracy. High voltage was applied to electrical contacts on upper and lower metalized surfaces of the microvalve. Closing voltage was recorded as the voltage when no flow was detected through the valve. Figure 16 shows the experimentally obtained flow rate change for a 0.9 mm wide microvalve when applied DC voltage is increased. Two data sets are taken, for P = 1 kPa (blue line) and P = 1.3 kPa (red line).

Hysteresis was observed in most experiments when the voltage was reduced back to 0V. Figure 17 shows the measured change of the air flow rate versus applied DC voltage at the valve electrical contacts. For 450 Pa applied air pressure, the voltage needed to close the 1 mm wide valve was 300 V. Reducing the voltage at that point showed that valve stays closed until ~200 V was reached, when the channel is opened and the flow rate increased to its starting value. The hysteresis has been reported in other electrostatically driven microvalves (Messner et al., 2006; Ohnstein et al., 1990; Yildirim and Kulah, 2011).

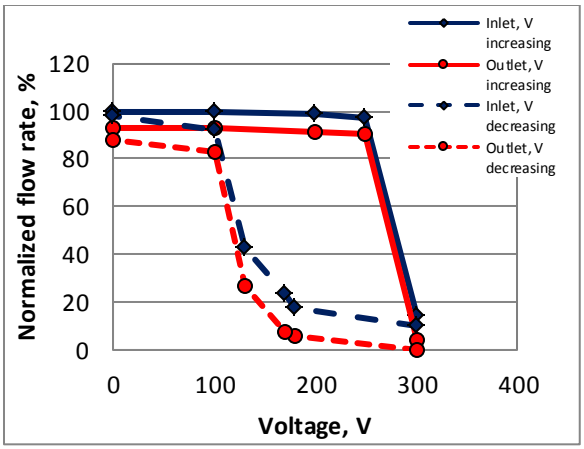

Figure 17. Measured flow rate (normalized to 10 sccm) versus applied closing voltage for a 1 mm wide microvalve and 450 Pa air pressure. Inlet and outlet flow rates are measured as voltage is increased (solid) or decreased (dashed). Difference between blue and red indicates a leak.

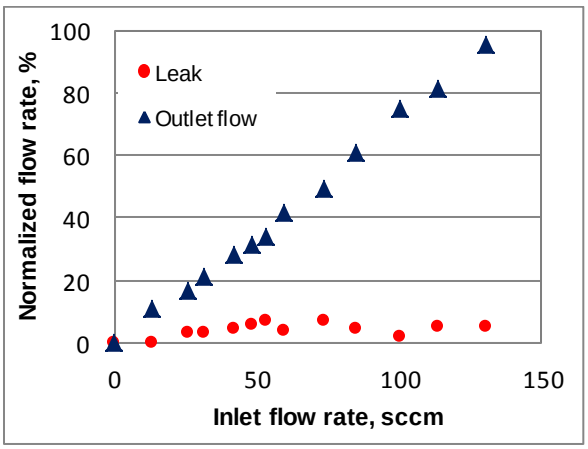

Figure 18. Measured leak as a function of inlet flow rate (range 10-150 sccm) for 1mm wide microvalve. Flow rates are measured with GILMONT flowmeters, max leak rate was 7.14 %.

Experiments were conducted to set an upper bound on microvalve leakage. A controllable air pressure was applied to the inlet, and microvalve was submerged in the container filled with water (previously saturated with air). The opening of the outlet tube was above the water level. The air pressure was then increased gradually until air bubbles start to form anywhere on the microvalve surface in the water. It was observed that when a leak occurs, it is either on the contact between Mylar channel and LDPE rings that provided the structural support for the valve, or within the valve Mylar region. The first one is a dominant reason for a leak, and it is due to the error in manufacturing when LDPE rings were not completely melted around LLDPE tube and Mylar channel. Therefore a small gap between LDPE rings and Mylar would exist and become a leakage point. Leaks occurring at the valve Mylar region were either due to incompletely welded lines, or valves damaged due to the applied pressure.

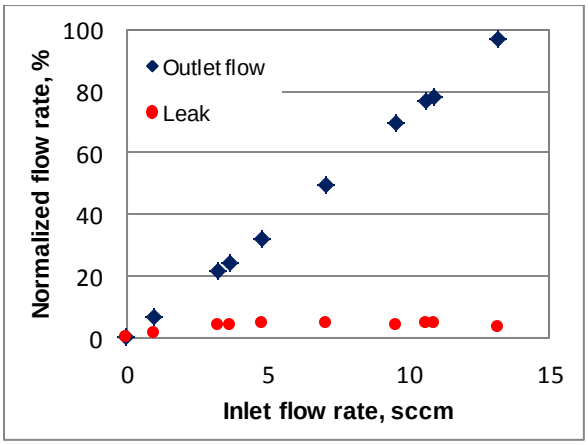

Figure 19. Measured leak as a function of inlet flow rate (range 1-15 sccm) for 1mm wide microvalves. The flow rates are measured using Omega flowmeters, max leak rate was 4.85 %. (Not the same microvalve as in Figure 18.)

The leak was measured using the same experimental set up as in Figure 14b. The air flow rate was controlled using valve V1, and flow rates recorded at the inlet and outlet of the valve. The difference in recorded flow rates is the leak caused by incomplete welding to LDPE support rings, and/or from errors in laser drawn weld lines. The results of leak tests for 1 mm wide valves with relatively good welded support rings and for two different ranges of flow rates are shown in Figures 18 and 19. Measured leak was 0-10% of flow rate.

H. Conclusion

We presented an electrostatically driven normally open microvalve made of thermoplastic materials. A new technique has been developed to make valves and other microfluidic structures by patterned welding of compliant thermoplastic films. Electrical contacts, packaging, and low leakage connections with external tubing to these structures have also been demonstrated. The microvalves are compatible with a wide range of fluids. Equation (2.6) is an estimate on the voltage required to close the microvalve, since it doesn't take into account the mechanical forces (deformation and stretching energies of the thermoplastic film) that work to close the structure. These mechanical forces reduce the maximum opening O_{max} of the microvalve to be less than the D_{valve} predicted by equation (2.2). This decreases the cross-sectional area A_{valve} from the value predicted by equation (2.3) and reduces the voltage required to close the microvalve. The microvalve is limited to actuation voltages less than 600 V because of the breakdown voltage limitation of 1.4 μm thick Mylar film. The pressure range is limited by the value of the closing voltages to few kPa, although the valve can withstand much higher applied pressures (~20 kPa). The operating temperature should be limited to 100 ºC because of the low melting point of the

LLDPE tubing and support rings. The measured leak rate for well manufactured microvalves was less than 10% of the flow rate.

III. MIXERS

A. Introduction and Motivation

A mixer is a microfluidic device that can rapidly and efficiently mix two or more fluids. W. Ehrfeld defined the mixing as follows: "Mixing is a physical process with the goal of achieving a uniform distribution of different components in the mixture, usually within a short period of time" (Ehrfeld et al., 2000). This function is necessary in: chemistry, μTAS systems, DNA sequencing, biochemical analysis and many others. The advantage of having mixer of a smaller size is to use less materials (fluids, reagents) for mixing, and potentially be able to do analysis in shorter time.

Most often we refer to mixer as either active or passive, depending whether they need external actuation for proper operation or not (Nguyen and Wu, 2005; Capretto et al., 2011; Mansur et al., 2008; Nguyen, 2008; Wu and Nguyen, 2009). Active mixers have an important advantage because the mixing length needed to complete the mixing process can be much smaller than for passive mixers because external energy applied to stir the fluid enhances the mixing process. There are many kinds of active mixers depending on the type of external actuation used for mixing process, which can be pressure, temperature, acoustic waves, electrophoresis, electrokinetic, etc. Depending on the applied energy the fluid to be mixed can be subjected to increased temperature or high agitation that can be very damaging if biological samples are involved. Moreover, the fabrication process has to include the connection to external energy suppliers and the experimental set-up may become quite complicated.

Passive mixers are easier to make and they can operate using one of the following: parallel lamination, chaotic advection (Stroock et al., 2002; Mouza et al., 2008; Saatdijian et al., 2012; Li et al., 2012), injection or droplet forming (Song et al., 2003; Song and Ismagilov, 2003; Song et al., 2006; Tice et al., 2003). The mixer designs that we investigated are all passive mixers, although they can be turned into active mixers with bifurcated microvalve technology reported elsewhere (Paya et al, 2008). For passive mixers the most common mechanisms for mixing are diffusion and chaotic advection.

Because of the smaller size of devices and smaller flow rates, the fluid flow in mixers is laminar. Reynolds number Re is defined as:

$$Re = \frac{\rho\, v\, D_h}{\mu} \tag{3.1}$$

where ρ is the density of the fluid, v its velocity, D_h is hydraulic diameter and μ is dynamic viscosity of the fluid. Hydraulic diameter is defined as:

$$D_h = \frac{4\,A}{P} \tag{3.2}$$

where A is the area of the smallest cross section in the channel and P is its perimeter. Reynolds number shows the ratio of inertial and viscous forces acting on the fluid. The turbulent fluid flow is characterized by Reynolds numbers larger than 2300. There is a transition region from laminar to turbulent flow in the Reynolds number region from 1500 to 2300 (Kovacs, 1998). Other authors report various values, for example (Capretto et al., 2011) gives 2500 as the beginning of the turbulent flow. In microfluidics application the channel cross sectional dimensions are small and Reynolds numbers are most often in the range less than 100, which is the laminar flow. In this flow regime two fluids can flow in parallel along the microfluidic channel with mixing occurring only on the interfacial area between two fluids due to the molecular diffusion. Molecular diffusion is a slow process and can take excessively long time on the order of minutes

or even tens of minutes (Nguyen, 2008). Diffusion time t_d is defined as (Falk and Commenge, 2009):

$$t_d = \frac{x^2}{(p+1)(p+3)D} \tag{3.3}$$

Dimension x is the half width of the aggregate. Parameter p depends on the channel shape and for a slab is equal 0, for cylinder p = 1, and for a sphere p = 2. For microfluidic channel with rectangular cross section diffusion time is calculated as:

$$t_d = \frac{x^2}{2D} \tag{3.4}$$

where x is width of the mixing fluid (half-width of the channel for two mixing fluids). D is the diffusion coefficient which depends on the fluid dynamic viscosity μ, and size of the diffusing particles (radius R):

$$D = \frac{k\,T}{6\,\pi\,\mu\,R} \tag{3.5}$$

Small particles has larger coefficient of diffusion, usually in the range 10^{-9} to 10^{-10} m^2/s, but for larger molecules such as most biomolecules this coefficient can be much smaller, in the order of 10^{-13} to 10^{-14} m^2/s, which means that much longer diffusion time is needed for mixing process to complete. Diffusion mixing length, L_d is defined as a length of the microfluidic channel needed for diffusion to complete:

$$L_d = v\,t_d \tag{3.6}$$

Other dimensionless numbers are used in microfluidic, for example Pecklet number Pe is defined as:

$$Pe = \frac{v\,D_h}{D} \tag{3.7}$$

where v its velocity, D_h is hydraulic diameter and D is diffusion coefficient.

When the fluid flow in microchannels is characterized by small Reynolds numbers, the diffusion mixing length can be very large (on the order of meters). The goal of many research projects is to reduce the mixing length to more practical values. Diffusion process is completed when the concentration of all mixing particles or fluids is equal across the cross sectional area of the channel. Therefore to enhance the diffusion mixing we can try to increase the interfacial area between mixing fluids and to try to obtain as thin fluid striations as possible applying designs of the mixer geometries. A large number of designs have been proposed in the literature to reduce the mixing distance between mixing species and therefore reduce the needed mixing time and accordingly the mixing length (as mixing length is directly proportional to mixing time and fluid velocity). Passive mixers use one of the following methods: lamination (parallel or sequential), chaotic advection, injection and droplet (Nguyen and Wu, 2005; Nguyen, 2008; Ottino and Wiggins, 2004; Mansur et al., 2008; Carpetto, 2011; Kovacs, 1998). In this study only lamination and chaotic injections are considered.

Lamination can be parallel and sequential. An example of very simple parallel lamination is a T mixer or Y mixer, where a long channel serves for parallel flow of two fluids delivered through T, Y or arrow shaped inlets. Many papers are reported on those types of mixers, for example: Kamholtz, 1999; Gobby, 2001; Schönfeld et al., 2004; Wong et al., 2004; Tofteberg et al., 2010. Mixing fluids can be delivered through more than one pair of inlets in such a way that they flow next to each other in thinner layers which enables faster diffusion. Examples of this type of parallel lamination can be seen in the following papers: Kamper, 1997; Ehrfeld et al., 1999a; Koch et al., 1999; Lee and Kwon, 2009; Hinsman, 2001. Serial lamination includes splitting and recombining stages and a number of different mixers are reported such as: Munson and Yager, 2004; Lee et al., 2006; Bertsch et al., 2001; Chen and Meiners, 2004.

Advection can also be used to enhance the mixing process. In mixer types described above advection (e.g. fluid mass transport) occurs in the direction of the main channel axes, e.g. in the fluid flow direction. However, if channel is designed in such a way that its geometry encourages the transport in direction other than the main channel axes, the chaotic advection may occur which may lead to formation of the vortices and improving the mixing significantly (Mizuno and Funakoshi, 2002; Wiggins and Ottino, 2004). Many designs are proposed in this category (Kim et al., 2004; Stroock, 2002; Bhagat, 2007; Bhagat, 2008a; Villermaux et al., 2008; Tsai and Wu, 2011, Tsai and Wu, 2012; Li, X.B. et al., 2012). One can change the width of the simple mixer channel to induce the vortices (Gan et al., 2006; Sousa et al., 2012), or place obstacles in the channel for the same effect. Obstacles may be in the form of patterned channel walls, or bottom or top surfaces.

The channel can change its direction from inlet to outlet in the form of a zigzag (Mengeaud et al., 2002; Chung and Shih, 2008), serpentine shape (Groisman and Steinberg, 2001), labyrinth (Li, P. et al., 2012), or use modified Tesla or other structures using Coanda effect (Jeon et al., 2005). All those methods are convenient for planar mixers.

Inducing the three-dimensionality (Yi and Bau, 2003; Liu et al., 2004; Chang and Cho, 2005; Liu et al., 2000; Vijayendran et al., 2003) showed better mixing results in all cases, although the fabrication usually becomes more complicated because of the additional photolithographic processes. Some of the reported works on micromixers are presented below.

B. Previous Work

Jeon et al. described the passive micromixer based on Coanda effect. Mixer was made of PDMS (using the standard technique with SU-8 resist as a mold) and two glass plates (Jeon et al., 2005). The passive mixers are useful for biological applications, when temperature of the mixing fluids should not be increased as often happens when active mixers are used. At the inlet the combined fluid flow is brought from two main inlets. The mixer chamber is divided into two main paths which recombine at the outlet. For each of these main channels there is a side channel of smaller cross sectional area which serves for the recycled fluid. Both experiments and simulations showed that there is a critical Reynolds number when the pressure at the inlet of the side channel becomes the same as at its outlet, and above the critical Re the fluid starts to flow in the reverse direction through the side channel, i.e. toward the inlet. The fluid emerging from the smaller channel back into the main channel can behave as a jet and cause the circular flows of the fluid which enhances the mixing. The mixing was better for higher Reynolds numbers because the recycled flow is larger for higher Re. If more units of the basic mixer design are used in series, the mixing process is enhanced after each unit until mixing is complete. The used fluid was ink and distilled water. The mixing of NaOH and phenolphthalein solutions dissolved in water and ethanol was observed across the cross section of the outlet. Phenolphthalein changes the color from clear when in neutral or acidic solution to pink when the base is present. Here the pink or red colors indicate the complete mixing with the basic NaOH solution. The mixer is designed for small Re and tested for Re values from 7 to 42.

Kämper et al. described the use of LIGA technology in fabrication of different kinds of microfluidic devices such as mixers, heat reactors, and micropumps, or microfilters (Kämper et

al., 1997). For reaction channels, the micro electro discharge machining (µEDM) can be used for the fabrication, especially if steel is to be used as the device material.

Ehrfeld proposed a micromixer made using LIGA and µEDM technologies (Ehrfeld et al., 1999a). The mixing element is made by LIGA, either in nickel on copper, or in silver. The element has two small circular chambers for the incoming fluids and multiple sinusoidal shaped long and thin channels which prevent mixing of the liquid but separates each inlet flow into many laminar sheets. The top and bottom parts of the housing are made by µEDM. The top part has two inlets and an outlet, as well as a discharge slit where two liquids are mixed and brought to the outlet. The mixing quality was characterized using two fluids that can undergo to two different chemical reactions, one fast and the other ultrafast, depending on the mixing quality. The absorption of the iodine in the 300-400 nm spectrum was a measure of the mixing quality. They investigated both single mixers and mixer arrays, both for different slit widths and different widths of the channels in mixing elements. Mixers with narrower widths of the channels as well as narrower slit widths show better mixing results. Also the single mixing units show very good results, in some cases better than mixing arrays. Arrays can be very efficient for large volume flow rates. The volume flow can be enhanced in the individual mixing unit either by making the channels somewhat deeper, or/and by increasing the number of channels for each fluid within the mixing element.

Kang and Kwon proposed the color particle tracking method for the numerical simulations of the mixing two or more fluids for periodically structured mixers and throughout the mixer length (Kang and Kwon, 2004). Previously the similar simulation methods were performed only for one or two periods of the mixer units. The proposed method consists of three steps. In the first the velocity field is calculated for one period assuming the periodicity of the velocity field in

the down channel direction. In the second step the particles are induced and colored, and tracked along the mixer channel using the information on velocity field obtained in the first step. In the last step, the entropy of the mixing is used to quantify the mixing process at the desired cross sections along the fluid path through the mixer. The results of the simulation for three reported mixer designs (slanted groove SGM, staggered herringbone SHM, and barrier embedded BEM micromixers) are reported. For the SHM mixer the obtained simulation results show a great similarity as published experimentally obtained results for the same mixer.

Groisman and Quake constructed the microfluidic rectifier made of PDMS, that shows large fluid flow resistance in one direction (backward), and much smaller resistance in other (forward) (Groisman and Quake, 2004). The main channel has 43 triangular shaped segments connected linearly one to the other. The fluid passes through the narrow passage to adjacent triangular segments. The aqueous solution with small amount of the high molecular weight polymer was used, and it was found that for small Reynolds numbers and small differential pressure across the segment, flow is reversible (very similar in both direction). For the larger Re and larger pressure across each segment, there is considerable difference in fluid behavior. In the forward direction consistent vortices were formed. The main flow is restricted to the central part where the flow can be approximated as a tubular flow of the diameter approximated by the dimension of the bottleneck connections between the segments. In the backward direction larger fluid resistance is observed and vortices formed at much higher pressures than in the forward direction. It was noticed that these vortices are not consistent in time as a difference to the vortices in forward direction. The same channel was used for testing the water flow, and it was noticed that for Re smaller than 3, the flow is reversible. For the larger Re numbers the inertia contributes to the nonlinearity. The vortices are mostly formed in the backward direction after

the fluid emerges from the narrow passage, similar as with jets. This structure may be used for the directional flow of the liquid, pumps or mixers.

Chung and Shih proposed a planar passive micromixer made of PDMS using SU-8 photoresist as a master and soft lithography technique (Chung and Shih, 2008). The mixer is completed when second PDMS layer is bonded to the first one (containing the mixer channels) after exposing them to an oxygen plasma. The mixer works with two fluids, one delivered in-line with the mixer direction, and the other fluid is brought by two channels perpendicular to the main direction and of smaller channel diameter. The mixer body was modification of the zigzag mixer, and the mixing element had a rhombic shape. In front of the outlet the channel narrows and then expands to the outlet diameter – this part of the mixer is called converging-diverging elements. In simulations and experiments it is found that this element contributes to better mixing efficiency. Mixing efficiency is enhanced with larger number of mixing elements (rhombs), smaller turning angles, larger Reynolds numbers in case when the converging diverging element is present. If the outlet does not have this element, the increased Reynolds number reduces the mixing efficiency for zigzag mixer and rhombic mixer with only one element. However if two or more elements are present, mixing efficiency is enhanced. This is because of the longer mixing length and more angles and diversion areas where recirculation occurs. The mixing efficiency is evaluated using image gray levels.

Kamholz et al. described the use of T sensor for the qualitative analysis of molecular interactions (Kamholz et al., 1999). The Re numbers are very small for the given geometries and fluid flow rates, and the flow is laminar. Mixing is characterized by measuring the fluorescent intensity of reacting fluids. This technique can be used to determine the local diffusion coefficients and viscosities for different concentrations of reacting fluids.

Hinsmann et al. developed a micromixer for mixing the chemicals rapidly and immediately before recording the chemical reaction (Hinsmann et al., 2001). Usually there would be some dead time because the measurements of the reaction would occur after the reaction chemicals are already mixed, and part of the reaction would not be recorded at all. The mixer has Y inlets for two different reactants. Each inlet is divided into many narrow and parallel flow paths by SU-8 made channel structures. The two inlet fluids flow independently through levels separated by thin silver layer before the fluids are brought into the same channel. The top of the mixer is closed with CaF_2 layer which is transparent for infrared (IR) light used in reaction measurements made by Fourier transform infrared spectroscopy (FTIR). Since the fluid flow rate was around 100 ml/min the flow was laminar. The fluids in the main channel are not separated but still follow the independent stream lines. For the fast chemical reaction such as the one with acetic acid and sodium hydroxide, mixing occurs even when flow is not stopped. Slower reaction of monochloroacetate and sodium hydroxide does not occur within the mixer unless the flow is stopped. The mixing time of 100 ms is obtained experimentally as well as in simulations.

Wu et al. reported on the theoretical and experimental results for the Y mixer (Wu et al., 2004). The mixer was made of PMMA. Two PMMA pieces and an adhesive sheet were cut using the CO_2 laser. The mixer was assembled using the lamination technique, where the thickness of the adhesion layer determined the depth of the mixer channel (50 μm). The mixer length was ~4 mm and the channel width 850 μm. The analysis was developed for both linear and nonlinear model of the micromixer. The mixer was illuminated with the laser light to excite the fluorescent dye and the image was recorded and analyzed using MATLAB. Experimental results confirm the presented analysis. The flow rates used were from 40-310 μl/h, and Re numbers very small (0.0183 to 0.1417). The mixing process was due to the molecular diffusion.

Yi and Bau investigated the mixer consisting of bended micro conduits (Yi and Bau, 2003). The passive Y- mixer is designed of 5 layers: bottom plate, right bends, connections, left bends and inlet channels, and inlet and outlet holes. The material used is co-fired ceramic tapes and glass plates for the top and bottom layer in order to provide transparency. The numerical model is developed where the particle tracing was used to determine the position of particle after going through the bended section. Then the periodicity is used for in plane and out of plane bends. The model is tested for small Reynolds numbers, from 0.5 to 80. After each bend the length of the interface between two inlet flows is increased. Simulations and experiments showed that out of plane bends enhance the vortices formation and mixing much better then in plane bends.

Wong et al. discussed a micro T mixer (Wong et al., 2004). The mixer channel and inlet and outlet ports were etched in silicon wafer, and then bonded to Pyrex glass to close the fluid channel. Inlet and outlet ports are connected through the backside of the wafer. The mixers with 4 different hydraulic diameters (defined by channel widths and depths) were investigated. The mixing efficiency was tested using the blue colored solution on one inlet and DI water on the other. The images of the channel were captured and analyzed for different flow rates of incoming fluids. To compare the mixing process and find the mixing length, the images were converted to the gray scale and normalized to the image of the completely mixed fluids. Mixing was also observed using the chemical process in which the fluid becomes red colored when reaction occurs between two incoming fluids. The first incoming fluid is clear diluted NaOH, and the other fluid is dichloroacetyl phenol red dissolved in acetic buffer which makes it yellow in color. The applied fluid pressures were from 100 kPa (1 bar) to 600 kPa (6 bar) and corresponding Reynolds number from 50 to 300 for the device with smallest hydraulic diameter, and from 400 to 1400 for the device with the largest hydraulic diameter. Experiments showed that for Re

smaller than 100 mixing did not complete by the outlet. When Re were around 450-500 the cross flow was noticed which helped the mixing process and mixing was completed with mixing time in the order of millisecond, except in the mixer with the smallest hydraulic diameter. Simulations performed using Fluent 6 software corroborate the experimental results.

Wong et al. simulated the mixing process in a cross shaped micromixer using two software packages, CoventorWare and Fluent 5 (Wong et al., 2003). Since the volume of mixing samples was required to be very small (1 μl), the mixer was designed to operate in a non-continuous flow mode. The main inlet of the mixer serves for one fluid, while two other inlets which are perpendicular to the main channel bring the other type of liquid to both sides of the first one. Changing the flow rates of inlet fluids will determine the diffusion distance between contacting areas. Three mixer designs were simulated: mixer without static mixing elements, mixer with two static mixing elements, and mixer with five static mixing elements. Static mixing element was constructed as rectangular protuberance in the main channel which can generate the vortices to enhance the mixing process in the laminar flow regime. It will also contribute to the larger pressure drop from inlet to outlet which is not desired in most applications. The mixing efficiency was described by the following parameters: intensity of segregation, and variation coefficient. For the perfectly mixed fluids both mentioned parameters are zero. The simulation results showed that mixer with two and five static mixing elements have greatly improved intensity of segregation (from 0.3 in the case with no static mixing elements to 0.02 and 0.0006 for two and five static mixing elements) while the flow rate was reduces at the same time from 11.9 μl/s to 8.55 μl/s and 7.45 μl/s respectively. The simulations predict mixing time shorter than 1 ms for inlet pressures of 200 kPa.

Gobby et al. used computational fluid dynamics software to simulate the mixing process of gaseous fluids in a T type micro mixer (Gobby et al., 2001). It was shown that for the Pecklet numbers in the range from 0.027 to 13. 49 the mixing length increases from ~ 0.6 mm to ~4 mm, which is consistent with the theoretical prediction except for the very small flow rates. Keeping the channel width constant, the simulations showed that mixing length decreases for the channel aspect ratio smaller than 1.5, and above this value the mixing length is independent of the channel depth (channel aspect ratio is defined as its height/width). The initial shortening of the mixing length is explained as an influence of the wall shear for the shallow channels. Basic T type of the mixer can have inlets at different angles in respect to the main channel (arrow, T, Y inlets). Simulation results reported minimal influence of the inlet positions on mixing length and pressure drop. The only benefit of having inlets under higher angle may be the smaller area that device takes in experiments. The simulations were performed to investigate the influence of throttle at the beginning of the mixer channel. It showed that varying the throttle size from small values to the full channel width, simulated mixing length increases as well. Similar result was obtained when changing the inlet flow rates, the mixing length increases with the increase of the fluid velocity.

Veenstra et al. proposed a mixer for the micro flow injection analysis systems, with the laminar flow and diffusion mixing (Veenstra et al., 1999). This was achieved by simply narrowing the central part of the channel in order to reduce the diffusional distance for mixing process. The needed channel length can be predicted if flow rate, mixing time, width and depth of the channel are known. The pressure drop is larger for shorter diffusion time. The mixer has two symmetrical outputs and the mixing quality is measured as a concentration of fluid at the

outputs, when at the inputs the concentrations were known. Both outputs would have same concentration with complete mixing.

Koch et al. et al. proposed use of colored inks and image processing to observe the mixing process in their mixer (Koch et al., 1999). The mixing occurs due to diffusion and therefore to reduce the diffusional distance multiple inlets for both mixing species are created and fluids are brought by close contact feeding channels. Previously mixing was determined as a change of color when certain threshold pH value is obtained, however that did not show the mixing process quality for different pH values (bellow threshold pH value the fluids are colorless, and above the mixed fluid shows the same color regardless of the pH value). Using colored inks allows mixing to be observed to observe mixing throughout the entire mixing process. Inlet fluids are colored by different inks (red and green) and photographs were taken along the mixer length. The images are then converted to a gray scale and analyzed. It was shown that the mixing process improves along the mixer length and the color intensity becomes more uniform across the mixer width.

Walker et al. proposed to use the micromixer to obtain the gradual concentration of viruses within a device in order to optimize the recombinant protein production (Walker et al., 2004). Two versions of mixers were made of PDMS, for non-gradient and gradient infection. The non-gradient infection mixers consist of 5 straight channels of different widths and same lengths. The gradient mixer has 3 inlets and one outlet, and viruses are delivered through the central inlet, and medium through the side inlets thus focusing the virus liquid flow so that the stream of viruses is 100 μm wide. Since PDMS is transparent the reactions can be observed using fluorescence.

Mengeaud et al. investigated the zigzag structure for the mixer channel (Mengeaud et al., 2002). Mixers were made by laser ablation of Mylar substrate and geometries were varied. The width and depth of the channel were kept constant (100 μm and 48 μm) and the lengths of the

zigzag pattern were changed from 100 μm to 800 μm. In this paper mixing efficiency was defined as the ratio of minimal and maximal concentrations at the cross-section at a 2mm distance from the inlets. Simulations were performed such that Pecklet number was kept constant while Reynolds number was changed from 0.26 to 800, and significant improvement in mixing efficiency was obtained for Reynolds numbers larger than 80. Experiments showed that increasing the flow rate up to ~0.9 ml/h increases the intensity slope (obtained from normalized intensity of fluorescence across the mixing channel cross section at the outlet) which indicates that mixing efficiency was reduced. Above the flow rate of 0.9 ml/h, the intensity slope decreases and this enhanced mixing efficiency is due to the formation of vortices in the zigzag structure. This was also confirmed by simulations of the velocity field along the zigzag structure.

Groisman and Steinberg showed that mixing of viscous fluids in a mixer with N repeated curved turns, and with low Reynolds numbers (well below 1) can be greatly enhanced if very small amount of polymers is added to the mixing solution (1 ppm). This leads to the enhanced elastic instability of the fluid mixture and enhances the irregular flow which helps better mixing. Possible applications were suggested for laboratory or industrial use (Groisman and Steinberg, 2001).

Liu et al. performed the numerical simulations on three different micromixers reported by other researchers, the square-wave mixer, three dimensional serpentine mixer, and staggered herringbone mixer, taking care that hydraulic diameters and lengths for all three mixers were the same (Liu et al., 2004). The simulations were done for two different Reynolds numbers (Re = 1 and Re = 10) and for two different fluids, water and glycerol-water solution. It was shown that for the Re = 1, mixing was dominated by molecular diffusion and it was best for the serpentine mixer type. Increasing of the mass fraction of glycerol did reduce the mixing efficiency for small

Reynolds number flow for both mixer types. When the Reynolds number was increased to 10, serpentine mixer showed much better mixing for increased glycerol concentration due to increased flow advection. For the herringbone mixer very similar results were obtained both for Reynolds number 1 and 10, and there was no improvement in mixing as with serpentine mixer for large Re and larger glycerol content.

Lee et al. designed, fabricated and simulated a split and recombination micromixer made of PDMS (Lee et al., 2006). The experiments were done for a large range of Reynolds numbers, from 0.012 to 120. Two inlets bring the fluids (with one common interface) to the horizontal membrane which splits flow to the upper and lower channels. Further on the flows are recombined in such a way that three interfaces are obtain after the first mixing unit. The mixing quality was proved using phenolphthalein and NaOH solutions at inlets and comparing the result of the mixing process in proposed mixer to the simple T mixer of the same dimensions as the one investigated. When phenolphthalein and NaOH are brought together the red color appears, and experiments showed that a T mixer with the same length will have the red line only in the center of the mixing channel, whereas the proposed mixer will have a mixed region throughout the channel cross section. The exact mixing efficiency was measured using blue dye at one inlet and clear water on the other. Taking images of the mixing process along the channel and converting images to the gray scale (while normalizing the values of light intensity at inlets to 1 and 0) showed that mixer has ~90% mixing efficiency for Reynolds number 0.06.

Munson and Yager fabricated the lamination mixer made of five Mylar sheets (Munson and Yager, 2004). The top and bottom sheet serve as covers, the second and fourth sheet define the channels which are connected through the vias defined in the middle (third) layer. Channels and vias are cut using the Universal Laser System CO_2 laser. Mylar sheets (covered with adhesive)

were aligned and pressed together to complete the mixer. Buffered solutions of fluorophore (pH sensitive material) at different pH values are injected at two inlets. The mixing was observed as a change in fluorescent intensity (the fluorescence depends on pH value). Images were captured for different flow rates along the lines perpendicular to fluid flow along the channel and the intensity values were analyzed using Matlab. The mixer was tested for small flow rates and Reynolds number from 0.9 to 7.9. Both experiments and Coventor simulations showed that mixing was better for increased residence time (reduced flow rate), and that proposed mixer was showing much better results than the equivalent straight channel mixer. It was also shown that even for higher flow rates the mixing was improved as the number of mixing units increased.

Chang and Cho proposed micromixers with alternating whirl (AW) units (in clockwise and counter clockwise direction), and micromixer with alternating whirl and lamination (AWL) units (Chang and Cho, 2005). They compared those two types with two previously reported mixers, the straight channel (diffusion mixing) and serial lamination mixer (diffusion mixing and lamination). All four mixers were made of PDMS, and had the same dimensions of the channel cross sections and total channel lengths (6.2 mm). The fluids used in experiments were phenolphthalein and NaOH diluted in ethanol (which are often used for the characterization of the mixing process, since it turns red when mixed and pH is above 8). The experiments were done for the Reynolds numbers from 0.26 to 26. It was shown that only the mixer with combined diffusion, alternating whirl and lamination, AWL has the mixing lengths smaller than the mixer channel length (6.2 mm) for all Re values used.

Lee and Kwon proposed the micromixer with recirculating zones where the formation of vortices would increase the mixing process (Lee and Kwon, 2009). Mixer was made of photosensitive glass. The etching control was achieved by exposing the desired areas to UV

light, which after thermal treatment turns into ceramic material that has higher etch rate then original glass. Different layers are then aligned and bonded at higher pressure and temperature. Simulating this structure for Reynolds numbers from 10 to 1000 it was shown that mixing was enhanced and mixing efficiency for Re >400 was above 90%. In comparison, the conventional multilamination mixer has decreased mixing efficiency with the increased Reynolds numbers because for the larger flow rate the residence time decreases and affects the diffusion process. Experimental results confirmed the enhancing role of the recirculating zones on mixing, since the mixing efficiency was lager for this mixer than for the multilamination mixer for Reynolds numbers from 40 to 1000. For flow with Re<40 there were no observed vortices in the recirculating zones, and the recirculation mixer showed worse results in mixing which was due to the enlarged diffusion widths between mixing fluids in this region.

Kim et al proposed the barrier embedded micromixer (BEM) as an improvement to slanted groove mixer (SGM) (Kim et al., 2004). Mixer was compared favorably to Y-mixer and slanted grooves mixer. Adding the barrier either on top of the mixer channel or at the bottom, induces the appearance of the hyperbolic point and two elliptic points at the channel cross section, in comparison to only one elliptic point and no hyperbolic point in regions with only slanted grooves present. This enhances the helical flow and therefore the mixing process. The fabrication of PDMS micromixers involves one additional photolithography step for BEM than for SGM. The experimental results show linear dependence of the characteristic mixing length versus Reynolds number for the Y mixer, which is characteristic for diffusion based mixing, and logarithmic dependence of mixing length versus Re for SGM and BEM, which implies that chaotic mixing was induced. Reynolds numbers were varied from 0.228 to 2.28, and corresponding mixing lengths were 6.26 mm, 7.98 mm, and 12.94 mm, while total mixer length

was 21 mm. Mixing length was defined as the downchannel length where normalized mixing intensity was 0.632 (it is 0 at the inlet, and can be max 1 for perfectly completed mixing).

Neils et al. developed a combinatorial mixer of laminated Mylar sheets (Neils et al., 2004). The intended application is to enable automatic fabrication of multiple different mixtures (16 in the presented work) made of two different dye colors and diluter (water). Nine Mylar layers were cut using laser, and then aligned to form four level structure which involved four inlets, four sizes of serpentine mixers at different structure stages from inlet to outlet. The efficiency of the serpentine mixers was modeled and tested comparing the gray scale levels from inlet to mixer outlet. It was shown that flow rate (and Pecklet number) has great influence on mixing quality.

Liu et al. reported a passive three-dimensional serpentine micromixer made using standard silicon wafer technology (Liu et al., 2000). Mixer was compared to simple straight channel and to square channel mixer. The design is based on previous design of twisted pipe which proved to be efficient for mixing at Reynolds numbers larger than 60, while this mixer showed very good results for Reynolds numbers from 6 to 70. Twisted pipe was modified to involve rotation of the fluid by 90º in two successive steps, and those two C-sections comprised one mixing segment. The viewing windows were made at each 90º turn to monitor the mixing progress. Two benchmark mixers had viewing windows at the outlet. All three mixers had the same total length of 18 mm, 300 μm width and 150 μm depth. In experiments the phenolphthalein was used to show the change of color from transparent to red when mixed with NaOH at the pH value larger than 8. The standard deviation of the pixel intensity was not convenient to use because the intensity increases from the inlet as the mixing progresses along the channel. It was noted that prior to entering the first mixing segment, mixing by diffusion was dominant and better mixing was achieved for smaller Re. The normalized average intensity is below 0.3 for all tested flows.

After several mixing segments the normalized average intensity increases and reaches the plateau for all Reynolds numbers. The serpentine mixer showed much better results than both straight channel (where mixing decreases with increase of Re) and square channel mixer (where mixing increases at Re larger than 70), while for serpentine mixer increases significantly at Re = 25.

Bertsch et al. used microstereolithography process to build mixromixers with the design similar to mixers used in the industry for large scale mixing (Bertsch et al., 2001). Material used is a liquid resin (such as SU-8) which is polymerized by laser light at desired areas layer by layer until the whole structure was built. Two types were made: with intersecting channels and helical elements. Qualitative experiments were performed by mixing colored liquids for Reynolds numbers from 1 to 100. Both experiments and simulations showed that mixer with intersecting channel had better mixing efficiency than mixer with helical elements.

Stroock et al. discussed two mixing structures made of PDMS using soft photolithography process, to induce the anisotropy in the channel in order to enable chaotic flow at Re less than 100 (Stroock et al., 2002). The first structure had fabricated ridges at the channel bottom which help to generate a transverse flow component and helical flow of the flow in the channel. The second structure had a staggered herringbone mixer (SHM) where groove shapes were not straight and where their dominant orientation was varied along the channel bottom. Using standard deviation of pixel intensity across the channel cross section, it was shown that SHM performs mixing much better that simple channel (where deviation remains very close to 0.5 value at cross sections along the channel length which indicates very poor mixing) and also better than the first structure (mixer with straight grooves).

Niu and Lee investigated the active mixer with multiple side channels for inducing pressure perturbances at the main fluid flow and in such way contribute to the chaotic mixing (Niu and

Lee, 2003). They showed that such mixer can reduce the needed mixing length by two orders of magnitude compared to the straight channel with diffusion mixing only. The minimum mixing length depends significantly on the diffusion coefficient *D* which depends on fluid properties and is smaller for larger molecules which would lead to longer mixing lengths.

Wang et al. studied the mixing quality of the mixers with grooves on the channel bottom by performing numerical simulations using computational fluid dynamics software (Wang et al., 2003). They investigated the slow flow rates and consequently the small Reynolds number regime, and found out that mixing was very dependent on channel dimensions, particularly on the aspect ratio of the patterned grooves in respect to channel height. The mixers with grooves of larger aspect ratio showed better mixing comparing to those with smaller aspect ratio for the Reynolds numbers 1 to 5. This result confirmed results previously published by Stroock et al (2002).

Park et al. presented two micromixers (made of PDMS using soft photolithography) where the dimensional component was induced by forcing the fluid through two levels of mixing channels (Park et al., 2004). For mixer 1, fluid successively goes through lower and upper level in each mixing segment. Mixer 2 has somewhat complicated structure since upper level also induces the breakup process. Both lower and upper levels have five mixing units in parallel and upper level is shifted by half mixing unit width. The upper channels divide the fluid flow into two separate paths. Each of these fluid paths combines in the next, lower level with fluid from neighboring mixing units making the mixing process more efficient. Both simulations and experiments showed that mixer 1 was efficient for large Reynolds numbers (Re =50) where interfacial area between two mixing fluids was distorted and increased significantly after several mixing segments. For smaller Reynolds numbers (Re = 1 and below 1) there was no significant

difference between results and the interfacial area was barely distorted. It was also shown that shorter segments produced better mixing results. Mixer 2 was tested for three Reynolds numbers (1, 10 and 50) and results were the best for Re = 10 (84% mixing compared to 78.5% for Re = 1 and 72.5% for Re = 50). For small Re diffusion and breakup of the flow were main factors to contribute to mixing, while for larger Re (50) dominant factor was breakup and stretching and folding. For Re = 10, all three processes were present which explained better results.

Chen and Meiners proposed topological mixing mechanism for mixer fabricated of PDMS and encapsulated by epoxy resin (Chen and Meiners, 2004). The three dimensional mixer has two levels. At each level, flow is divided into two smaller flows which after two 90º turns merge again at the second level. The needed channel length for mixing decreases exponentially with the number of mixing segments. The experiments were done for Reynolds numbers from 0.1 to 2 using fluorescent protein solutions and mixing process was recorded by Charge-coupled device (CCD) camera. Better mixing results were obtained for smaller Re.

Bhagat et al. investigated the mixing enhancement in Y-type mixer by placing obstacles in the main channel (Bhagat et al., 2007). Mixer was made of PDMS using patterned SU-8 photoresist as a mold. The channel depth was 55 μm, and width 200 μm wide. PDMS channel was bonded to glass slide in order to close the mixer channel. Simulation and experiments were conducted for wide range of Reynolds numbers (0.01 to 100 in simulations and 0.02 to 10 in experiments). In experiments the fluorescence was used for mixing characterization. Obstruction height was simulated for obstruction heights from 0 to 55 μm (channel height), and it was shown that best mixing was achieved with 55 μm obstacle height. This also simplifies the fabrication reducing the lithography steps to one, with the cost of increasing the pressure drop along the mixer channel. Various shapes of obstructions were investigated (circular, triangular, rhomboid

and stepped rhomboid) and stepped rhomboid obstructions showed best mixing results in simulations. It was shown that best location of the obstructions was not in the middle of the channel, but certain offset (45 μm) is desired. Experimental results for the mixing quality was performed for the Re from 0.02 to 10 for both mixer with rhomboid obstructions and Y-mixer, showing better mixing efficiency of the mixer with obstacles in all investigated Re range. Also it was noted that mixing efficiency decreases from 0.02 to 1, and for Re larger than 1 again increases. It was concluded that for lower Re range mixing was dominated by diffusion, while at larger Re range mixing was dominated by convection. The experimental results closely followed the simulations. This mixer in effect behaves as a split and recombine mixer.

Bhagat et al. proposed a particle mixer with obstacles in the channel to enhance the lateral velocity component of the mixing fluids (Bhagat et al, 2008; Bhagat and Papautsky, 2008). The main channel was 100 μm wide and 50 μm high, and obstacles of rectangular shapes and same height as the mixer channel were placed at 45º in respect to the main fluid flow in order to increase the fluid flow length with tolerable pressure drop from inlet to outlet regions (pressure drop was measured at 3 mm from the inlet and was found to be 80 Pa).The particle mixer performance was compared to modified Tesla mixer and Y-mixer. Simulation results showed that particle mixer is comparable to modified Tesla mixer in mixing efficiency and much better than Y mixer for mixing two fluids. The experimental data confirmed the simulation results. Particle distribution was also modeled and the particle mixer was much better in distributing the particles across the channel width: at 3 mm from the inlet, for particle mixer particles were spread at 90% of the channel width and for modified Tesla mixer at 60% of the channel width. For Y mixer particles remained in one half of the channel (50%). The size of particles was also taken into account and it was shown that sizes from 59 nm to 5.9 μm were similarly distributed

across the particle mixer channel since the distance from side wall to obstacles was large enough for all particles (15 μm).

Villermaux et al. analyzed mixing in a staggered herringbone structure for small Reynolds numbers Re and large Pecklet numbers Pe (Villermaux et al., 2008). They confirmed that mixing length can be approximated as *ln(Pe)* as pointed out by other researchers (Stroock 2002).

Vijayendran et al. investigated the application of the three-dimensional serpentine mixer in surface-based biosensors (Vijayendran et al., 2003). The straight channel mixer of the same residence time was used as a benchmark. One wall of each mixer was covered with immobilized protein A, while fluid going through the mixer contained Immunoglobulin G (IgG) antibodies. Three-dimensional serpentine mixer showed two times faster binding of the IgG antibodies to protein A. The authors suggested that modified mixer design can lead to more significant improvement in detection in order to justify additional cost for serpentine mixer fabrication compared to simple straight channel mixer.

Fang and Lee experimentally investigated the mixer efficiency for the micro Kenics mixer (Hobbs and Muzzio, 1997) and for Reynolds numbers from 66 to 1020 (Fang and Lee, 2001). The benchmark mixer was straight tube mixer of the same dimensions (without the helices as in Kenics mixer). It was shown that Kenics mixer has transition from laminar to turbulent flow at Re =150, as compared to the straight tube having the transition at Re >2100. No details on mixer fabrications were given, except for dimensions (0.8 cm diameter, and 9.4 cm length).

Sudarsan and Ugaz presented two mixers, planar split and recombine (P-SAR) and asymmetric serpentine micromixer (ASM), both showing good mixing results due to the formation of the Dean vortices. Dean vortices form in the vertical plane when fluid path is

curved and radius of the path is larger than the hydraulic diameter of the channel (Sudarsan and Ugaz, 2006a; 2006b).

C. Fabrication

Two Mylar™ sheets (1.4 μm thick, coated on one side with ~10nm of gold, Knowles Electronics, Itasca, IL) are held in close contact by applying a partial vacuum between them while keeping gold layers on the outer surfaces. The whole set-up is placed on the platform of the Universal Laser System CO_2 laser. The laser head follows the path determined by an AutoCAD drawing and corresponding weld lines are obtained. The welding parameters are: power used for welding is 3.5 W (the Universal Laser Systems CO_2 has 100W total power), head speed is ~63 - 76 mm/second, and there are 39 pulses/mm.

The focusing is done above the Mylar film surface in order to avoid focusing on a very small area and burning the Mylar. After welding the Mylar material is removed from the laser workbench and gold layer is etched away from the mixer region in order to enable observing the mixing process through transparent Mylar film. After gold etching, redundant Mylar is cut around the mixer channel. LDPE support has contact with Mylar only at inlet and outlet regions in order to enable better melting between LDPE support structures. Leak tight inlet and outlet connections are provided by inserting LLDPE (linear low density polyethylene) or Tygon tubes into the Mylar inlet and outlet welded channels. To make the device more robust, welded films and tubing are placed between two LDPE rings (or rectangles) and fused together at elevated temperature and pressure. To prevent the collapsing of the LDPE tubing at high temperature, thin Teflon tubes were inserted into LPDE tubing. When the device is cooled to the room temperature Teflon tubes are easily removed. The fabrication process is illustrated in Figures 20 and 21.

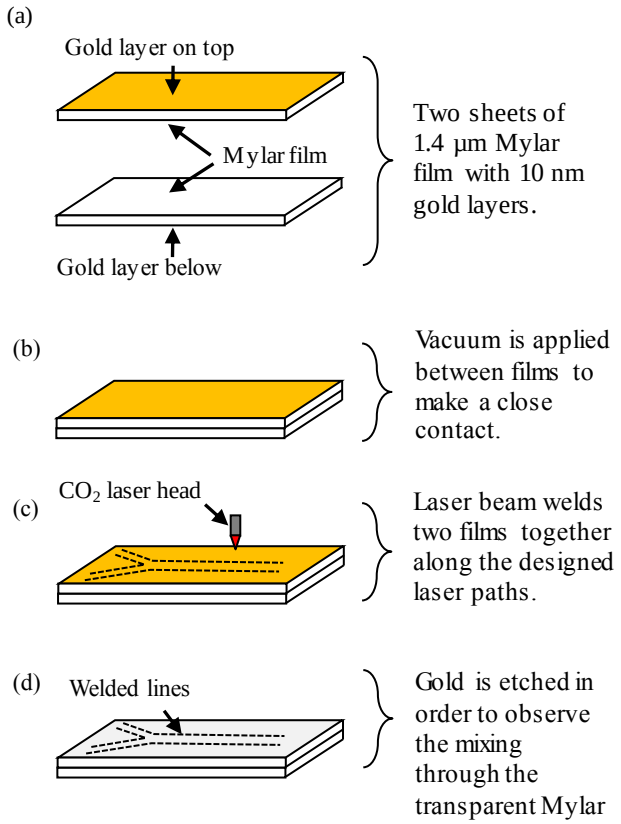

Figure 20. Laser welding of thermoplastic films. (a) Two sheets of Mylar film with metallized layers on opposite sides; (b) vacuum is applied; (c) Laser head follows the computer guided path; d) Gold is etched in order to observe the mixing. (Drawings are not to scale.)

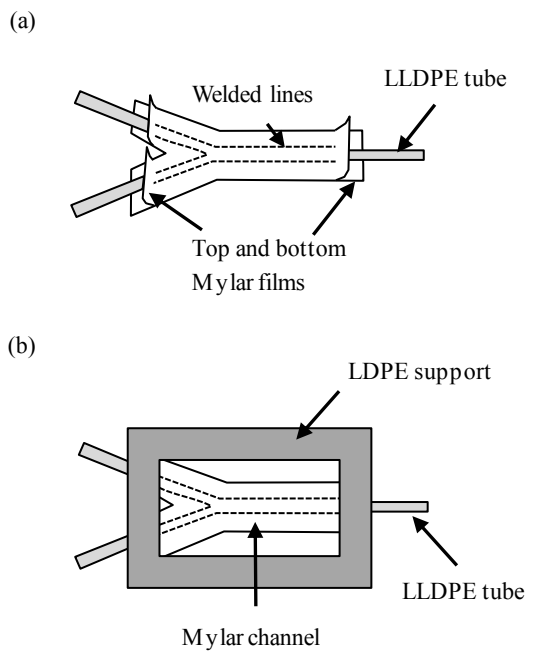

Figure 21. Assembling the device. (a) Inserting LLDPE tubes between top and bottom Mylar film into welded inlet and outlet channels; (b) LDPE provides the support and tight connection between LLDPE tubes and Mylar channels.

D. Proposed Mixer Structures

We have developed a novel fabrication technique for a passive, planar, continuous flow micromixer with laminar flow (Feinerman, 2006). The device is made by welding thin thermoplastic sheets using a simple manufacturing procedure which reduces the total cost of the device, and enables frequent changes to the design as necessary. Several types of devices were fabricated in order to present the applicability of described fabrication technique in microfluidics.

All devices have Y-type inlets. Other configurations such as T-type or arrow are also possible, although there is no clear advantage in mixing process for any of those (Gobby, 2001). However Y-type requires smaller area and was chosen as the most convenient. All fabricated

mixers have 5.2 mm long mixing channels. The inlet and outlet welded lines are separated to such width that when opened, their diameters match the LLDPE tubing outer diameter (OD = 1.016 mm).

1. Serpentine micromixer

Serpentine mixer has mixing channel meandering along the main flow direction which increases the available flow length for a smaller device foot print. The serpentine mixer is shown in Figure 22. Two versions are made, with wider and narrower main channel. In both versions the mixing period is 4.5 mm, and average channel widths are 1.2 to 2 mm for wider mixer and 1 to 1.3 mm for narrower.

(a)

(b)

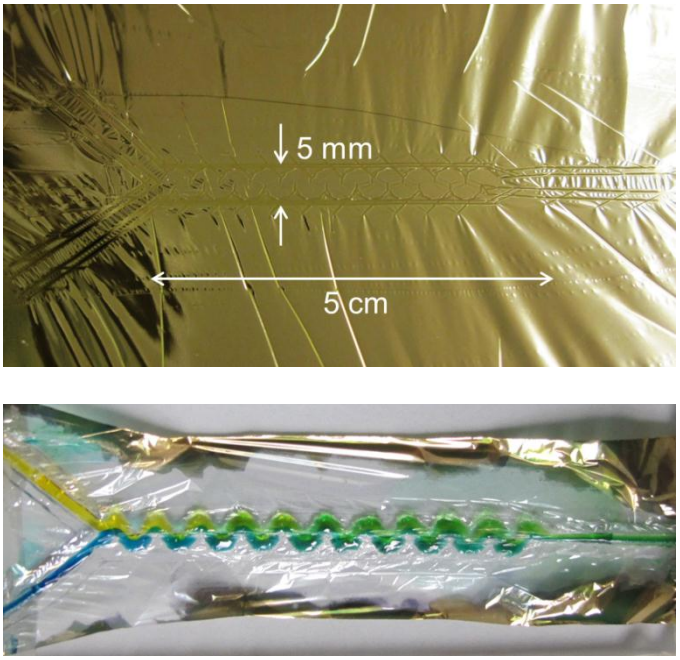

Figure 22. Serpentine mixer. (a) Mixer channel after the laser welding; (b) mixing of yellow and blue colored water solutions in wide serpentine mixer.

2. Micromixer with obstacles

The obstacles in our design were welded lines (~0.5 to 0.7 mm thick) that separated the mixing chamber into a series of interconnected channels thus forced the fluid to separate into two or three directions within the chamber. Obstacles are designed to have slightly curved shape toward the central mixer channel axis, while leaving the narrow fluid paths along the central channel axes and along the upper and lower channel walls. The curved sections were intended to induce the fluid velocity components in directions other than main fluid flow and the appearance of vortices. The shape of obstacles can vary from straight lines to more or less curved sections. More curved sections proved to be more effective in better mixing. If there was no offset between upper and lower obstacles, mixing is further enhanced but the pressure drop is expected to be much larger and certain compromise has to be made. The mixer channels widths are 3.4 mm and 2.8 mm when flat (no fluid going through), and approximately 3 mm and 2.5 mm with fluid going through. The width of the upper and lower narrow fluid paths are ~ 200 μm. Obstacles have 2.5 mm period.

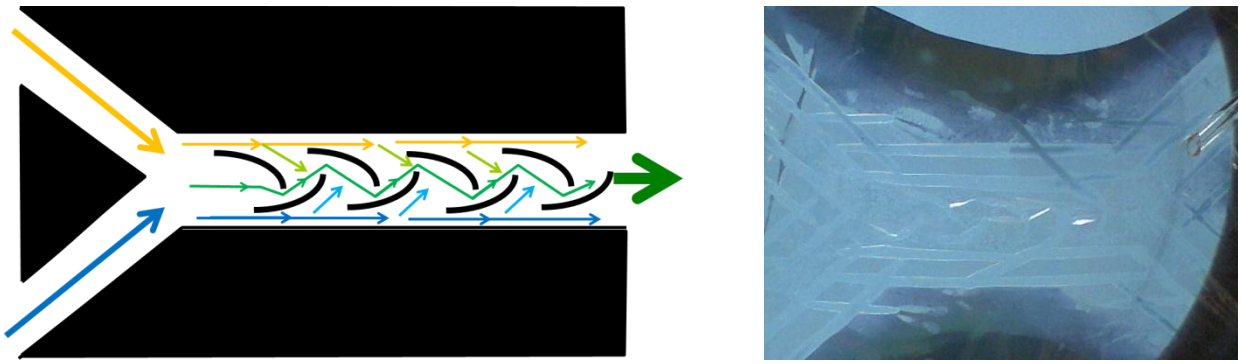

(a) (b)

Figure 23. Mixer with obstacles. (a) Schematic presentation of mixing principle. (b) The welded mixer channel with 6 obstacles.

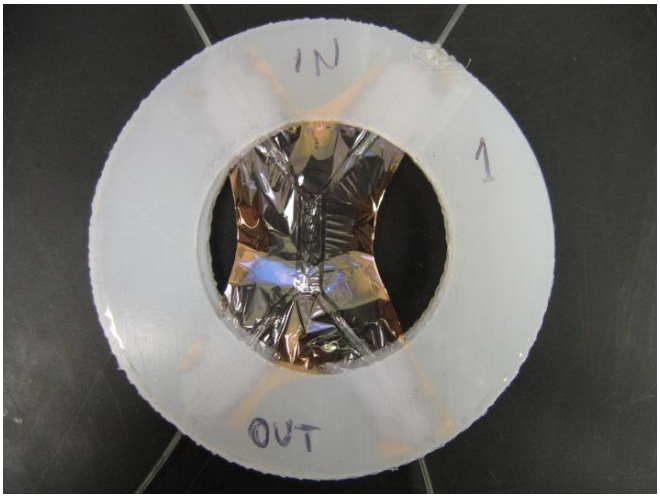

Figure 24. The first version of mixer with obstacles after manufacturing. Tygon tubes are inserted into the inlets and outlets, and the entire device is sandwiched between two LDPE rings which also create leak tight connections.

3. Split and recombine micromixer

Split and recombine mixer was constructed as a long straight main channel with periodic obstructions in the middle of the channel and on its edges. This would cause the fluid to separate into two flows around the obstacle, and merge again when channel narrows, i.e. after one split-and-recombine segment. Dimensions of the main channel width are 2.8 mm when flat and 2.2 mm with fluid flow for the narrower mixer version. For the same mixer the recombine region has width of 1.8 mm and mixing segment length is 4 mm. The wider split-and-recombine mixer has main channel width 3.5mm when flat and 2.6 mm with fluid flow and 5 mm split-and-recombine segment length. The narrow recombine region is made smaller in this version and it is 1mm wide. The split and recombine mixer is shown in Figure 25.

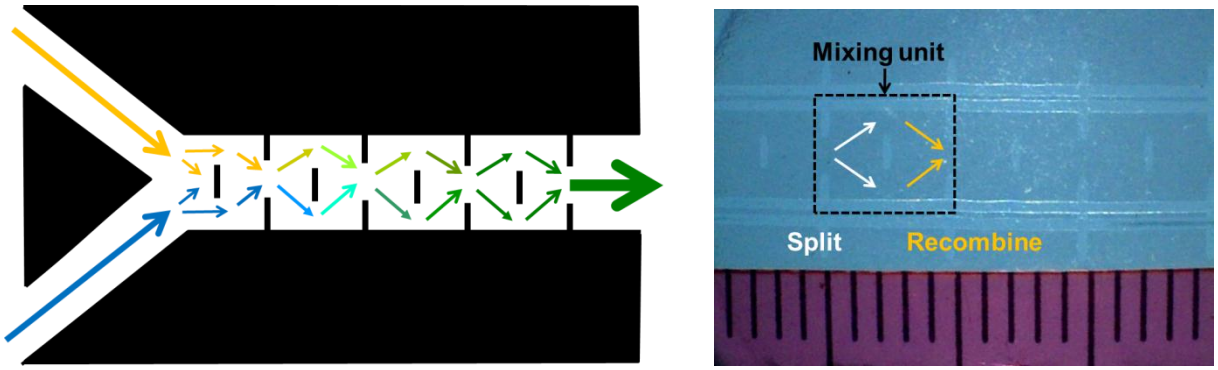

(a) (b)

Figure 25. Split and recombine mixer. (a) Schematic presentation of mixing principle. (b) Mixer with 5 mm long mixing segments after welding and gold layer removal. Horizontal weld lines define the mixer channel. Short vertical lines periodically arranged in the middle and edges of the channel provide the required mixing segments for splitting and recombining the fluid. The scale is in millimeters.

4. Y-mixer

Y mixer is a simple straight channel mixer with Y-inlets and one outlet, and is presented here in order to compare the mixing efficiency of other proposed mixers. The mixing in long narrow channels is due to molecular diffusion which is a slow process. Depending on channel width and material properties of fluid, diffusion process can require long channel length to complete the mixing. Y-mixer main channel has 1.2 mm diameter when flat and ~0.8 mm with fluid flow through it.

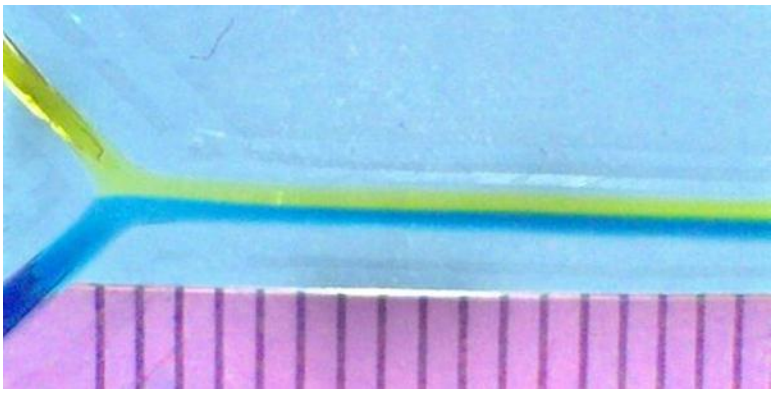

Figure 26. Y-mixer. The scale is in millimeters.

E. Experimental Results

The mixing quality was demonstrated using two different colored water solutions and observing the mixing along the channel length. The color dyes used were FD&C (Federal Food, Drug, and Cosmetic Act) colors: Blue No. 1 and Yellow No. 5 (McCormick and Company). The diffusion coefficient of those dyes was reported to be $D = 4.5*10^{-10}$ m^2/s (Neils et al., 2004). The particle size is less than 1 μm (von Elbe and Schwartz, 1996). The flow rate of the fluids was controlled by KD Scientific 780200 syringe pump. Reynolds numbers were varied from 0.01 to 10 in all cases except for the short micromixers with obstacles where the range was from 0.005 to 5.24. Reynolds numbers were calculated at the entrance of the main mixer channel for the average fluid velocity and characteristic dimension. The channel dimensions are changing as the fluid flows toward the outlet, and the characteristic dimension was taken at the entrance of the main mixer channel. For most mixers it was assumed that channel cross section is a circle of the same area as sum of the two inlets' cross sectional areas. For serpentine and Y-mixer the hydraulic diameter is taken as the diameter of the main channel at the inlet (Kovacs, 1998).

The flow rate was adjusted accordingly for the syringe pump to fit the desired Re range. The limitations were between the minimum flow rate available for syringe pump for the given syringe diameter, and maximum flow rate that mixer can withstand without the channel being damaged. Fluid flow for all values of Reynolds numbers used in experiments is laminar. Those values of Reynolds numbers are smaller than for the micromixer designs reported earlier (Paya et al., 2008).

The observed colored patterns are photographed using Digital Blue™ QX5 microscope. The main mixer channel for all mixers was designed to be 5.2 cm, and the images are taken at the inlet region (covering inlet tubes and 0- ~ 1.5mm), middle region (~1.5-~3.5mm) and outlet region (~3.5-~5.2mm). Images were then converted to the gray scale, and using publicly available open source software ImageJ, the 8-bit pixel values were recorded at desired regions. The obtained pixel values range was scaled to cover the entire 0-255 range. There were three data conversion problems noticed during mixer evaluation: reflection off the Mylar (polyester) surface, appearance of dark lines, and different overall darkness obtained for three imaged regions. Reflection of Mylar and dark lines are illustrated in Figure 27.

Mylar reflection caused very bright spots or lines (close to 255 values) at the illuminated areas where fluid color should be darker. Wherever possible those areas were avoided in taking the data, but for large number of images that was not possible. As a result of Mylar reflection there are some unusual upward spikes in the normalized pixel value data. The three-dimensionality of the channel also leads to the lighter color at the edges of the completely open mixer channel. This effect can be seen as the increase in the pixel intensity near the channel edges, and is especially noticeable for the darker colored fluid.

The appearance of the dark lines are caused by folding the Mylar material when three dimensional structure is formed from the two dimensional welded pattern or due to not completely opened channel at certain location (for example in the Y-channel). Dark lines can be observed in the main flow direction along the central axial position (at the entrance region of the main channel between two inlets, or along the central axes for serpentine mixers), at upper and lower channel edge (for example in the Y-channel) or around the channel segments in split-and-recombine mixers. Dark lines can be noticed as sudden drop in pixel intensity.

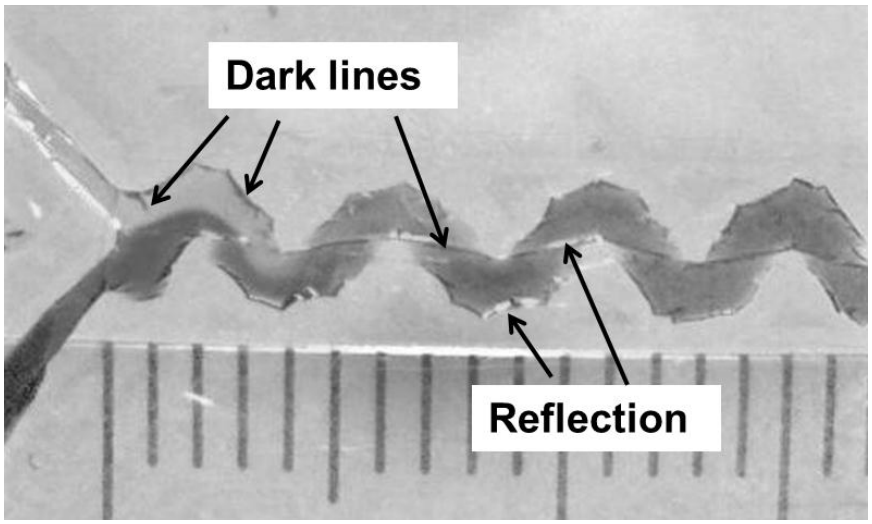

Figure 27. Illustration of Mylar reflection (bright spots) and Mylar folding (dark lines).

Different overall darkness was caused by slightly different position of the main channel in respect to the microscope objective. The reason for this is that the channel is compliant, sags due to gravity and is not in the same plane from inlet to outlet. The created shadows are recorded as

changed pixel values. This issue was only partially overcome by adjusting the darkness level of middle and outlet region to the inlet region images.

To quantify the mixing quality one of the values to measure is the standard deviation of normalized pixel intensity. It can be calculated as follows:

$$\sigma = \sqrt{\frac{\sum_{i=1}^{N}(I_i - I_m)^2}{N}} \tag{3.8}$$

I_m is the mean normalized pixel intensity for pixels 1 to N defined as:

$$I_m = \frac{1}{N}\sqrt{\sum_{i=1}^{N} I_i} \tag{3.9}$$

When fluids are completely unmixed, the standard deviation value is 0.5. When mixing is completed (100%), the standard deviation is 0. Standard deviation of 0.4 would correspond to 20% mixing, 0.3 to 40% mixing, etc. The standard deviation is calculated for each mixer at different positions along the mixing channel and for different Reynolds number. At each position of interest the rectangle area of the mixer channel cross section is analyzed in ImageJ. The rectangular area is divided into equal smaller areas (bins) and pixel intensities are averaged in each bin. The results are presented as normalized pixel intensity changes across the channel width for different Reynolds number to show the influence of Reynolds number on the mixing quality, and also along the channel for the same Reynolds number to determine the needed mixing length. Mixing length is defined as the distance along the general fluid flow where standard deviation is below 0.05 (90% mixing).

1. Serpentine micromixer

The serpentine mixer was made in two versions, with different channel widths. The width of the channel is not uniform, and it is widest at the curved upper and lower sections and narrowest at positions along the main channel direction (x-axis). The change of the channel width showed in previous works to be helpful for better mixing and the same is true for Mylar serpentine mixers as can be seen in Figures 28 and 31. Figure 28 shows mixing in serpentine mixer with wider channel for Reynolds numbers from 0.01 to 10.

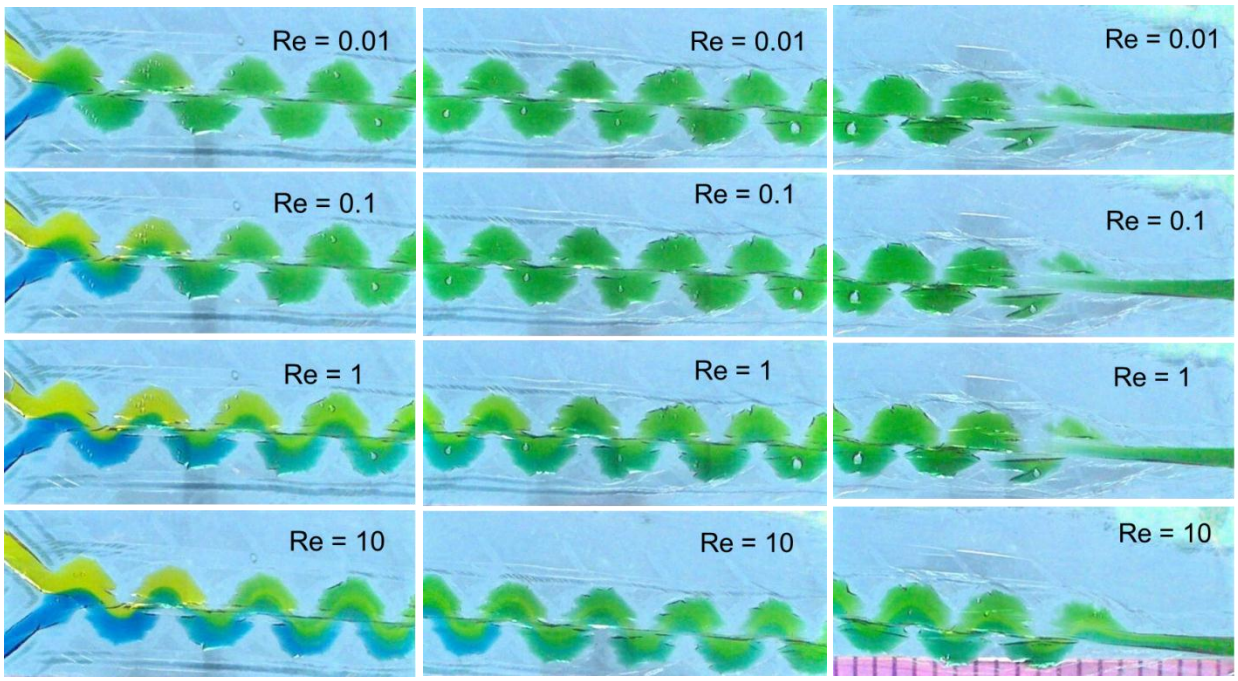

(a) (b) (c)

Figure 28. Images showing the mixing results for wider serpentine channel and Reynolds numbers from 0.01 to 10; (a) Inlet region, (b) middle section, and (c) outlet of the mixer. Scale is in millimeters.

For small Reynolds numbers mixing by diffusion is completed close to the inlet region. For Re smaller than 1, the flow in the channel is called creeping flow. Results are very similar for Re = 0.01 and Re = 0.1 and it can be noticed that uniform mixing is achieved after one and two serpentine periods respectively. For Re = 1 longer mixing length is needed but mixing is still completed within the mixer channel, while for Re = 10 it is clearly visible that fluid in the outlet is not uniformly mixed since various shades of green color are present. In addition, portion of the blue colored fluid transverse to the other side of the channel and light green colored fluid flows between dark green and blue regions.

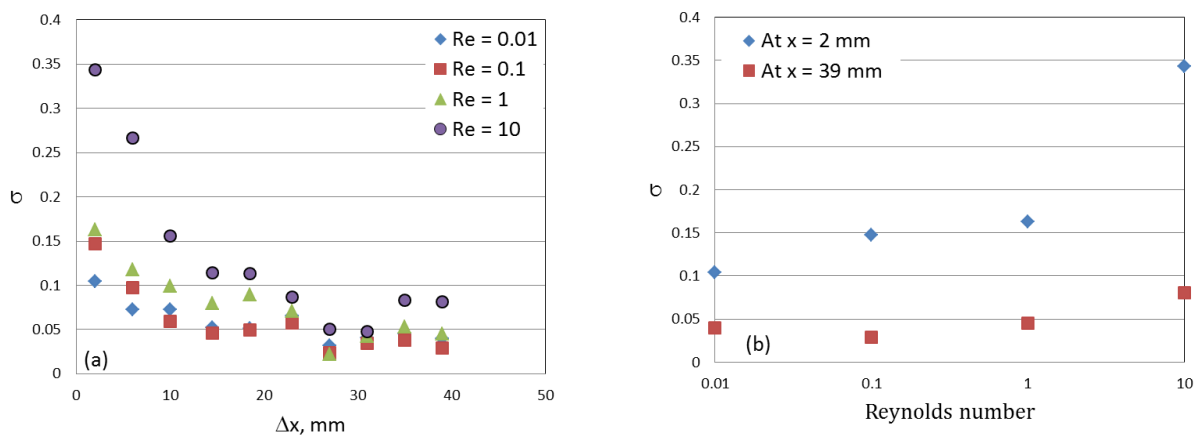

(a) (b)

Figure 29. Standard deviation of pixel intensity (a) along the main channel direction of the wide serpentine micromixer; (b) as a function of Reynolds number.

Figure 29a shows calculated standard deviation of the pixel intensity along the main channel direction for Reynolds numbers 0.01, 0.1, 1 and 10. Mixing of 80% is achieved for Re = 0.1 at 6 mm horizontal distance from inlets, and 10 mm for Re = 1. For Re = 10, 80% mixing was completed at 23mm. The measurements were somewhat imprecise due to the reflection of the Mylar surface. Figure 29b shows the dependence of standard deviation measured at the inlet and outlet of the mixer on Reynolds number. The mixing is improved as the fluid progress from inlet toward the outlet for all Re, reaching 90% at 14.5 mm for Re smaller than 0.1. Figure 30 shows the normalized pixel intensities at different cross-sections along the main channel direction and for various Reynolds numbers. The width of the channel at cross-section is normalized to 100% in order to easier compare different mixer types. The normalized intensity at inlet has a larger range from minimum to maximum values because fluids are not mixed yet. For high Re there is a sharp step in intensity values from high values close to 1 to low values close to 0 because two fluids flow parallel to each other and there is no mixing near the inlet for high Re. The transition from high to lower normalized pixel intensity becomes less steep as Re is reduces, and for Re = 0.01 normalized pixel intensity changes uniformly across the channel width - that means the mixing is already occurring at this position as can also be seen in Figure 28. Normalized pixel intensities further down the fluid flow tend to have more uniform values across the channel cross-section. For completely mixed fluids normalized pixel intensity is 0.5 across the channel width. Figure 30c shows that at 27mm from inlet, normalized pixel intensities do not change significantly across the channel width and values are near 0.5.

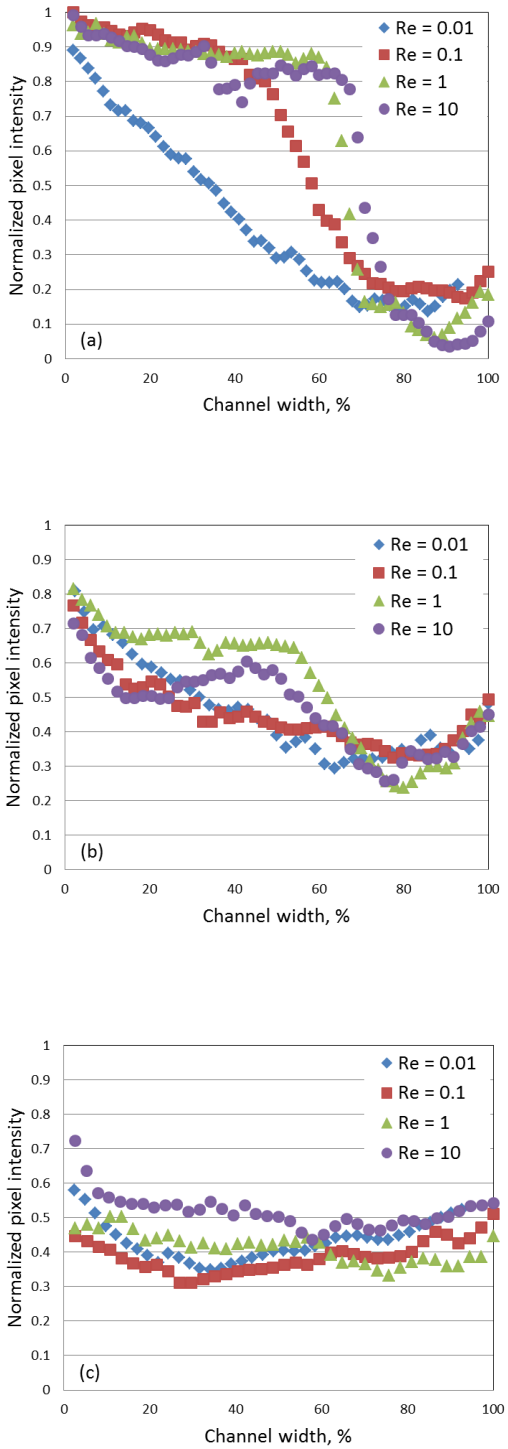

Figure 30. Standard deviation of pixel intensity at the cross section of the mixer channel: (a) At 2 mm from inlet; (b) at 14.5 mm; (c) at 27 mm.

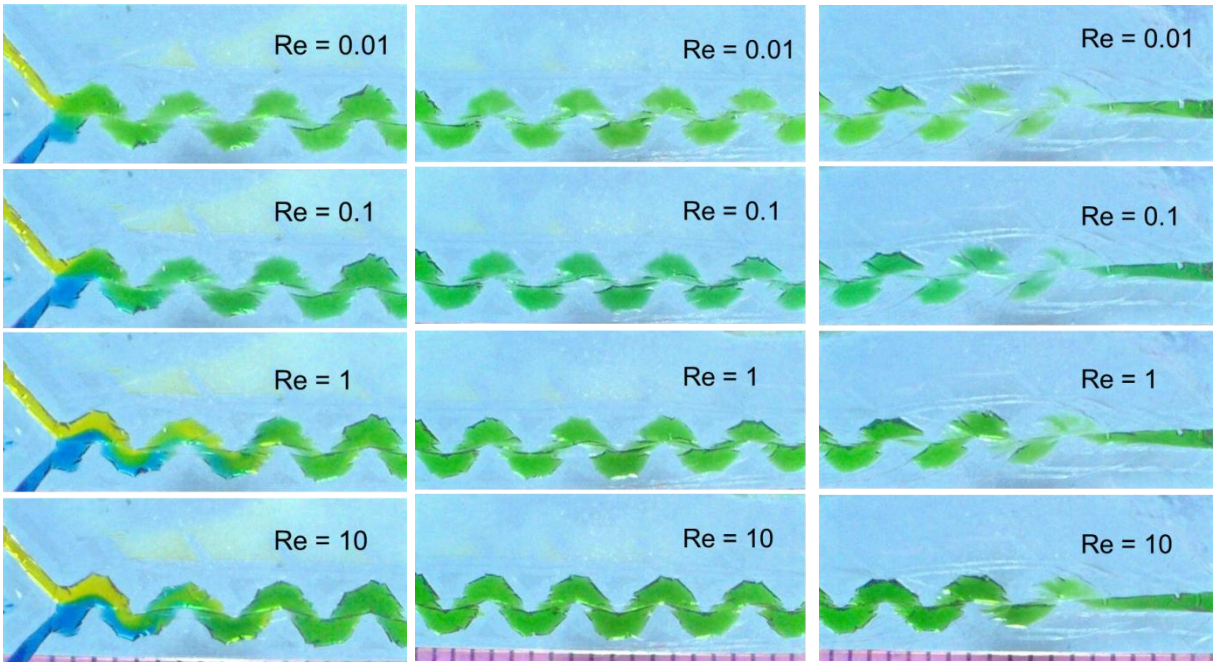

(a) (b) (c)

Figure 31. Images showing the mixing results for narrower serpentine channel and Reynolds numbers from 0.01 to 10; (a) Inlet region; (b) middle section; (c) outlet of the mixer.

The mixing of the narrower serpentine mixer is shown in Figure 31. The results are very similar to the previous for wider channel with the exception of flow at Re = 10, where mixing results at the end of the channel is better than for wider serpentine channel. Visual observations is confirmed by calculated standard deviation of pixel intensity shown in Figure 32 – for narrower serpentine channel it drops to 0.04 indicating mixing of 92% (in comparison, wider serpentine mixer at same cross section and same Re has $\sigma = 0.08$ and mixing 84%).

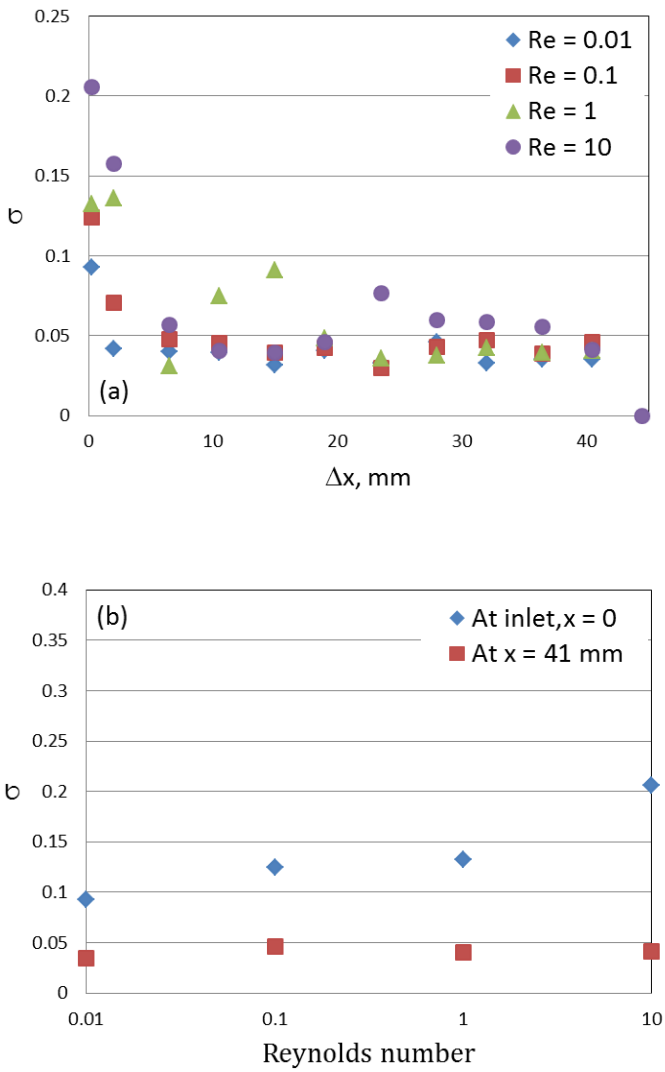

Figure 32. Standard deviation of pixel intensity (a) along the main channel direction of the narrower serpentine micromixer. (b) as a function of Reynolds number.

Figure 33 shows the normalized pixel intensities at two different cross-sections along the main channel direction (at 2 mm and at 13 mm) and for various Reynolds numbers. As compared to the wider serpentine channel (Figure 30), normalized pixel intensity becomes more

uniform across the channel width at shorter distance from the inlet. Comparing pixel intensities at Figure 30b (at 14.5 mm from the inlet) with pixel intensities at Figure 33c (at 13 mm), we can conclude that narrower serpentine channel shows better mixing results than wider serpentine channel.

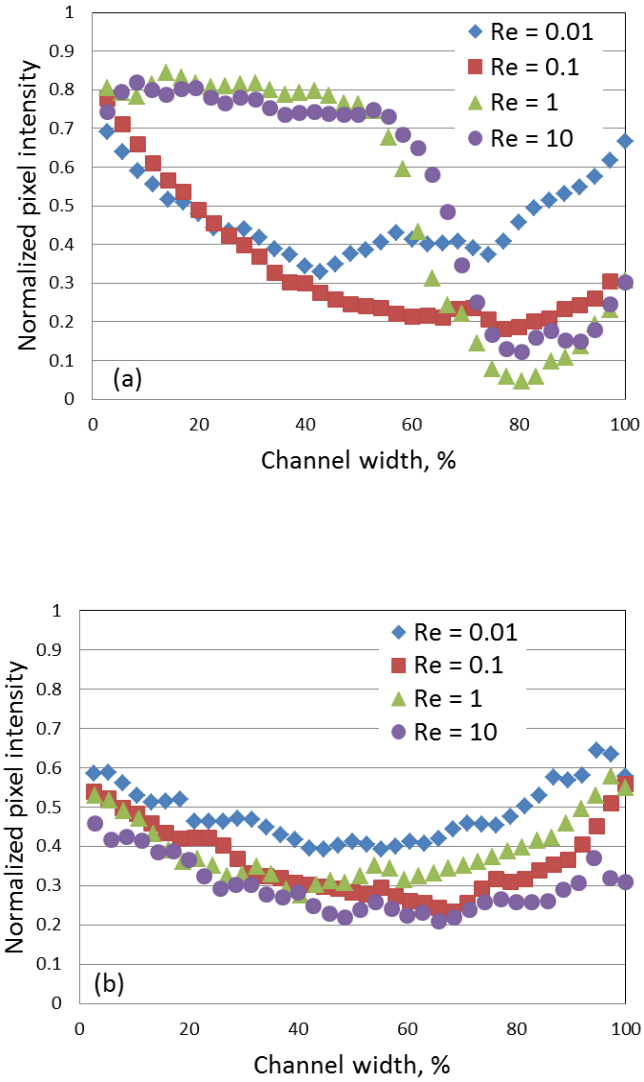

Figure 33. Standard deviation of pixel intensity at the cross section of the mixer channel; (a) at 2 mm from inlet; (b) at 13 mm.

2. Micromixer with obstacles

Micromixer with obstacles was made in order to induce the lateral velocity component of the fluid as well as velocity component parallel to the main channel direction. Lateral movement may lead to forming vortices and enhancing the mixing. The mixing result of colored water solutions are presented in Figures 34 and 37 for two versions of the mixer with obstacles with different channel widths. Results show that for Re = 0.01 and Re = 0.1 (creeping flow), mixing was efficient due to slow diffusion process that completes very near the inlet region. When Reynolds number is increased to Re = 1, the mixing quality deteriorates and we can notice that fluids are not completely mixed at inlets for both mixer versions. At those Reynolds numbers another phenomenon is noticed: eddy formation in the inlet region prior to dividing the channel by obstacles. This is due to sudden change in channel width since all fluid mass from wide channel abruptly needs to flow through three narrow paths. For Re = 10 one fluid starts to flow below the other: we notice more yellow colored fluid at the surface while blue colored fluid is below.

Figure 35 presents calculated standard deviation of pixel intensity across the channel width at different locations along the mixer channel and for different Reynolds numbers. Those results show that mixing is efficient for creeping flow, and not very good for Re = 1 and 10. A similar result is seen in Figure 36, where normalized pixel intensities across the channel widths are shown at the inlet and outlet regions. As Reynolds number increases, normalized intensity at the outlet becomes steeper indicating incomplete mixing.

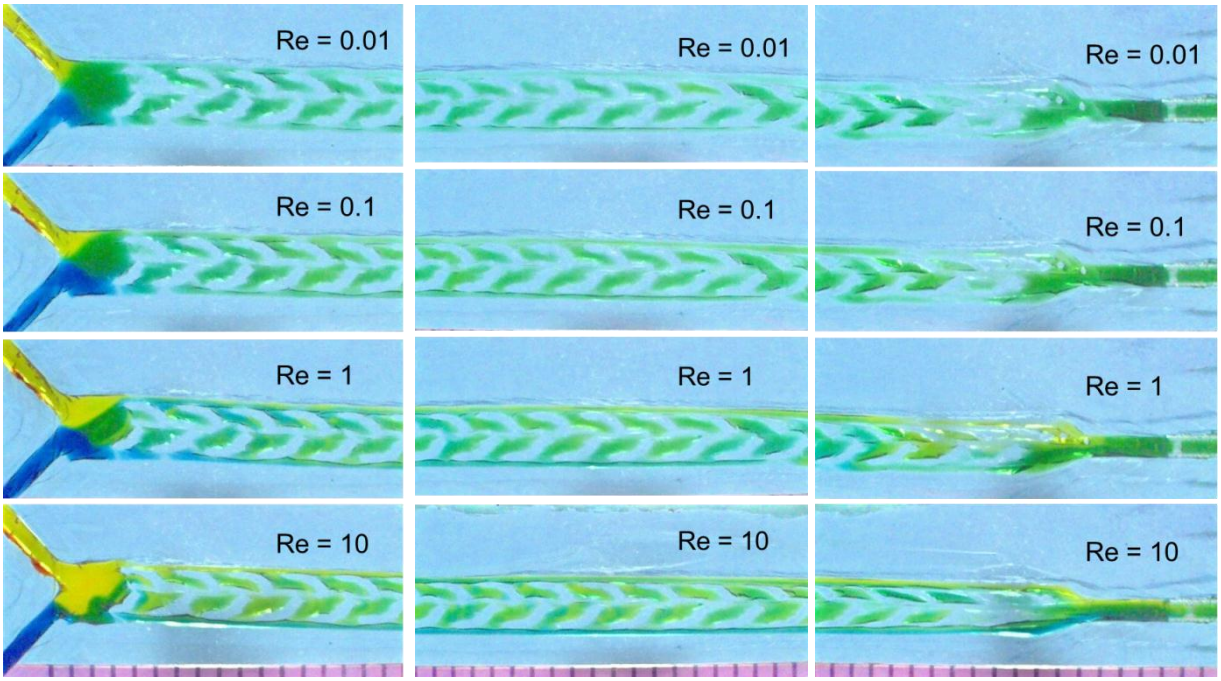

(a) (b) (c)

Figure 34. Images showing the mixing results for mixer with obstacles with wider channel and Reynolds numbers from 0.01 to 10. (a) Inlet region, (b) middle section, and (c) outlet of the mixer.

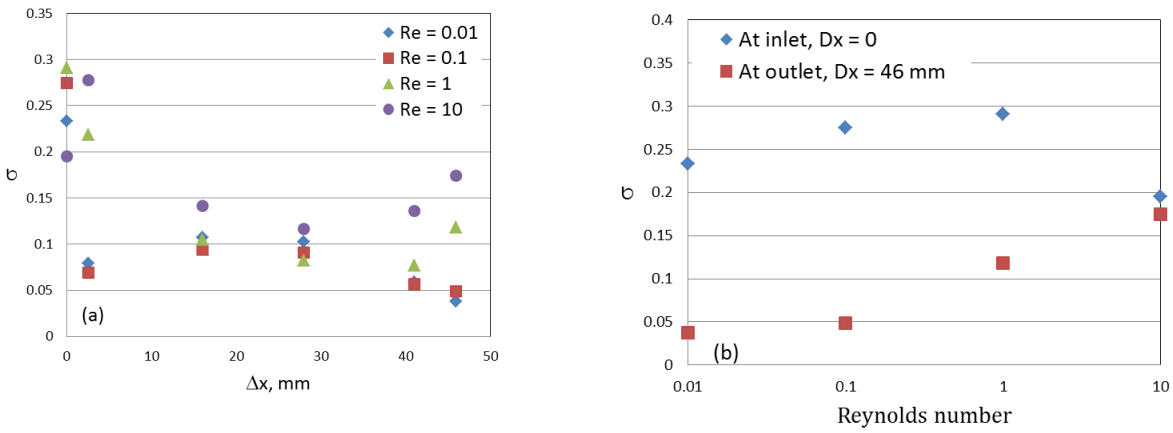

(a) (b)

Figure 35. Standard deviation of pixel intensity (a) along the main channel direction of mixer with obstacles and wide channel; (b) as a function of Reynolds number.

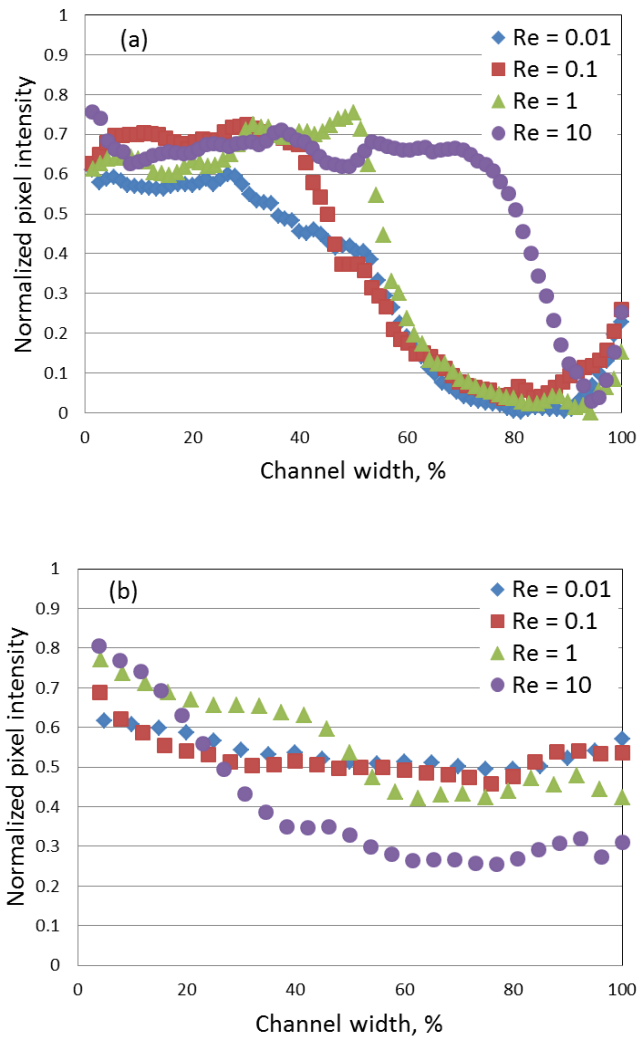

Figure 36. Standard deviation of pixel intensity at the cross section of the mixer channel; (a) At inlet; (b) at outlet.

The results for the narrower version show even less efficient mixing, as presented in Figure 38 and Figure 39. The reason for this is that the fluid path along the central mixer axes is much narrower here and at the inlet region fluid preferably flows toward the upper and lower narrow passages next to the channel walls. Some mixing does occur as fluid is moved along the

obstacle lines downward or upward from the central axes, but that is not very efficient at large Reynolds numbers (1 and 10) because there is a significant flow in the upper and lower narrow paths that provides a straight path through the through the mixer from inlets to outlets. If the welded obstacle lines were made somewhat longer to force the fluid to meander through the channel, the mixing would be more efficient.

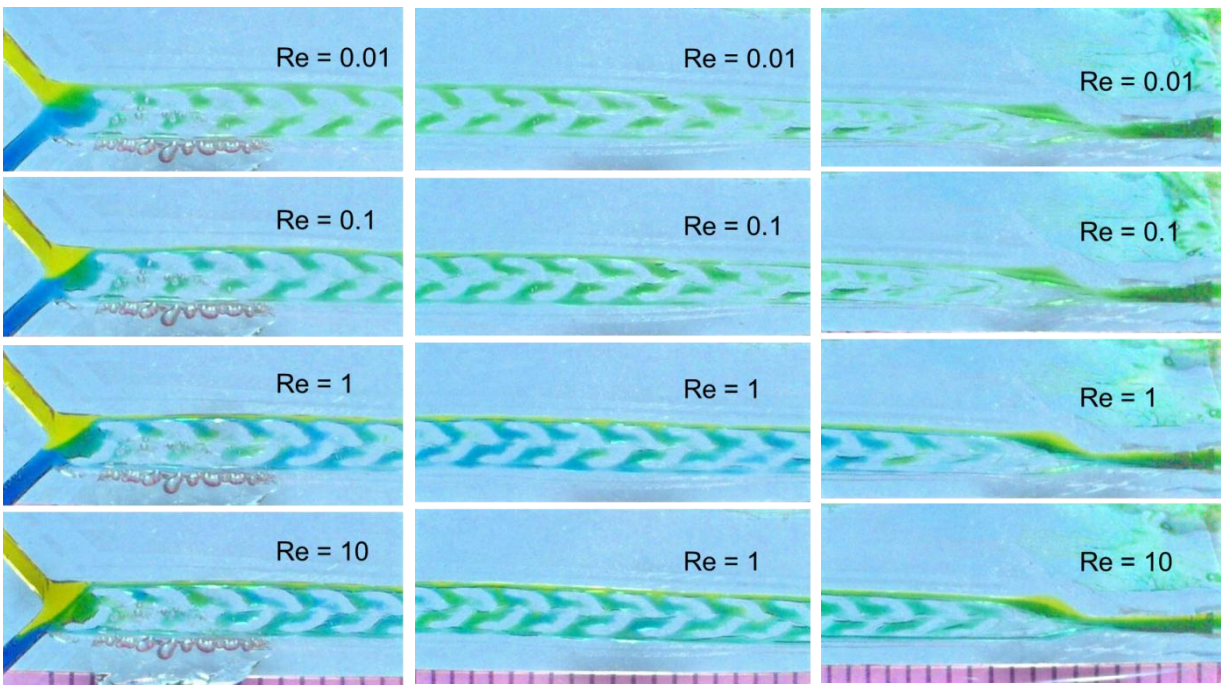

(a) (b) (c)

Figure 37. Images showing the mixing results for mixer with obstacles with narrower channel and Reynolds numbers from 0.01 to 10; (a) Inlet region, (b) middle section, and (c) outlet of the mixer.

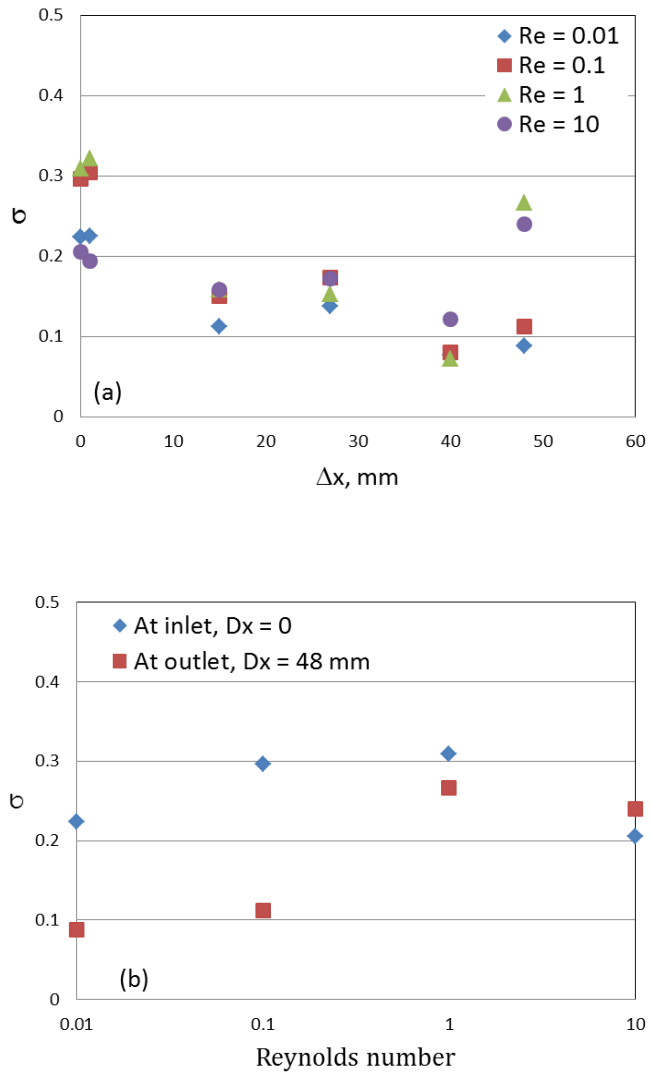

Figure 38. Standard deviation of pixel intensity (a) along the main channel direction of the mixer with obstacles and narrow channel; (b) Standard deviation as a function of Reynolds number.

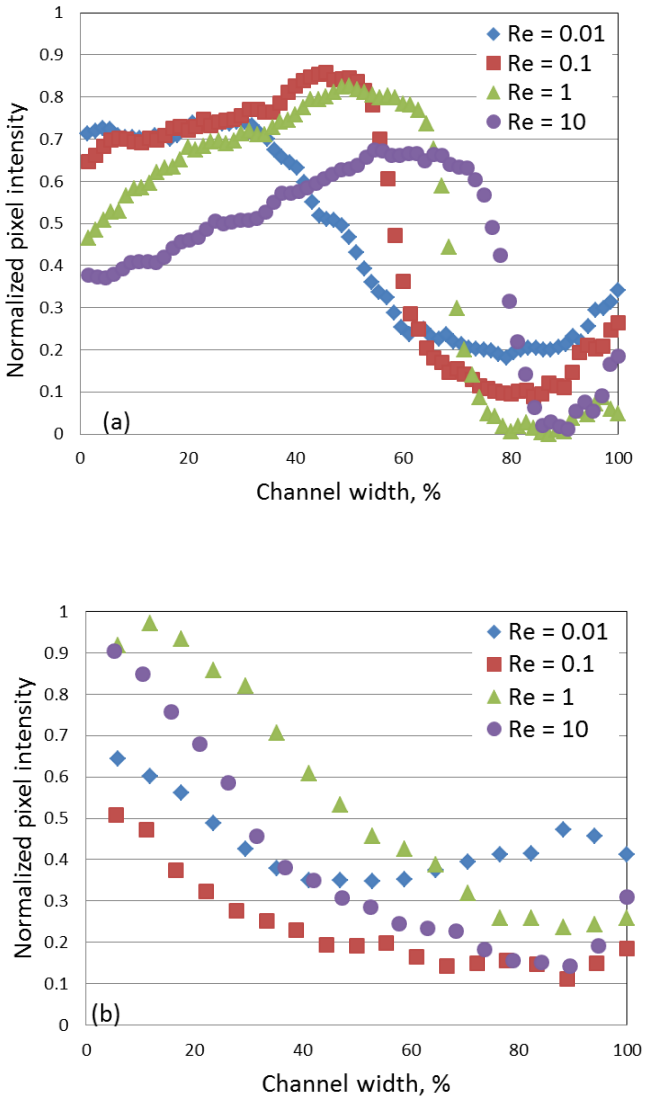

Figure 39. Standard deviation of pixel intensity at the cross section of the mixer channel. (a) at inlet; (b) at outlet.

Better results should be obtained if obstacles were not limited to one half of the mixer channel but are crossing the central mixer axes as shown in Figure 40. Those mixers were of shorter lengths, with only few obstacle segments in the channel, and it is expected that longer

channel would provide better mixing results. However those mixers have much larger pressure drop along the channel and this configuration was not made in long channel version.

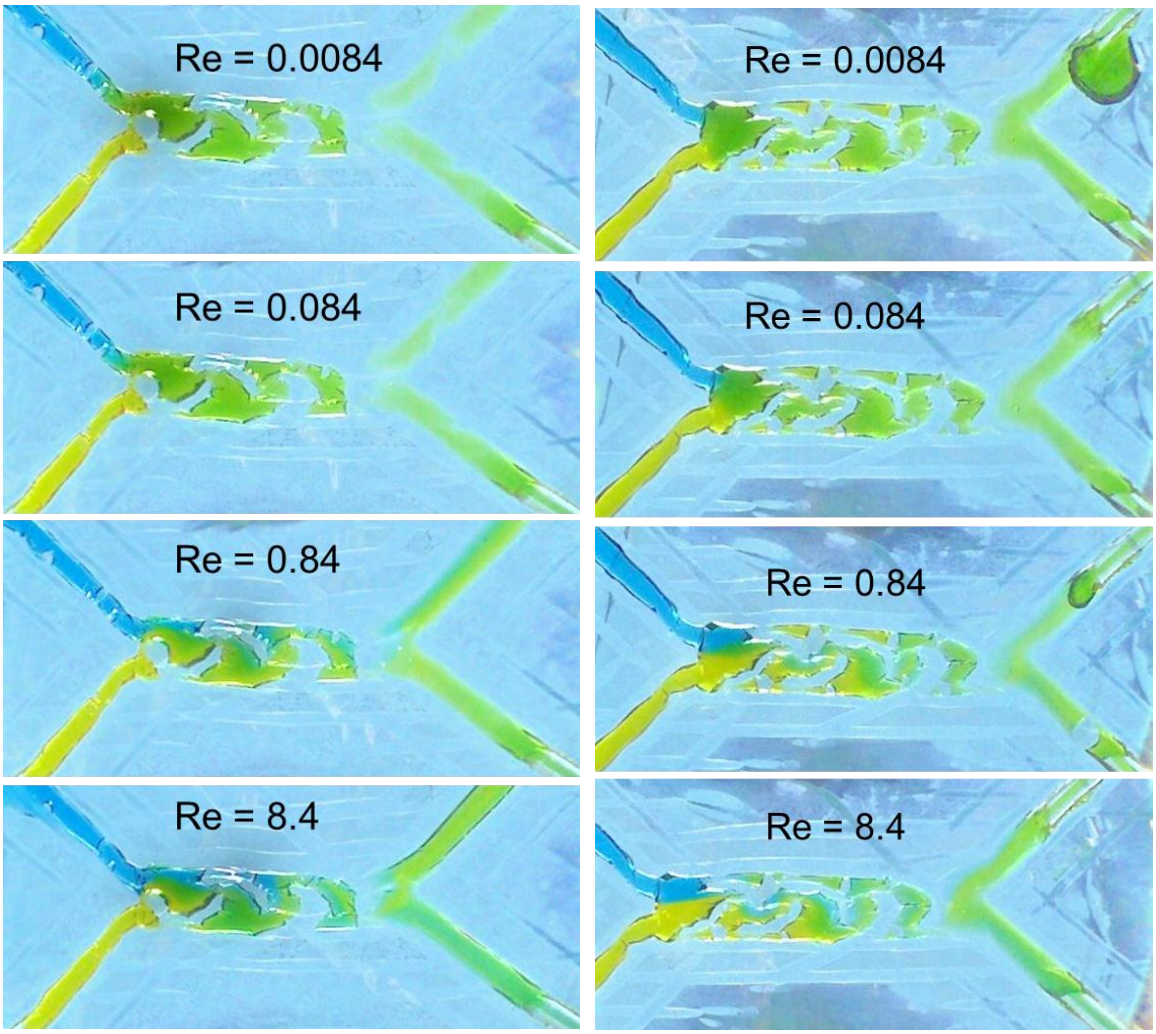

Figure 40. Images showing the mixing results for mixer with obstacles with short channel and Reynolds numbers range from 0.008 to 8.4;

3. Split and Recombine Micromixer

Mixing of two colored water solutions in split-and-recombine mixers is shown in Figure 41 and Figure 44 for two mixer versions. For both, mixing was completed for small Reynolds number and not completed for Re = 1 and Re = 10. Mixer with wider channel have better mixing percent due to the narrower 'recombine' segment – fluid after being split into two paths recombine at narrower part of the channel that in other mixer version.

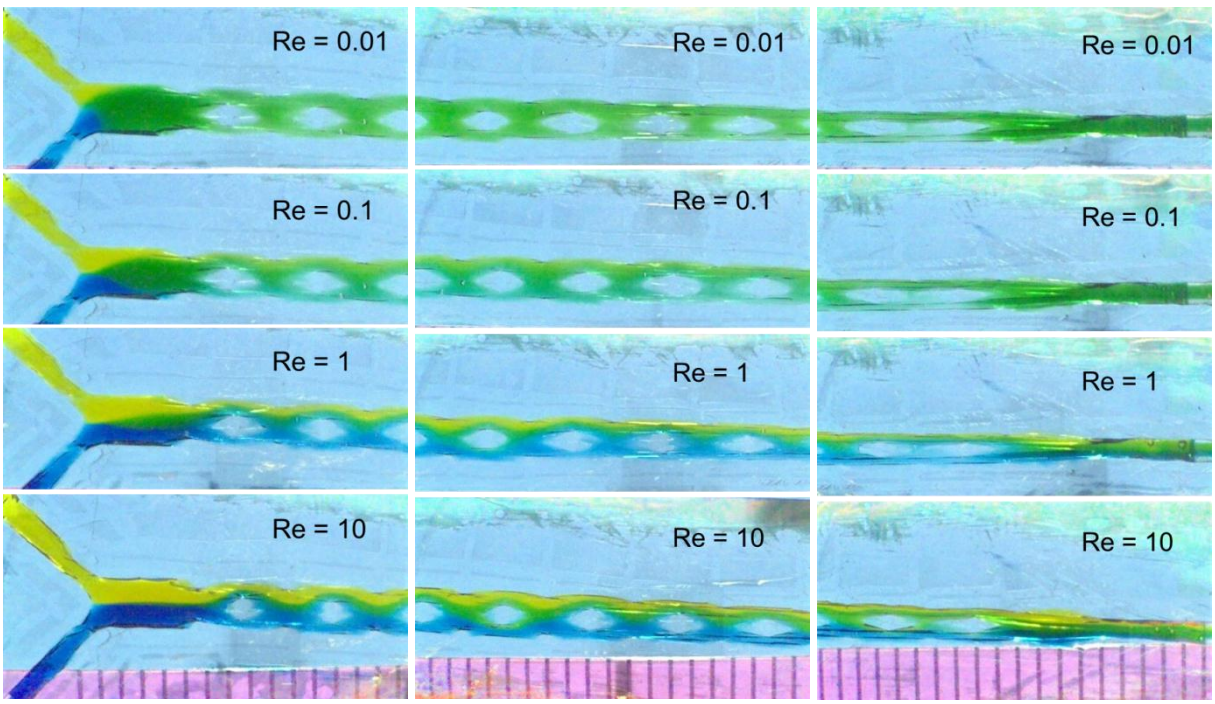

(a) (b) (c)

Figure 41. Images showing the mixing results for split and recombine mixer and Reynolds numbers from 0.01 to 10: (a) Inlet region, (b) middle section, and (c) outlet of the mixer. Length of split and recombine segment is 4 mm.

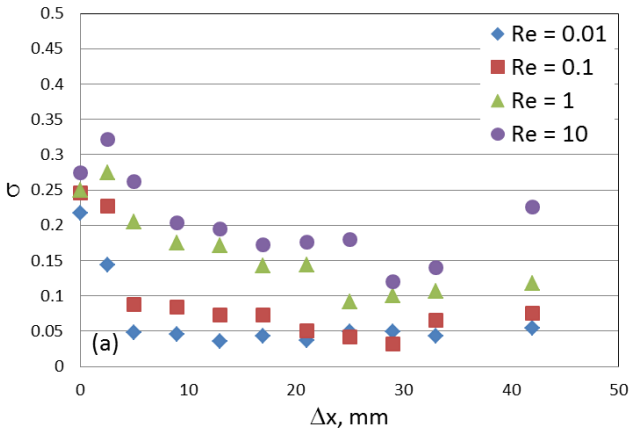

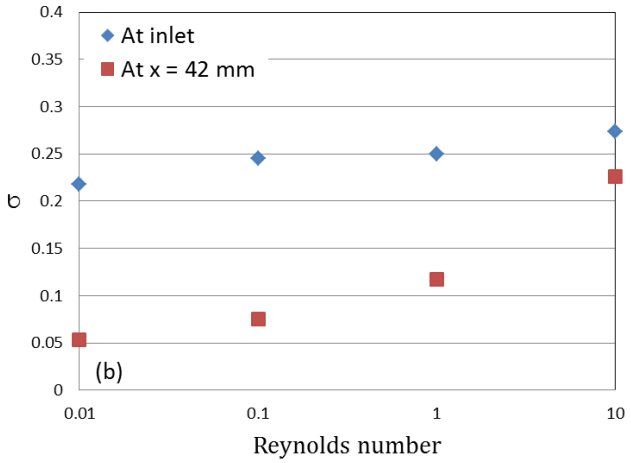

Figure 42. Standard deviation of pixel intensity (a) along the main channel direction of the split and recombine mixer with 4 mm segment length; (b) as a function of Reynolds number.

Figures 42 and 45 show calculated standard deviation of pixel intensity across the channels width and for several positions along the channel length. For Re = 10, standard deviation of wider mixer is 0.1723 (which corresponds to 65.5% mixing) , while for narrower mixer it is 0.2257 (54.9% mixing).

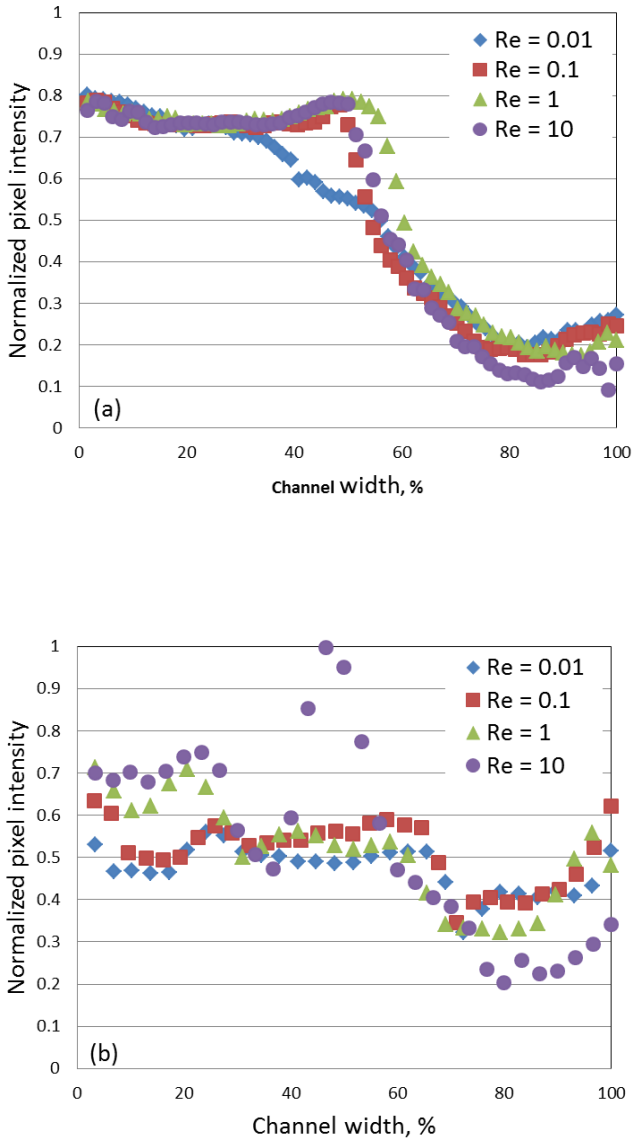

Figure 43. Standard deviation of pixel intensity at the cross section of the mixer channel. (a) at inlet; (b) at 42 mm from inlet.

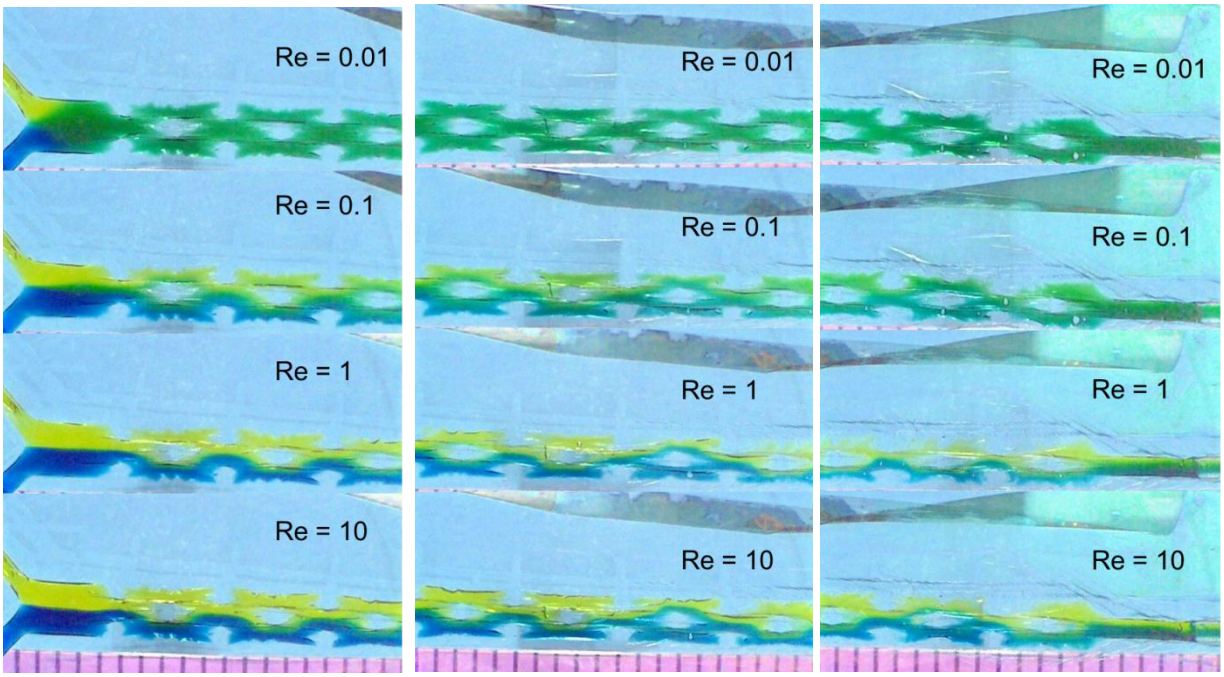

(a) (b) (c)

Figure 44. Images showing the mixing results for split and recombine mixer and Reynolds numbers from 0.01 to 10; (a) Inlet region, (b) middle section, and (c) outlet of the mixer. Length of split and recombine segment is 5 mm.

Figure 43 and Figure 46 show the normalized pixel intensities of the channel cross-section for both mixers, at the inlet and after the tenth mixing segment. The inlet region is characterized with insignificant change in normalized pixel intensities for all Reynolds number. Near the outlet, after tenth segment, pixel intensity has broad range of values for Re = 1 and Re = 10. For wider mixer there is less steep profile for all Reynolds numbers from 0.01 to 10.

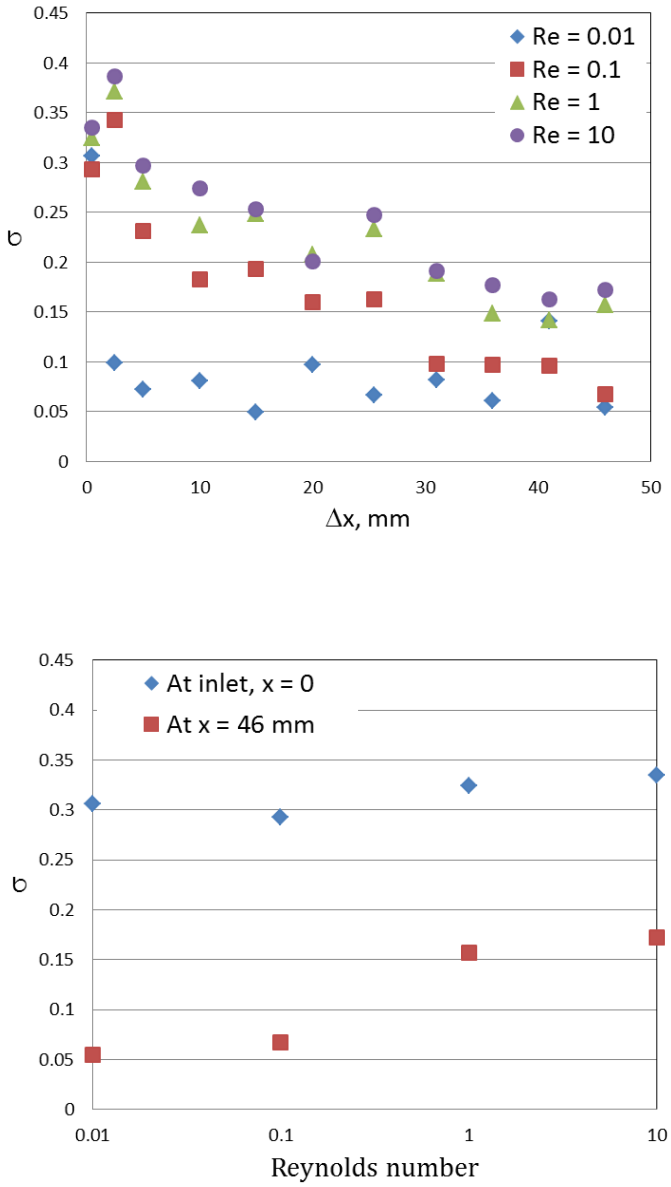

Figure 45. Standard deviation of pixel intensity (a) along the main channel direction of the split and recombine mixer with 5 mm segment length; (b) as a function of Reynolds number.

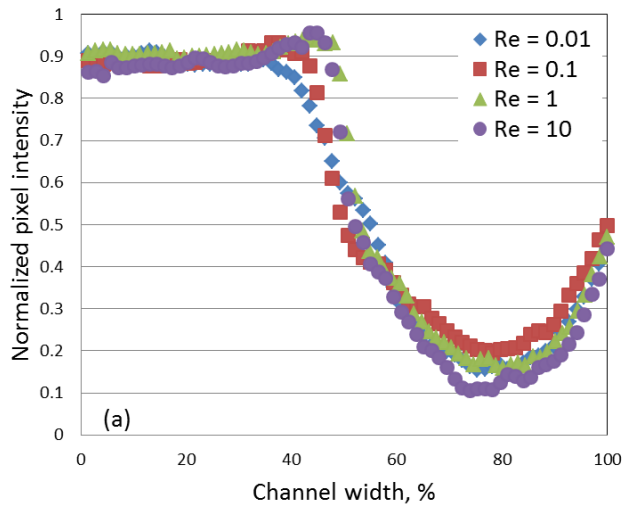

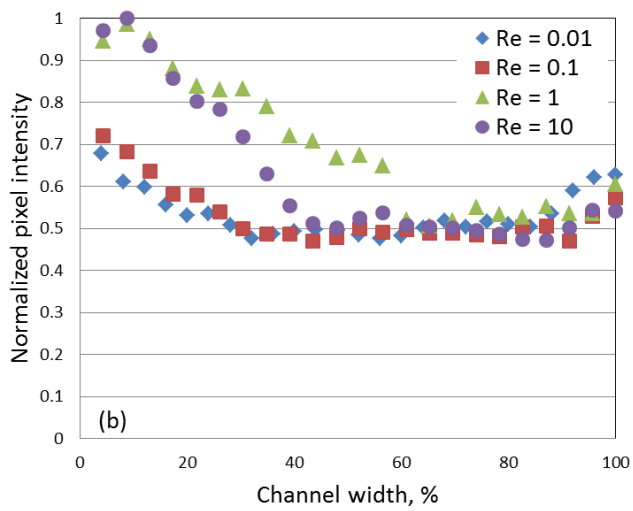

Figure 46. Standard deviation of pixel intensity at the cross section of the mixer channel. (a) at inlet; (b) at 46 mm from inlet.

4. Y-mixer

Mixing results of the colored water solutions in Y-mixer are shown in Figure 47. Mixing for the small Reynolds number Re = 0.01 and Re = 0.1 completes within the channel. For Re = 1 and Re = 10 mixing does not complete in the channel as expected according to equation (3.6).

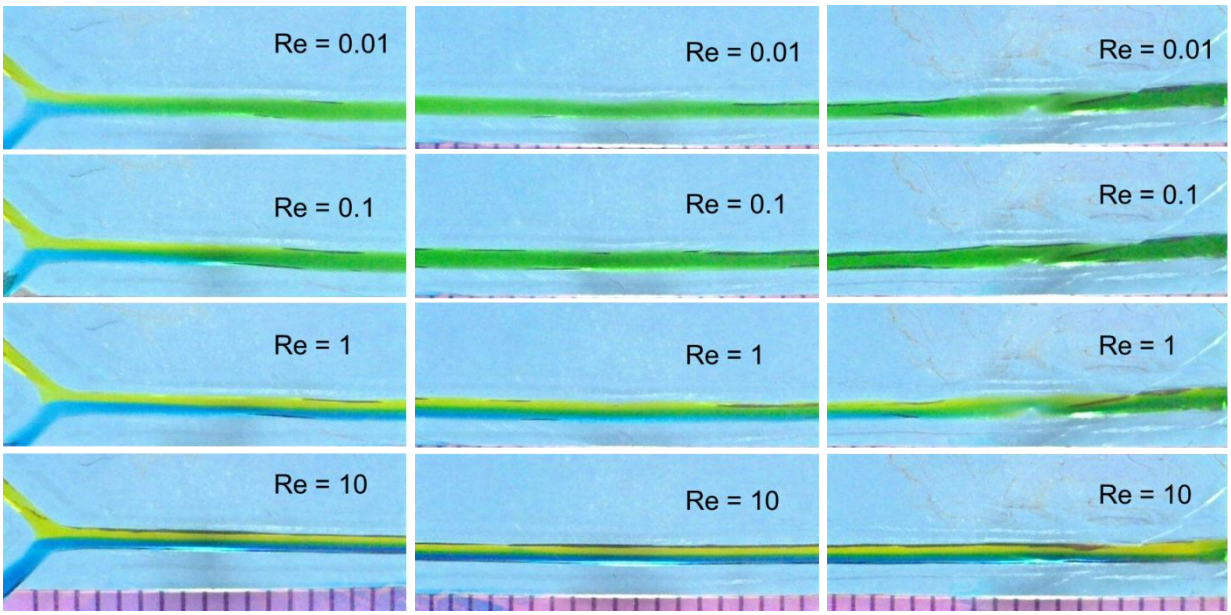

(a) (b) (c)

Figure 47. Images showing the mixing results for Y-mixer and Reynolds numbers from 0.01 to 10. (a) Inlet region, (b) middle section, and (c) outlet of the mixer.

Figure 48 shows the standard deviation of pixel intensity at the inlet and outlet of the mixer for different Reynolds numbers. It is noticeable that standard deviation increases with increase of Re. Figure 49 shows normalized pixel intensities at the inlet region, and at 25 mm and 50 mm

distance from inlet. For creeping flow normalized pixel intensity levels at the end of the channel, but for Re = 1 and Re = 10 the different levels of pixel intensities indicate low mixing, especially for Re = 10 where there is a steep transition from two main levels.

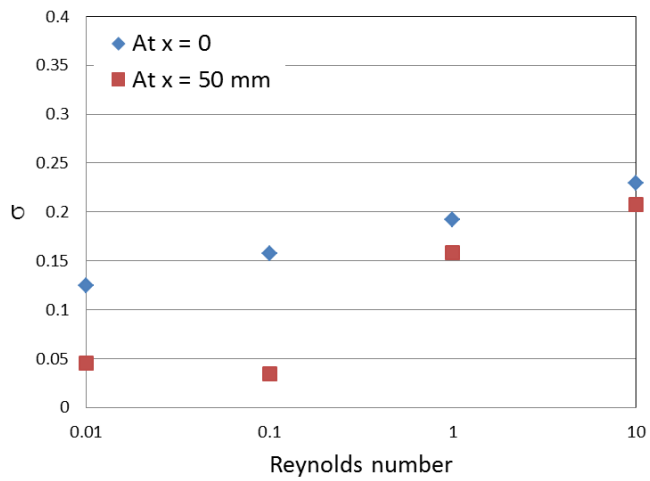

Figure 48. Standard deviation of pixel intensity for the Y-mixer channel as a function of Reynolds number.

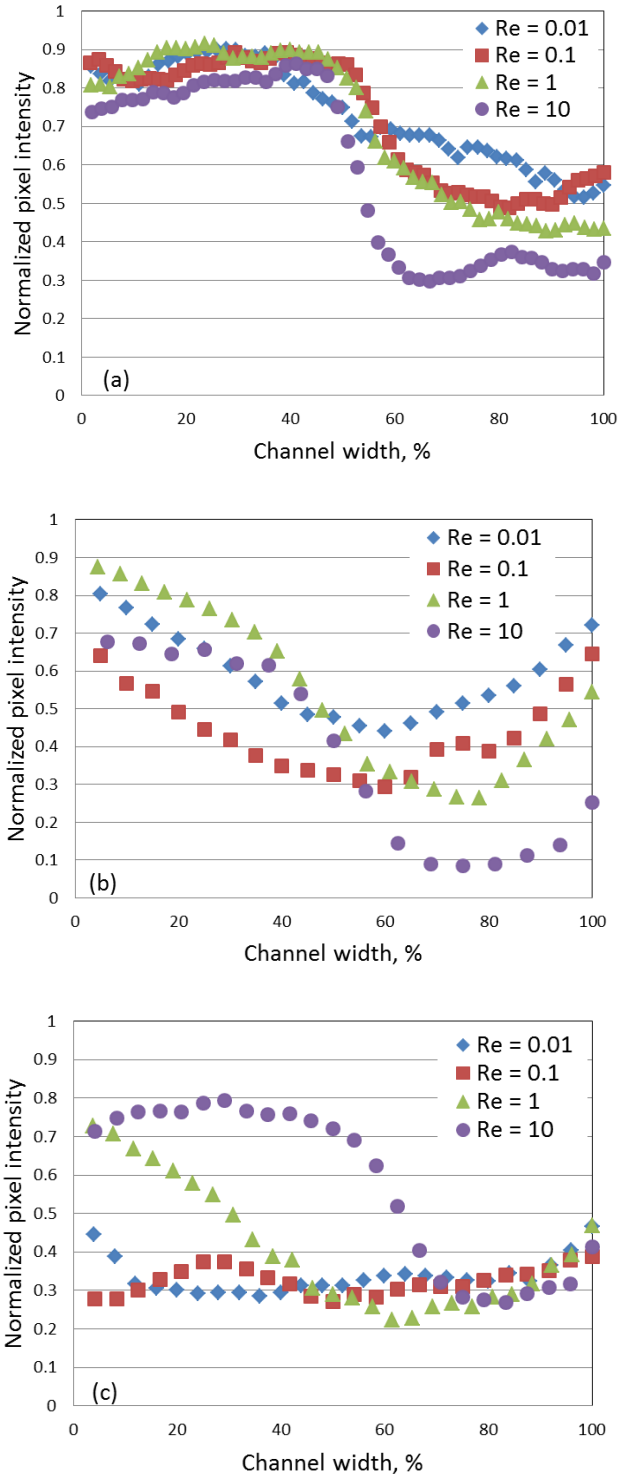

Figure 49. Standard deviation of pixel intensity at the cross section of the mixer channel (a) At inlet; (b) at 25 mm from inlet; (c) at 50 mm from inlet.

F. Conclusion and Future Work

The proposed fabrication method for welding very thin polyester sheets was used to produce several types of micromixers and demonstrate its potential use for producing different designs of mixer structures that can be modified as needed without the need for a photolithography or microfabrication facilities. The proposed fabrication technique limits the design of the mixer to planar types. The possibility of creating three dimensional structures is still under investigation. It would require an alignment step that we were able to avoid in the present fabrication method.

The comparison of mixers characteristics is given in Table 1. The best mixing results are obtained for serpentine mixers, and for the narrow version mixer we can see that mixing of more than 90% was completed for all tested flow rates and Reynolds numbers. Wider version also performs well – the mixing is above 90% for all Reynolds number except for Re = 10 where it is 83.8%.

Mixer with obstacles shows better results for wider model because it allows larger flow through the central path that flows through the upper and lower branches near the channel's lateral edges. The result might be better if obstacles were more curved and interdigitated, but that would contribute to larger pressure drop from inlet to outlet region. Pixel data were taken across the entire mixer channel width which also includes the obstacles, so mixing quality is actually better than the results shown in the Table 1.

Split-and-recombine unexpectedly showed better result for wider channel and longer mixing segments and that was due mostly to narrower channel width in the regions between the mixing segments. Y-channel was made for comparison to other mixer types. Not taking the creeping flow data into account, serpentine mixer has the best mixing quality, then mixer with obstacles, while split-and-recombine mixer has results approximately same as Y-mixer.

TABLE I

COMPARING MIXING RESULTS OF FABRICATED MICROMIXERS

Mixer type		Reynolds number	Standard deviation at outlet	Mixing at outlet, %
Serpentine	Narrow	0.01	0.034977	93.00456
		0.1	0.046115	90.77697
		1	0.040802	**91.83957**
		10	0.04117	**91.76593**
	Wide	0.01	0.039937	92.01264
		0.1	0.028843	94.23137
		1	0.045396	**90.92081**
		10	0.080914	**83.81713**
With obstacles	Narrow	0.01	0.087964	82.40718
		0.1	0.111866	77.62679
		1	0.266051	**46.78988**
		10	0.239632	**52.07352**
	Wide	0.01	0.027869	94.42619
		0.1	0.040481	91.9038
		1	0.097771	**80.44578**
		10	0.123204	**75.35922**
Split-and-recombine	Narrow	0.01	0.05365	89.26997
		0.1	0.074832	85.03369
		1	0.117484	**76.50329**
		10	0.225771	**54.84574**
	Wide	0.01	0.054465	89.10693
		0.1	0.067591	86.48183
		1	0.157329	**68.53421**
		10	0.172281	**65.54375**
Y-mixer		0.01	0.045378	90.92449
		0.1	0.088891	93.16008
		1	0.074862	**68.27806**
		10	0.149774	**58.53795**

Compliant nature of described devices can be very useful for mixer operations. The problem that occurs in many experiments is the appearance of bubbles. With compliant structure bubble can carefully be moved through the channel by gently applying pressure on the outside of the channel.

It was noted that fluid mass is large compared to the mass of the mixer channel, due to very thin Mylar layers used in mixer fabrication. The density of water and Mylar are comparable (1g/cm^3 for water and 1.4 g/cm^3 for Mylar), but the volumes are very different. For example, calculations show that water mass in a Y-channel (5.2 mm long and 0.076 mm^2 cross-section area) is ~0.024 g, and for the Mylar material (same length, thickness 2.8 μm and width of Mylar strip ~1.5 cm) it is only 0.003 g. This can cause the bending of the channel especially if the Mylar is not tightly stretched from inlet to outlet on the LDPE supports.

Due to very thin polyester material used devices show a certain fragility which must be taken into account when using the devices. This fragility can manifest itself at higher fluid flow rates when fluid can damage the channel weld line, especially at regions where there is a sudden change in channel width. This limits the range of fluid flow rates for proposed compliant mixers.

IV. CONCLUSIONS AND FUTURE WORK

The proposed fabrication method for welding very thin polyester sheets was demonstrated in creating different microfluidic devices such as microvale and micromixer presented in Chapter 2 and Chapter 3. Other microdevices were researched: microvalve, electrophoresis channels and pressure sensor. All devices are characterized with planar layout since the three-dimensional branching is not developed yet.

The main goal should be obtaining repeatedly thin welded line thicknesses, both in experiments and production. This would enable the creation of microfluidic devices with smaller channel widths. For micromixers the thinner weld line would allow more complex devices while keeping the fluid channels narrow. It is also important for electrophoresis channels where the channel diameter should be kept under 100 μm diameter for channel lengths ~10 cm.

To achieve the thin welded lines without trying to focus directly on to the Mylar sheet surface (since that proved to be very sensitive situation due to imperfect stretching of the film), the properly designed mask may be positioned on top of the vacuum tool and stretched Mylar, so that widening the laser beam below the focus point could be prevented by making the beam pass through slit openings. This however will require including an alignment step if vector option is used as described. There is the possibility to use a rastering option where the alignment step could be avoided, but the laser processing time will be largely increased. The rastering may need to be tested in more details to make sure that no gaps are left in the weld lines.

In previous experiments the photolithography process applied on thin Mylar sheets proved the possibility of etching the gold layer in microfabrication facility and creating precisely defined

gold pattern on its surface. Figure 50 shows the patterned gold resistors with 20 μm metal line thickness. Standard photolithography process was used with the addition of designed plastic holders to keep the Mylar flat and stretched during the process. The metal etching can be used to fabricate complex systems consisting of few devices (valves, mixers, pumps, reservoirs) fabricated on the same Mylar piece where electrostatically actuated devices are electrically connected via gold pattern resistor lines to the peripheral electrical contacts.

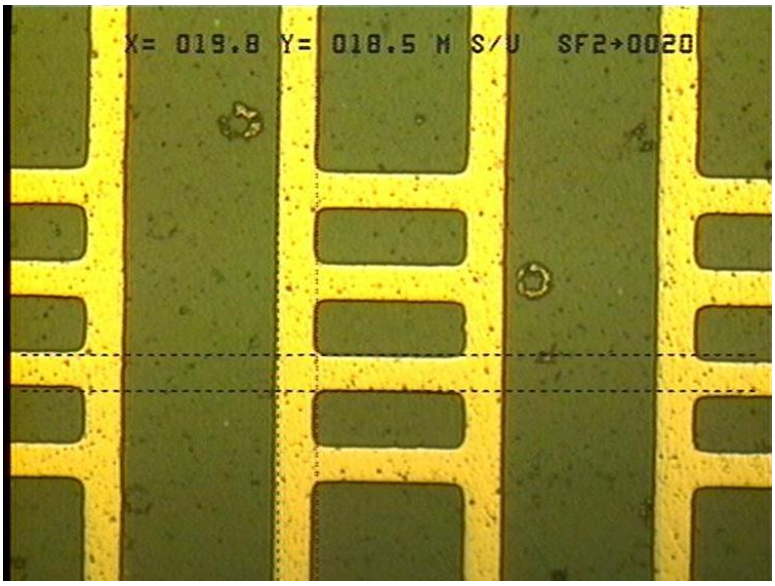

Figure 50. Patterned gold structure on Mylar film after etching the 10 nm gold layer, using standard photolithography process.

Micropump is one of the most investigated microfluidic devices. Since the first reported pumps appeared about thirty years ago, many different designs and techniques for manufacturing were proposed. The micropump that we propose would consist of a series of at least three identical electrostatically actuated microvalves. The schematic drawing of the micropump is

shown in Figure 51. Red lines show the weld lines for the device. The AutoCAD drawing would be very similar to the microvalve drawing with the only difference in the length of the channel since three microvalves are required to be placed in series. Metallization (thin gold layer) has to be removed from certain regions to electrically isolate contacts for all three valves. On the drawing light blue rectangles are gold regions on the upper side of the device. On the bottom side (dark blue region) the optimal solution would be to use only one metallized region (although it is possible to construct completely separate contacts for each valve).

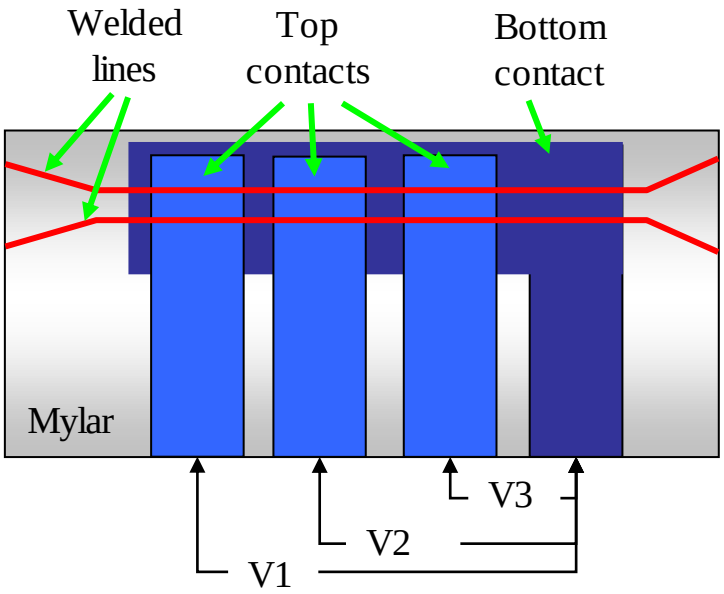

Figure 51. Schematic representation of the micropump. Top (light blue) and bottom (dark blue) gold regions are then connected to conductive black plastic to form electrical contacts for valves operation.

Each valve would be operated independently using the voltages appropriate for the valve channel diameters. Since we propose all three valves to be the identical, voltages would be of equal value. Microvalves would close and open in certain order as shown in Figure 52: close the first, then the second, and at last the third valve so that fluid which was present in their channels would be pushed toward the outlet. This ends in the third fifth of the cycle. Then we can start opening the first valve (in the fourth fifth of the cycle), then the second (in the last fifth of the cycle). Closing the first valve again begins in the next cycle. The bidirectional pumping can easily be achieved by reversing the voltages on individual valves, since geometry of the structure is completely symmetrical.

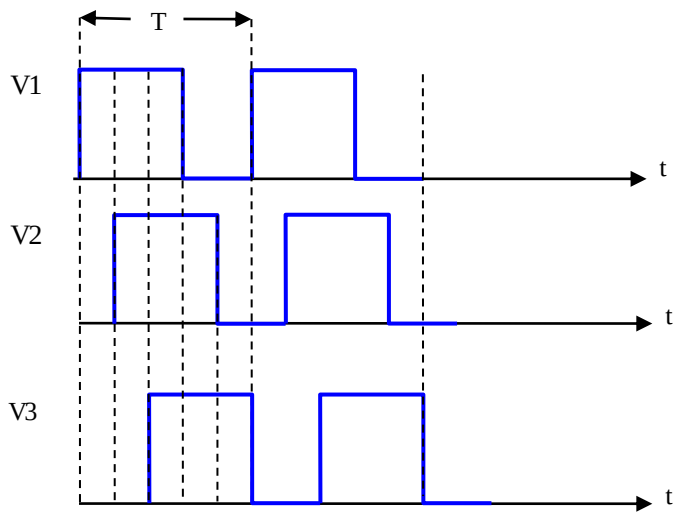

Figure 52. Voltages applied to micropump.

The fabrication of microvalve will require an alignment step because metal should be patterned on both upper and lower Mylar sheets. Laser welding can be done prior to metal etching. As a future work on micropumps, the electronic switch for accurate voltage delivery has to be constructed and testing of device performed.

CITED LITERATURE

1. Aiiborski, L.E. and Flierl, D.W.: Physical properties of terephthalate polyethylene films. *Industrial and Engineering Chemistry*, 45: 2290-2295, 1953.

2. Anamelechi, C.C., Truskey, G.A., Reichert W.M.: Mylar^{TM} and Teflon-AF^{TM} as cell culture substrates for studying endothelial cell adhesion. *Biomaterials*, 26: 6887-6896, 2005.

3. Anjewierden, D., Liddiard, G.A. and Gale, B.K.: An electrostatic microvalve for pneumatic control of microfluidic systems. *Journal of Micromechanics and Microengineering*, 22: 025019 (9pp), 2012.

4. Arora, A., Simone, G., Salieb-Beugelaar, G.B., Kim, J.T., and Manz, A.: Latest developments in micro total analysis systems. *Analytical Chemistr*y, 82: 4830-4847, 2010.

5. Ashby, M.F.: Materials selection in Mechanical Design. Oxford, Butterworth-Heinemann, 1999.

6. Auroux, P.A., Iossifidis, D., Reyes, D.R., and Manz, A.: Micro total analysis systems. 2. Analytical standard operations and applications. *Analytical Chemistry*, 74: 2637-2652, 2002.

7. Barth, P.W.: Silicon microvalves for gas flow control. In Proceedings, *Transducers '95 - Eurosensors IX*, 2: 276 -279 1995.

8. Becker, H., and Gartner, C.: Polymer microfabrication methods for microfluidic analytical applications. *Electrophoresis*, 21: 12-26, 2000.

9. Becker H., and Locascio, L.E.: Review of *Polymer microfluidic devices*. *Talanta*, 56: 267-287, 2002.

10. Becker, H., and Gartner, C.: Polymer microfabrication technologies for microfluidic systems. *Analytical Bioanal. Chem.*, 390: 89-111, 2008.

11. Beebe, D.J., Mensing, G.A., and Walker, G.M.: Physics and applications of microfluidics in biology. *Annu. Rev. Biomed. Eng*, 4: 261-286, 2002.

12. Bertsch, A., Heimgartner, S., Cousseau, P., and Renaud, P.: Static micromixer based on large-scale industrial mixer geometry. *Lab on a Chip*, 1: 56-60, 2001.

CITED LITERATURE (continued)

13. Bhagat, A.A.S., Peterson, E.T.K., and Papautsky, I.: A passive planar micromixer with obstructions for mixing at low Reynolds numbers. *Journal of Micromechanics and Microengineering*, 17: 1017-1024, 2007.

14. Bhagat, A.A.S., Wurm, K.T., and Papautsky, I.: Evaluation of passive planar microfluidic devices for mixing of particle flows. In Proceedings of SPIE, *Microfluidics, BioMEMS, and Medical Microsystems VI*, 6886: 68860W-68860W-8, 2008.

15. Bhagat, A.A.S., and Papautsky, I.: Enhancing particle dispersion in a passive planar micromixer using rectangular obstacles. *Journal of Micromechanics and Microengineering*, 18: 085005(9pp), 2008.

16. Böhm S., Olthuis W., and Bergveld P.: A plastic micropump constructed with conventional techniques and materials. Sens. Actuators A, Phys., 77: 223-228, 1999.

17. Boone, T.D., Fan, Z.H., Hooper, H.H., Ricco, A.J., Tan, H., and Williams, S. J.: Plastic Advances Microfluidic Devices. *Analytical Chemistry*, 74: 78A-86A, 2002.

18. Bourouina, T., Bosseboeuf, A., and Grandchamp, J.P.: Design and simulation of an electrostatic micropump for drug-delivery applications. *Journal of Micromechanics and Microengineering*, 7: 186-188, 1997.

19. Cabuz, C.: Dielectric related effects in micromachined electrostatic actuators. In proceedings of IEEE, *IEEE Conference on Electrical Insulation and Dielectric Phenomena*, 1: 327-332, 1999.

20. Cabuz, C., Cabuz, E.I., Ohnstein, T.R., Neus, J., and Maboudian, R.: Factors enhancing the reliability of touch-mode electrostatic actuators. *Sensors and Actuators*, 79: 245-250, 2000.

21. Cabuz, C., Herb, W.R., Cabuz, E.I., Liu, S.T.: The dual diaphragm pump. In Proceedings of IEEE, *The 14th IEEE International Conference on Micro Electro Mechanical Systems, 2001. MEMS 2001*, 519-522. 2001.

22. Capretto, L., Cheng, W., Hill, M., and Zhang, X.: Micromixing within microfluidic devices. *Top. Curr. Chm*. 304: 27-68, 2011.

23. Chang, S., and Cho, Y.H.: Static micromixers using alternaling whirls and lamination. *Journal of Micomechanics and Microengineering*, 15: 1397-1405, 2005.

24. Chen, H., and Meiners, J.C.: Topological mixing on a microfluidic chip. *Applied Physics Letters*, 84: 2193-2195, 2004.

CITED LITERATURE (continued)

25. Chung, C.K., and Shih, T.R.: Effect of geometry on fluid mixing of the rhombic micromixers. *Microfluidics and Nanofluidics*, 4: 419-425, 2008.

26. Dankovic, T., and Feinerman, A.: Compliant Micromixers. In Proceedings, *2010 ASME International Mechanical Engineering Congress*, 10: 777-782, 2010.

27. Dankovic, T., and Feinerman, A.: Electrostatically actuated compliant microvalve. In Proceedings, *2012 ASME International Mechanical Engineering Congress*, 2010.

28. Dubois, P., Guldimann, B., Gretillat, M.A., and de Rooij, N.F.: Electrostatically actuated gas microvalve based on a Ta-Si-N membrane. In Proceedings of IEEE, *The 14th IEEE International Conference on Micro Electro Mechanical Systems, 2001. MEMS 2001*, 535 -538, 2001.

29. Easley, C.J., and Landers, J.P.: Practical fluid control strategies for microfluidic devices. In: *Handbook of Capillary And Microchip Electrophoresis And Associated Microtechniques*, ed. J.P. Landers, pp. 1153-1168, Boca Raton, CRC Press, Taylor & Francis Group, 2008.

30. Ehrfeld, W., Golbig, K., Hessel, V., Löwe, H., and Richter, T.: Characterization of mixing in micromixers by a test reaction: single mixing units and mixer arrays. *Industrial & Engineering Chemistry Research*, 38: 1075-1082, 1999.

31. Ehrfeld, W., Hessel, V., Löwe, H., Schulz, C, and Weber, L.: Materials of LIGA technology. *Microsystem Technologies*, 5: 105-112, 1999.

32. Ehrfeld, W., Hessel, V., and Löwe, H.: *Microreactors: New Technology for Modern Chemistry*, page 41, Weinheim, WILEY-VCH Verlag GmbH, 2000.

33. von Elbe, J.H., and Schwartz, S.J.: Colorants, In: *Food Chemistry*, ed. O.R. Fennema, pp. 651-722, New York, Marcel Dekker, Inc., 1996, p. 717.

34. Fahrenberg, J., Bier, W., Maas, D., Menz, W., Ruprecht, R., and Schomburg, W.K.: A microvalve system fabricated by thermoplastic molding. *Journal of Micromechanics and Microengineering*, 5: 169-171, 1995.

35. Falk, L., and Commenge, J.M.: Characterization of mixing and segregation in homogeneous flow systems. In: *Micro Process Engineering. A Comprehensive Handbook, Volume 1: Fundamentals, Operations and Catalysts*. eds. V. Hessel, A. Renken, J.C. Schouten, and J. Yoshida, pp. 147-174, Weinheim, Wiley-VCH Verlag GmbH & Co., 2009, p. 149.

CITED LITERATURE (continued)

36. Fang, J.Z., and Lee, D.J.: Micromixing efficiency in static mixer. *Chemical Engineering Science*, 56: 3797–3802, 2001.

37. Feinerman, A.: Thin Welded Sheets Fluid Pathway. U.S. 2009/0217997 A1, Appl. 11/909,834, 4 May 2006; 22 pp, 3 Sep 2009.

38. Felton, M.J.: The new generation of microvavles. *Analytical Chemistry*, 75: 429-432, 2003.

39. Feng, Y., Zhou, Z., Ye, X., and Xiong, J.: Passive valves based on hydrophobic microfluidics. *Sensors and Actuators A*, 108: 138-143, 2003.

40. Fiorini, G.S., Lorenz, R.M., Kuo, J.S., and Chiu, D.T.: Rapid prototyping of thermoset polyester microfluidic devices. *Analytical Chemistry*, 76: 4697-4704, 2004.

41. Fiorini, G.S., and Chiu, D.T.: Disposable microfluidic devices: fabrication, function, and application. *BioTechniques*, 38: 429-446, Mar. 2005.

42. Fiorini, G.S., Yim, M., Jeffries, G.D.M., Schiro, P.G., Mutch, S.A., Lorenz, R.M., and Chiu, D.T.: Fabrication improvements for the thermoset polyester (TPE) microfluidic devices. *Lab on a Chip*, 7: 923-926, 2007.

43. Gan, H.Y., Lam, Y.C., and Nguyen, N.T.: Polymer-based device for efficient mixing of viscoelastic fluids. *Applied Physics Letters*, 88: 224103, 2006.

44. Gilbert, J.R., Ananthasuresh, G.K., and Senturia, S.D.: 3D modeling of contact problems and hysteresis in coupled electro-mechanics. In Proceedings, *The 9th Annual international Workshop on MEMS*, 127-132, 1996.

45. Gobby, D., Angeli, P., and Gavriilidis, A.: Mixing characteristics of T-type microfluidic mixers. *Journal of Micromechanics and Microengineering,* 11: 126-132, 2001.

46. Goll, C., Bacher, W., Bustgens, B., Maas, D., Menz, W., and Schomburg, W. K.: Microvalves with bistable buckled polymer diaphragms. *Journal of Micromechanics and Microengineering*, 6: 77-79, 1996.

47. Goll, C., Bacher, W., Bustgens, B., Maas, D., Ruprecht, R., and Schomburg, W. K.: An electrostatically actuated polymer microvalve equipped with a movable membrane electrode. *Journal of Micromechanics and Microengineering*, 7: 224-226, 1997.

48. Gorkin, R., Park, J., Siegrist, J., Amasia, M., Lee, B.S., Park, J.M., Kim, J., Kim, H., Madou, M., and Cho, Y.K.: Centrifugal microfluidics for biomedical applications. *Lab on a chip*, 10: 1758-1773, 2010.

CITED LITERATURE (continued)

49. Groisman, A., and Steinberg, V.: Efficient mixing at low Reynolds numbers using polymer additives. *Nature*, 410: 905-908, 2001.

50. Groisman, A., and Quake, S.R.: A microlfuidic rectifier: anisotropic flow resistance at low Reynolds numbers.*Physical Review Letters*, 92: 094501(4 pages), 2004.

51. Haji-Babaei, J., Kwok, C.Y., and Huang, R.S.: Integrable active microvalve with surface micromachined curled-up actuator. In Proceedings, *International Conference on Solid-State Sensors and Actuators, Transducers '97*, 2: 833 – 836, 1997.

52. Hatch, A., Kamholz, A.E., Hawkins, K.R., Munson, M.S., Schilling, E.A., Weigl, B.H., and Yager, P.: A rapid diffusion immunoassay in a T-sensor. *Nat. Biotechnol.*, 19: 461-465, 2001.

53. Heckele, M., and Schomburg, W.K.: Review on micro molding of thermoplastic polymers. *Journal of Micromechanics and Microengineering*, 14: R1-R14, 2004.

54. Henning, A.K.: Microfluidic MEMS," In Proceedings, *IEEE Aerospace Conference*, 1: 471-486, 1998.

55. Hinsmann, P., Frank, J., Svasek, P., Harasek, M., and Lendl, B.: Design, simulation and application of a new micromixing device for time resolved infrared spectroscopy of chemical reactions in solution. *Lab on a Chip*, 1: 16-21, 2001.

56. Hobbs, D.M., and Muzzio, F.J.: The Kenics static mixer: a three-dimensional chaotic flow. Chemical Engineering Journal, 67: 153–166, 1997.

57. Hsu, C.H., Neils, C.M., Tourovskaia, A., and Folch, A.: 'Microcanals' for modulation of the microfluidic environment of cultured cells. In Proceedings, *IEEE 2nd Joint EMBS/BMES Conf.*, 1681-1683, 2002.

58. Huff, M.A., Mettner, M.S., Lober, T.A. and Schmidt, M.A., 1990, "A pressure-balanced electrostatically-actuated microvalve. In Proceedings, *Solid-State Sensors and Actuator Workshop, 4th Technical Digest, IEEE*, 123–127, 1990.

59. Huff, M.A., and Schmidt, M.A.: Fabrication, packaging, and testing of a wafer-bonded microvalve. *Solid-State Sensor and Actuator Workshop, 5th Technical Digest, IEEE*, 194 – 197, 1992.

60. Jeon, M.K., Kim, J.H., Noh, J., Kim, S.H., Park, H.G., and Woo, S.I.: Design and characterization of a passive recycle micromixer. *Journal of Micromechanics and Microengineering*, 15: 346-350, 2005.

CITED LITERATURE (continued)

61. Kamholz, A.E., Weigl, B.H., Finlayson, B.A., and Yager, P.: Quantitative analysis of molecular interaction in a microfluidic channel: the T-sensor. *Anal. Chem*. 71: 5340-5347, 1999.

62. Kämper, K.P., Ehrfeld, W., Döpper, J., Hessel, V., Lehr, H., Löwe, H., Richter, T., Wolf, A.: Microfluidic components for biological and chemical microreactors. *Proceedings of the IEEE MEMS '97*, *10th Annual International Workshop on Micro Electro Mechanical Systems*, 338 – 343, 1997.

63. Kang, T.G., and Kwon, T.H.: Colored particle tracking method for mixing analysis of chaotic micromixers. *Journal of Micromechanics and Microengineering*, 14: 891-899, 2004.

64. Khan Malek, C., Saile, V.: Applications of LIGA technology to precision manufacturing of high-aspect-ratio micro-components and systems: a review. *Microelectronics Journal*, 35: 131-143, 2004.

65. Khan Malek, C.G..: Laser processing for bio-microfluidics applications (part I). *Analytical and Bioanalytical Chemistry*, 385: 1351-1361, 2006.

66. Khan Malek, C.G.: Laser processing for bio-microfluidics applications (part II). *Analytical and Bioanalytical Chemistry*, 385: 1362-1369, 2006.

67. Kim, D., and Beebe, D.J.: A bi-polymer micro one-way valve. *Sensors and Actuators A*, 136: 426-433, 2007.

68. Kim, D.S., Lee, S.W., Kwon, T.H., and Lee, S.S.: A barrier embedded chaotic micromixer. *Journal of Micromechanics and Microengineering*, 14: 798-805, 2004.

69. Kim, H., Astle, A.A., Najafi, K., Bernal, L.P., and Washabaugh, P.D.: A fully integrated high-efficiency peristaltic 18-stage gas micropump with active microvalves. In Proceedings, *20th International Conference on Micro Electro Mechanical Systems*, 131 – 134, 2007.

70. Kim, H., and Najafi, K.: Electrostatic hydraulic three-way gas microvalve for high-pressure applications. *Twelfth International Conference on Miniaturized Systems for Chemistry and Life Sciences*, 396-371, 2008.

71. Kim, J.Y., deMello, A.J., Chang, S.I., Hong, J., and O'Hare, D.: Thermoset polyester droplet-based microfluidic devices for high frequency generation. *Lab on a chip*, 11: 4108-4112, 2011.

CITED LITERATURE (continued)

72. Koch, M., Witt, H., Evans, A.G.R., and Brunnschweiler, A.: Improved characterization technique for micromixers. *Journal of Micromechanics and Microengineering*, 9: 156-158, 1999.

73. Koo, J.M., Im, S., Jiang, L., and Goodson, K.E.: Integrated microchannel cooling for three-dimensional electronic circuit architectures. *Journal of Heat Transfer,* 127: 49-58, 2005.

74. Kovacs, G.T.A.: *Micromachined Transducers Sourcebook*, p. 823, Boston, McGraw-Hill, 1998.

75. Kricka, L.J., Fortina, P., Panaro, N.J., Wilding, P., Alonso-Amigo, G., and Becker, H.: Fabrication of plastic microchips by hot embossing. *Lab on a Chip*, 2: 1-4, 2002.

76. Lee, A.P., Hamilton, J., Trevino, J.: A low power, tight seal, polyimide electrostatic microvalve. In Proceedings, *MEMS Symposium of DSCD, International Mechanical Engineering Congress and Exposition*, 9 pages, 1996.

77. Lee, J., Kwon, S.: Mixing efficiency of a multilamination micromixer with consecutive recirculation zones: *Chemical Engineering Science*, 64: 1223-1231, 2009.

78. Lee, J.N., Park, C., and Whitesides, G.M.: Solvent compatibility of poly(dimethylsiloxane) -based microfluidic devices. *Analytical Chemistry*, 75: 6544-6554, 2003.

79. Lee, S.W., Kim,D.S., Lee, S.S., and Kwon, T.H.: A split and recombination micromixer fabricated in a PDMS three-dimensional structure: *Journal of Micromechanics and Microengineering*, 16: 1067-1072, 2006.

80. Legtenberg, R., Gilbert, J., Senturia, S.D., and Elwenspoek, M.: Electrostatic curved electrode actuators," *Journal of Microelectromechanical Systems*, 6: 257 – 265, 1997.

81. Levine, L.M.: Developing diagnostic products using polymer laminate technology. Available: http://www.alineinc.com/technical_articles.html, llevine@alineinc.com

82. Li, K., Miville-Godin, C., Normandin, F., Roy, E., Veres, T.: Fabrication of thermal plastic microfluidic devices with peristaltic micropumps and microvalves. In Proceedings, *The 2nd European Conference on Microfluidics, Microfluidics 2010*, 1222-DD05-24 (6 pages)., 2010.

83. Li, P., Coswell, J., and Faghri, M.: Design and test of a passive planar labyrinth micromixer for rapid fluid mixing. *Sensors and Actuators B*, 174: 126-132, 2012.

CITED LITERATURE (continued)

84. Li, X.B., Li, F.C., Cai, W.H., Zhang, H.N., and Yang, J.C.: Very-low-Re chaotic motions of viscoelastic fluid and its unique applications in microfluidic devices: A review. *Experimental Thermal and Fluid Science*, 39: 1-16, 2012.

85. Liu, R.H., Stremler, M.A., Sharp, K.V., Olsen, M.G., Santiago, J.G., Adrian, R.J., Aref, H., and Beebe, D.J.: Passive mixing in tree-dimensional serpentine microchannel. *Journal of Microelectromechanical Systems*, 9: 190-197, 2000.

86. Liu, Y.Z., Kim, B.J., and Sung, H.J.: Two-fluid mixing in a microchannel. *International Journal of Heat and Fluid Flow*, 25: 986-995, 2004.

87. Madou, M.J.: *Fundamentals of Microfabrication: The Science of Miniaturization*, *Second Edition*, New York, CRC Press, 2002.

88. Mansur, E.A., Mingxing, Y., Yundong, W., and Youyuan, D.: A state-of-the-art review of mixing in microfluidic mixers. *Chinese Journal of Chemical Engineering*, 16: 503-516, 2008.

89. Manz, A., Graber, N., and Widmer, H.M.: Miniaturized Total Chemical Analysis Systems: a Novel Concept for Chemical Sensing. *Sensors and Actuators B*, 1: 244-248, 1990.

90. Meijer, J.: Laser micromachining. In: *Micromachining of Engineering Materials*. ed. J. McGeough, pp. 203-238, New York, Marcel Dekker, Inc., 2002.

91. Mengeaud, V., Josserand, J., and Girault, H.H.: Mixing processes in a zigzag microchannel: finite element simulations and optical study. *Analytical Chemistry*, 74: 4279-4286, 2002.

92. Messner, S., Schaible, J., Vollmer, J., Sandmaier, H., and Zengerle, R.: Electrostatic driven 3-way silicon microvalve for pneumatic applications. In Proceedings, *IEEE The Sixteenth Annual International Conference on Micro Electro Mechanical Systems*, 88 – 91, 2003.

93. Messner, S., Schaible, J., Sandmaier, H., Zengerle, R.: 3-way silicon microvalve for pneumatic applications with electrostatic actuation principle. *Microfluid nanofluid*, 2: 89-96, 2006.

94. Mizuno, Y., and Funakoshi, M.: Chaotic mixing due to a spatially periodic three-dimensional flow. *Fluid Dynamics Research*, 31: 129-149, 2002.

95. Mouza, A A., Patsa, C.M., and Schonfeld, F.: Mixing performance of a chaotic micro-mixer. *Chemical Engineering Research and Design*, 86: 1128-1134, 2008.

CITED LITERATURE (continued)

96. Munson, M.S., and Yager, P.: Simple quantitative optical method for monitoring the extent of mixing applied to a novel microfluidic mixer. *Analytica Chimica Acta*, 507: 63–71, 2004.

97. Neils, C., Tyree, Z., Finlayson, B., and Folch, A.: Combinatorial mixing of microfluidics streams. *Lab Chip*, 4: 342-350, 2004.

98. Nguyen, N.-T., and Wereley, S.T.: *Fundamentals and Applications of Microfluidics*. Boston, Artech House, 2002.

99. Nguyen, N.-T, and Wu, Z.: Mixromixers - a review. *Journal of Micromechanical Microelngineering*, 15: R1-R16, 2005.

100. Nguyen, N.-T.: *Micromixers: Fundamentals, Design and Fabrication*, Norwich, William Andrew Inc., 2008.

101. Niu, X., and Lee, Y.K.: Efficient spatial-temporal chaotic mixing in microchannels. *Journal of Micromechanics and Microengineering*, 13: 454-462, 2003.

102. Oh, K.W., and Ahn, C.H.: A review of microvalves. *Journal of Micromechanics and Microengineering*, 16: R13-R39, 2006.

103. Ohnstein, T., Tukiura, T., Ridley, J., and Bonne, U.: Micromachined silicon microvalve. In Proceedings, *Micro Electro Mechanical Systems '90*, 95–98, 1990.

104. Ottino, J.M, and Wiggins, S.: Introduction: mixing in microfluidics. *Phil. Trans. R. Soc. Lond. A*, 362: 923-935, 2004.

105. Park, S.J., Kim, J.K., Park, J., Chung, S., Chung, C., and Chang, J.K.: Rapid three-dimensional passive rotation micromixer using the breakup process. *Journal of Micromechanics and Microengineering*, 14: 6-14, 2004.

106. Pattanakul, R., Atiwongsangtong, N., Muanghlua, R., Titiroongruang, W., Niemchareon, S., and Chomnawang, N, Fabrication of a curled-up SU-8/metal closure plate for electrostatic microvalve. In Proceedings, *The 21st International Technical Conference on Circuits/Systems, Computers and Communications*, 3: 485-488, 2006.

107. Paul, D., Pallandre, A., Miserere, S., Weber, J., and Viovy, J.L.: Lamination-based rapid prototyping of microfluidic devices using flexible thermoplastic substrates. *Electrophoresis*, 28: 1115-1122, 2007.

CITED LITERATURE (continued)

108. Paya, N., Dankovic, T., and Feinerman, A.: 2008, A microfluidic mixer fabricated from compliant thermoplastic films. *Journal of Undergraduate Research* 2: 1-5 (2008). http://jur.phy.uic.edu/issue2/JUR-REU0801005.pdf

109. Pitchaimani, K., Sapp, B.C., Winter, A., Gispanski, A., Nishida, T., and Fan, Z.H., Manufacturable plastic microfluidic valves using thermal actuation. *Lab on a Chip*, 9: 3082–3087, 2009.

110. Reyes, D.R., Iossifidis, D., Auroux, P.A., and Manz,A.: Micro total analysis systems. 1. Introduction, theory, and technology. *Analytical Chemistry*, 74: 2623-2636, 2002.

111. Ribeiro, J.C., Minas, G., Turmezei, P., Wolffenbuttel, R.F., and Correia, J.H.: A SU-8 fluidic microsystem for biological fluids analysis. *Sensors and Actuators A*, 123-124: 77-81, 2005.

112. Rollier, A-S, Legrand, B., Collard, D., and Buchaillot, L.: The stability and pull-in voltage of electrostatic parallel-plate actuators in liquid solutions. *Journal of Micromechanics and Microengineering*, 16: 794-801, 2006.

113. Rowland, H.D., and King, W.P.: Micro- and nanomanufacturing via molding. In: *BioNanoFluidic MEMS*, ed. P.J. Hesketh, pp. 131-151, New York, Springer 2008.

114. Russek, U.A., Palmen, A., Staub, H., Pohler, J., Wenzlau, C., Otto, G., Poggel, M., Koeppe, A., and Kind, H.: Laser beam welding of thermoplastics. *Proceedings of SPIE*, 4977: 458-472, 2003.

115. Saatdjian, E., Rodrigo, A.J.S., and Mota, J.P.B.: On chaotic advection in a static mixer. *Chemical Engineering Journal*, 187: 289-298, 2012.

116. Sato, K. and Shikida, M.: An electrostatically actuated gas I valve with an S-shaped film element. *Journal of Micromechanics and Microengineering*, 4: 205-209, 1994.

117. Schaible, J., Vollmer, J., Zengerle, R., Sandmaier, H., Strobelt, T.: Electrostatic microvalves in silicon with 2-way function for industrial applications. In Proceedings, *11th International Conference on Solid-State Sensors and Actuators Transducers'01, Eurosensors XV*, 928-931, 2001.

118. Schilling, E.A., Kamholz, A.E., and Yager, P.: Cell lysis and protein extraction in a microfluidic device with detection by a fluorogenic enzyme assay. *Analytical Chemistry*, 74: 1798-1804, 2002.

CITED LITERATURE (continued)

119. Schomburg, W.K., Ahrens, R., Bather, W., Goll, C., Meinzer, S., and Quinte, A.: AMANDA-low-cost production of microfluidic devices. *Sensors and Actuators A*, 70: 153-158, 1998.

120. Schönfeld, F., Hessel, V., and Hofmann, C.: An optimized split-and-recombine micro-mixer with uniform 'chaotic' mixing. *Lab on a Chip*, 4: 65-69, 2004.

121. Sethu, P., and Mastrangelo, C.H.: Cast epoxy-based microfluidic systems and their application in biotechnology. *Sensors and Actuators B*, 98: 337-346, 2004.

122. Shao, P., Rummler, Z., and Schomburg, W.K.: Polymer micro piezo valve with a small dead volume. *Journal of Micromechanics and Microengineering*, 14: 305–309, 2004.

123. Shikida, M., Sato, K., Tanaka, S., Kawamura, Y., and Fujisaki, Y.: Electrostatically driven gas valve with high conductance. *Journal of Micromechanics and Microengineering*, 3: 76-80, 1994.

124. Shoji, S., and Esashi, M.: Microflow devices and systems. *Journal of Micromechanics and Microengineering*, 4: 157-171, 1994.

125. Snakenborg, D., Klank, H., and Kutter, J. P.: Microstructure fabrication with a CO_2 laser system. *Journal of Micromechanics and microengineering*, 14: 182-189, 2004.

126. Sollier, E., Murray, C., Maoddi, P., and Di Carlo, D.: Rapid prototyping polymers for microfluidic devices and high pressure injections. *Lab on a chip*, 11: 3752-3765, 2011.

127. Song, H., Bringer, M.R., Tice,J.D., Gerdts, C.J., and Ismagilov, R.F.: Experimental test of scaling of mixing by chaotic advection in droplets moving through microfluidic channels. Applied Physics Letters, 83: 4664- 4666, 2003.

128. Song, H., and Ismagilov, R.F.: Millisecond kinetics on a microfluidic chip using nanoliters of reagents. J. Am. Chem. Soc. 125: 14613-14619, 2003.

129. Song, H., Chen, D.L., Ismagilov, R.F.: Reactions in Droplets in Microfluidic Channels. Angewandte Chemie International Edition, 45: 7336–7356, 2006.

130. Sousa, P.C., Pinho, F.T., Oliveira, M.S.N., and Alves, M.A.: High performance microfluidic rectifiers for viscoelastic fluid flow. *Royal Society of Chemistry Advances*, 2: 920-929, 2012.

131. Srikar, V.T., and Spearing, S.M., Materials selection for microfabricated electrostatic actuators. *Sensors and Actuators A*, 102: 279-285, 2003.

CITED LITERATURE (continued)

132. Stone, H.A., Stroock, A.D., and Ajdari, A.: Engineering flows in small devices: Microfluidics toward a lab-on-a-chip. *Annu. Rev. Fluid Mech*., 36: 381-411, 2004.

133. Stroock, A.D., Dertinger, S.K.W., Ajdari, A., Mezic, I., Stone, H.A., and Whitesides, G.M.: Chaotic mixer for microchannels. *Science*, 295: 647-651, 2002.

134. Sudarsan, A.P., and Ugaz, V.M.: Multivortex micromixing. *PNAS*, 103: 7228-7233, 2006.

135. Sudarsan, A.P., and Ugaz, V.M.: Fluid mixing in planar spiral microchannels. *Lab on a Chip*, 6: 74-82, 2006.

136. Terry, S.C., Jerman, J.H., and Angell, J.B.: A Gas Chromatographic Air Analyzer Fabricated on a Silicon Wafer," *IEEE Transaction on Electron Devices*, 26: 1880-1886, 1979.

137. Teymoori, M.M., and Abbaspour-Sani, E.: Design and simulation of a novel electrostatic peristaltic micromachined pump for drug delivery applications. Sensors and Actuators A, 117: 222–229, 2005.

138. Tice, J.D., Song, H., Lyon, A.D., and Ismagilov, R.F.: Formation of droplets and mixing in multiphase microfluidics at low values of the Reynolds and the Capillary numbers. Langmuir, 19: 9127-9133, 2003.

139. Tofteberg, T., Skolimowski, M., Andreassen, E., and Geschke, O.: A novel passive micromixer: lamination in a plannar channel system. *Microfluid Nanofluid*, 8: 209-215, 2010.

140. Tsai, R.T., and Wu, C.Y.: An efficient micromixer based on multidirectional vortices due to baffles and channel curvature. *Biomicrofluidics*, 5: 014103 (13 pages), 2011.

141. Tsai, R.T., Wu, C.Y.: Multidirectional vortices mixing in three-stream micromixers with two inlets. *Misrosyst. Technol*., 18: 779-786, 2012.

142. Tsao, C.W., and DeVoe, D.L.: Bonding of thermoplastic polymer microfluidics. *Microfluid Nanofluid*, 6: 1–16, 2009.

143. Veenstra, T.T., Lammerink, T.S.J., Elwenspoek, M.C., and van den Berg, A.: Characterization method for a new diffusion mixer applicable in micro flow injection analysis systems. *Journal of Micromechanics and Microengineering,* 9: 199-202, 1999.

144. Vijayendran, R.A., Motsegood, K.M., Beebe, D.J., and Leckband, D.E.: Evaluation of a three-dimensional micromixer in a surface-based biosensor. *Langmuir*, 19: 1824-1828, 2003.

CITED LITERATURE (continued)

145. Villermaux, E., Stroock, A.D., and Stone, H.A.: Bridging kinematics and concentration content in a chaotic micromixer. *Physical Review E*, 77: 015301(R), 2008.

146. Walker, G.M., Ozers, M.S., Beebe, D.J.: Cell infection within a microfluidic device using virus gradients. *Sensors and Actuators B*, 98: 347-355, 2004.

147. Wang, H., Iovenitti, P., Harvey, E., and Masood, S.: Numerical investigation of mixing in microchannels with patterned grooves. *Journal of Micromechanics and Microengineering*, 13: 801-808, 2003.

148. West, J., Becker, M., Tombrink, S., and Manz, A.: Micro Total Analysis Systems: Latest Achievements. *Analytical Chemistry*, 80: 4403-4419, 2008.

149. Whitesides, G.M.: The origins and the future of microfluidics. *Nature*, 442: 368-373, 2006.

150. Wiggins, S., and Ottino, J.M.: Foundations of chaotic mixing. *Phil. Trans. R. Soc. Lond. A*, 362: 937-970, 2004.

151. van der Wijngaart, W., Ask, H., Enoksson, P., and Stemme, G.: A high-stroke, high-pressure electrostatic actuator for valve applications. *Sensors and Actuators A*, 100: 264-271, 2002.

152. Wong, S.H., Bryant, P., Ward, M., and Wharton, C.: Investigation of mixing in a cross-shaped micromixer with static mixing elements for reaction kinetics studies. *Sensors and Actuators B*, 95: 414-424, 2003.

153. Wong, S.H., Ward, M.C.L., Wharton, C.W.: Micro T-mixer as a rapid mixing micromixer. *Sensors and Actuators B*, 100: 359-379, 2004.

154. Wu, Z., Nguyen, N.-T., and Huang, X.: Nonlinear diffusive mixing in microchannels: theory and experiments. *Journal of Micromechanics and Microengineering*, 14: 604-611, 2004.

155. Wu, Z., and Nguyen, N.-T.: Passive and active micromixers. In: *Micro Process Engineering. A Comprehensive Handbook, Volume 1: Fundamentals, Operations and Catalysts*. eds. V. Hessel, A. Renken, J.C. Schouten, and J. Yoshida, pp. 175-204, Weinheim, Wiley-VCH Verlag GmbH & Co., 2009, p. 149.

156. Xie, J., Shih, J., and Tai, Y. C.: Integrated surface-micromachined mass flow controller. In Proceedings, *The 16th Annual International Conference on Micro Electro Mechanical Systems, 2003*, 20–23, 2003.

CITED LITERATURE (continued)

157. Yager, P., Edwards, T., Fu, E., Helton, K., Nelson, K., Tam, M.R., and Weigl, B.H.: Microfluidic diagnostic technologies for global public health. *Nature*, 442: 412-418, 2006.

158. Yang, B., and Lin, Q.: Planar micro-check valves exploiting large polymer compliance. *Sensors and Actuators A*, 134: 186-193, 2007.

159. Yang, R., Williams, J.D., and Wang, W.: A rapid micro-mixer/reactor based on arrays of spatially impinging micro-jets. *Journal of Micromechanics and Microengineering*, 14: 1345-1351, 2004.

160. Yeo, L.P., Ng, S.H., Wang, Z.F., Xia, H.M., Wang, Z.P., Thang, V.S., Zhong, Z.W., and de Rooij, N.F.: Investigation of hot roller embossing for microfluidic devices. *Journal of Micromechanics and Microelngineering*, 20: 015017 (10 pp.), 2010.

161. Yi, M., Bau, H. H.: The kinematics of bend-induced mixing in micro-conduits. *International Journal of Heat and Fluid Flow*, 24: 645-656, 2003.

162. Yildirim, E., and Kulah, H., Analysis and characterization of an electrostatically actuated in-plane parylene microvalve. *Journal of Micromechanics and Microengineering*, 21: 105009 (9pp), 2011.

163. Yildirim, E., Sahir Arikan, M. A., Kulah, H.: A normally closed electrostatic parylene microvalve for micro total analysis systems. *Sensors and Actuators A*, 81: 81–86, 2012.

164. Yobas, L., Huff, M.A., Lisy, F.J., and Durand, D.M.: A novel bulk-micromachined electrostatic microvalve with a curved-compliant structure applicable for a pneumatic tactile display," *Journal of Microelectromechanical Systems*, 10: 187-196, 2001.

165. Yobas, L., Durand, D.M., Skebe, G.G., Lisy, F.J., and Huff, M.A.: A novel integrable microvalve for refreshable braille display system. *Journal of Microelectromechanical Systems*, 12: 252-263, 2003.

166. Yoshida, K., Tanaka, S., Hagihara, Y., Tomonari, S., Esashi, M.: Normally closed electrostatic microvalve with pressure balance mechanism for portable fuel cell application. *Sensors and Actuators A*, 157: 290–298, 2010.

167. Yuen, P. K., Kricka, L. J. and Wilding, P.: Semi-disposable microvalves for use with microfabricated devices or microchips. *Journal of Micromechanics and Microengineering*, 10: 401–409, 2000.

CITED LITERATURE (continued)

168. Zhang, Q., Pekas, N., Juncker, D.: Design and fabricaton of novel compliant electrostatically actuated microvalves. *Advanced Materials Research,* 74: 179-182, 2009.

169. Zhou, J., Ellis, A.V., and Voelcker, N.H.: Recent developments in PDMS surface modification for microfluidic devices. *Electrophoresis*, 31: 2-16, 2009.

VITA

NAME: Tatjana Dankovic

EDUCATION:

B.S., Electrical Engineering, University of Belgrade, Belgrade, Serbia, 1995

M.S., Electrical and Computer Engineering, University of Illinois at Chicago, Chicago, Illinois, 2006

Ph.D., Electrical and Computer Engineering, University of Illinois at Chicago, Chicago, Illinois, 2013

PROFESSIONAL MEMBERSHIP:

Institute of Electrical and Electronics Engineers
American Society of Mechanical Engineers

JOURNAL PUBLICATIONS:

Gardiye Punchihewa, K., Zaker, E., Kuljic, R., Banerjee, K., Dankovic, T., Feinerman, A., and Busta, H.: Comparisons between membrane, bridge and cantilever miniaturized resistive vacuum gauges. *Sensors*, 12: 8770-8781, 2012.

Kuljic, R., Chang, J., Jayapratha, N., Dankovic, T., Banerjee, K., Feinerman, A., and Busta, H.: A MEMS-based vacuum gauge for measuring pressure and out-gassing rates in miniaturized vacuum microelectronic devices. *J. Vac. Sci. Technol. B*, 29: 02B114 doi:10.1116/1.3562271 (5 pages), 2011.

Paya, N. Dankovic, T., and Feinerman, A.: A microfluidic mixer fabricated from compliant thermoplastic films. *Journal of Undergraduate Research* 2: 1-5, 2008. http://jur.phy.uic.edu/issue2/JUR-REU0801005.pdf

CONFERENCE PUBLICATIONS

Dankovic, T., and Feinerman, A.: Electrostatically actuated compliant microvalves. 2012 ASME International Mechanical Engineering Congress, Nov 9-15, 2012, Houston, Texas, US IMECE2012-89499.

Dankovic, T., Gardiye Punchihewa, K.A., Zaker, E., Farid, S., Habibimehr, P. Feinerman, A., Busta, H.: Extension of operating range towards lower pressures of MEMS-based thermal vacuum gauges by laser-induced heating. *Procedia Engineering*, 26th European Conference on Solid-State Transducers, EUROSENSOR 2012, 47, 2012: 1243–1246, 2012.

VITA (continued)

Zaker, E.; Farid, S.; Selvaraj, S.K.; Bhavanarayana, C.; Sorto, D.; Kaur, R.; Svean, B.; Slusser, S.; Habibimehr, P.; Cheng, J.; Sliwa, K.; Habeebuddin, F.; Kirkpatrick, M.; Dankovic, T.; Punchihewa, K.A.G.; Feinerman, A.; Busta, H., : Thermal-based MEMS vacuum gauges for measuring pressures from 10−2 Torr to 10−6 Torr," *Vacuum Nanoelectronics Conference (IVNC), 2012 25th International*, pp. P1-64 (two pages), 2012.

Punchihewa, K.G.; Zaker, E.; Kuljic, R.; Rangaraj, A.; Liu, M.; Purahmad, M.; Saboonchi, H.; Vesa, A.; Gezahegne, G.; Hughes, C.; Humayun, M.; Huang, J.; Padmanabhan, A.; Seethapathy, S.; Shelton, J.; Hsu, B.; Prabhakar, A.; Jendo, M.; Sridhar, P.; Suh, A.; Banerjee, K.; Dankovic, T.; Feinerman, A.; Busta, H., "Improvement of the sensitivity and operating range of MEMS-based resistive-type vacuum gauges," Vacuum Nanoelectronics Conference (IVNC), 2011 24th International, pp. 191-192, 2011.

Feinerman, A., Dankovic, T., and Yarbrough, D.: Thermal model of area and edge losses for vacuum insulation panels using tensile supports and a stainless steel foil exterior. *Proceedings of the 31th International Thermal Conductivity Conference and the 19th International Thermal Expansion Symposium*, Saguenay, Quebec, June 26-30, 2011.

Dankovic, T., and Feinerman, A.,: Compliant micromixer. Proceedings of *2010 ASME International Mechanical Engineering Congress*, Nov 12-18, 2010, Vancouver, British Columbia, Canada IMECE2010-38991, pp. 777-782

J. Chang, N. Jayapratha, R. Kuljic, B. Salvador, M. Cantwell, K. Broughton, B. Kunzer, P. K. Ng, A. Selner, R. Razo, M. Harris, Q. He, S. Syerov, D. Harry, S. C. Kanneganti, A. Benison, B. Edlavitch, T. Dankovic, K. Banerjee, A. Feinerman, and H. Busta, "A MEMS-based vacuum gauge for measuring pressure and out-gassing rates in miniaturized vacuum microelectronic devices," Technical Digest of the 23rd International Vacuum Nanoelectronics Conference, Palo Alto, CA, USA, 2010

Dankovic, T., and Feinerman, A.: Compliant micromixers. 2010 ASME International Mechanical Engineering Congress, Nov 12-18, 2010, Vancouver, British Columbia, Canada

Feinerman, A., Dankovic, T., Zeng, H., and Wan, Z.: Compliant microvalves fabricated by direct laser welding," 2010 ASME International Mechanical Engineering Congress, Nov 12-18, 2010, Vancouver, British Columbia, Canada